

**UCGE Reports
Number 20294**

Department of Geomatics Engineering

**Development of Laser Fluorosensor Data Processing
System and GIS Tools for Oil Spill Response**

(URL: <http://www.geomatics.ucalgary.ca/research/publications>)

by

Maya Nand Jha

September 2009



UNIVERSITY OF CALGARY

Development of Laser Fluorosensor Data Processing System and GIS Tools for Oil Spill

Response

by

Maya Nand Jha

A THESIS

SUBMITTED TO THE FACULTY OF GRADUATE STUDIES
IN PARTIAL FULFILMENT OF THE REQUIREMENTS FOR THE
DEGREE OF (MASTER OF SCIENCE)

DEPARTMENT OF GEOMATICS ENGINEERING

CALGARY, ALBERTA

September, 2009

© Maya Nand Jha (2009)

Abstract

An oil spill detection and decision support system is a critical tool in protecting oceanic environment and reducing economic losses due to oil spill. Remote sensing data can help in detecting minor spills before they cause widespread damage. This thesis examines the characteristics and applications of different sensors with regard to oil spill surveillance. Laser Fluorosensors, such as the Scanning Laser Environmental Airborne Fluorosensor (SLEAF) sensor operated by Environment Canada, are among the most appropriate sensors for oil spill surveillance. Algorithms for detecting oil spills using laser fluorosensor datasets are analyzed. The algorithms are compared on the basis of their ability to identify oil in the Scanning Laser Environmental Airborne Fluorosensor (SLEAF) data as well as from the simulated data. A classification scheme is developed for oil spill detection and classification based on the analysis. The developed oil spill detection and classification scheme is employed to detect and classify oil from SLEAF data acquired in parts of west and east coast of Canada.

Though various components and software tools exist for managing specific tasks involved in oil spill response, there is a need to develop a comprehensive integrated system for oil spill response. An integrated oil spill detection and response system can greatly help disaster managers in directing resources and equipments for oil spill cleaning and containment operations to appropriate locations. A software system is developed to exhibit the feasibility of realizing such an integrated oil spill detection and decision support system. The oil spill trajectory modeling tool is developed as a part of the system.

Acknowledgements

This thesis is based on extensive research for around two years. This thesis would not have been possible without support from many people. First, I would like to thank my supervisor Dr. Yang Gao for his constant support, guidance and encouragement throughout my research. I sincerely thank ESTD, Environment Canada and particularly Dr. Brown for kindly providing the SLEAF dataset for this thesis. I wish to express my deep appreciation to Dr. Xin Wang, Dr. Ayman Habib and Dr. Ron Wong for carefully reading and providing comments concerning various aspects of this research.

I have been far from my parents Dr. Baua Nand Jha and Indira Jha during this research but I always felt the warmth of their affection with me. I would like to thank my brother Jaya Nand Jha and my sister-in-law Rashmi Jha for their constant encouragement and support. I am grateful to my sister Hema Jha and brother-in-law Dr. Mani Kumar for their love and support.

Members of PMIS research group have been really helpful and I am thankful to them. I am grateful to members of DPRG group for their friendliness. I want to particularly thank Ki In Bang for giving valuable suggestions in geo-referencing SLEAF data, and Anna Jarvis for help and emotional support. The stay at University of Calgary would not have been so much fun without my friends Sneha and Nidhi. Last but not the least, I appreciate help and support from my flat-mates Jaydeep Tailor and Sandeep Chandana during this research.

Dedication

*To my mother “Indira Jha” whose categorical love, affection
and occasional chiding has given me strength and guided me throughout
the life.*

Table of Contents

Approval Page.....	ii
Abstract.....	ii
Acknowledgements.....	iii
Dedication.....	iv
Table of Contents.....	v
List of Tables.....	vii
List of Figures and Illustrations.....	viii
List of Symbols, Abbreviations and Nomenclature.....	xi
CHAPTER ONE: INTRODUCTION.....	1
1.1 Damages Caused by Oil Spill.....	1
1.2 Oil Spill Surveillance.....	3
1.3 Oil Spill Trajectory Modeling.....	5
1.4 Oil Spill Response and GIS.....	8
1.5 Research Objectives.....	11
1.6 Thesis Outline.....	12
CHAPTER TWO: STATE-OF-THE-ART SENSORS TECHNOLOGY FOR OIL SPILL SURVEILLANCE.....	13
2.1 Remote Sensing for Oil Spill Surveillance.....	13
2.1.1 Visible Sensors.....	14
2.1.2 Infrared Sensors.....	16
2.1.3 Ultraviolet Sensors.....	16
2.1.4 Radar.....	17
2.1.5 Microwave.....	19
2.1.6 Laser fluorosensor.....	19
2.1.7 Laser-acoustic oil thickness sensor.....	21
2.2 Comparison of Remote Sensing Systems for Oil Spill Surveillance.....	22
CHAPTER THREE: EXISTING METHODS FOR LASER FLUOROSENSOR DATA PROCESSING.....	28
3.1 Oil Spill Detection using Laser Fluorosensors.....	28
3.2 Oil Spill Detection Methods and Algorithms.....	37
CHAPTER FOUR: A SCHEME FOR OIL SPILL DETECTION AND TRAJECTORY MODELING.....	40
4.1 Description of Dataset.....	40
4.2 Comparative Evaluation of Existing Methods for Oil Spill Detection.....	41
4.3 A Proposed Oil Spill Detection and Classification Scheme.....	53
4.4 Geo-referencing of SLEAF Data.....	58
4.5 Oil Spill Trajectory Modeling using Cellular Automata.....	67
CHAPTER FIVE: RESULTS AND DISCUSSION.....	71
5.1 Results of using Proposed Scheme on SLEAF Data.....	72
5.2 Oil Spill Disaster Products.....	76

CHAPTER SIX: DEVELOPMENT OF A TOOL FOR OIL SPILL DETECTION AND RESPONSE.....	84
6.1 System Architecture.....	84
6.2 Software Tool Development.....	89
CHAPTER SEVEN: CONCLUSIONS AND RECOMMENDATIONS.....	99
7.1 Conclusions.....	99
7.2 Recommendations.....	101
REFERENCES	103

List of Tables

Table 1.1: Appearance of Oil on a Calm Water Surface	3
Table 2.1: Remote Sensing Bands and Related Instruments used for Oil Spill Detection (Adapted from Goodman, 1994)	14
Table 2.2: Requirements for Oil Spill Detection (Adapted from Fingas et al., 1998).....	23
Table 2.3: Comparison of Various Sensors for Oil Spill Detection	26
Table 3.1: Technical Specifications for some Laser Fluorosensors	30
Table 4.1: Summary Statistics for Light Oils (Data Source: Environment Canada)	42
Table 4.2: Summary Statistics for Heavy Oils (Data Source: Environment Canada)	43
Table 4.3: Summary Statistics for Some Crude Oils (Data Source: Environment Canada)	43
Table 4.4: Summary Statistics for Background Materials (Data Source: Environment Canada)	44
Table 4.5: Classification Results using Various Algorithms for Simulated Data.....	53
Table 4.6: Typical Values of Thresholds for Oil Spill Detection and Classification Scheme	56

List of Figures and Illustrations

Figure 1.1: Sea Birds Affected by the Exxon Valdez Oil Spill (Photo Courtesy of the Exxon Valdez Oil Spill Trustee Council)	2
Figure 1.2: Processes Involved In Determining Fate and Behaviour of Oil Spill (Graph Courtesy Of ITOP. © International Tanker Owners Pollution Federation Limited (ITOPF))	7
Figure 2.1: Image of Exxon Valdez Oil Spill Captured by a Sensor in the Visible Range (Source: NOAA, 2007)	15
Figure 2.2: SAR Image (RADARSAT-1) of Oil Spill Caused by Katrina Hurricane (2005) in the Gulf of Mexico	18
Figure 2.3: Schematic Diagram of the Laser Fluorosensor (source: Laser Diagnostic Instruments AS (LDI))	20
Figure 3.1: Fluorescence Spectra of Light Oils. Data Source: Environment Canada.....	31
Figure 3.2 Fluorescence Spectra of Crude Oils (Data Source: Environment Canada).....	32
Figure 3.3: Fluorescence Spectra of Heavy Oils (Data Source: Environment Canada) ...	32
Figure 3.4: Fluorescence Spectra of Background Materials (Data Source: Environment Canada)	33
Figure 3.5: Fluorescence Spectra of Natural Water for Excitation Wavelength as 308 nm (Adapted from Grüner, 1991)	34
Figure 3.6: Laser Induced Fluorescence (LIF) spectrum for Oil Slick and Sea Water (Adapted from Hoge and Swift, 1980)	35
Figure 4.1: Sample Simulated Data Generated for Light Oil by adding 10% Gaussian Noise	45
Figure 4.2: Eigenvalues for the PCs Computed for Reference Spectrum.....	49
Figure 4.3: PC Loading for Reference Materials.....	50
Figure 4.4: 3D Scatter Plot of Reference Materials in the PC Space	50
Figure 4.5: 2D Scatter Plot of Reference Materials in the PC Space (PC1 and PC2)	51
Figure 4.6: Eigenvalues for the PCs Computed for Ratio Components	51
Figure 4.7: 3D Scatter Plot of Reference Materials in the PC Space for Ratio Components	52

: Figure 4.8: Correlation Map for Reference Fluorescence Spectra	56
Figure 4.9: Scheme for Oil Spill Detection and Classification.....	57
Figure 4.10: Components and Coordinate Systems for a Typical LiDAR System	60
Figure 4.11: Coordinate Systems for SLEAF.....	61
Figure 4.12: Angular Field of Views for Elliptical Scanner.....	64
Figure 4.13: Angular Position of a Point in Elliptical Footprint.....	65
Figure 4.14: The Von Neumann Neighborhood	67
Figure 4.15: The Moore Neighborhood	67
Figure 4.16: Oil Masses in Neighbourhood of Cell (i,j) at Time t	68
Figure 5.1: Study Area Displaying Locations of SLEAF Test Flights Conducted by Environment Canada.....	72
Figure 5.2: Observed Fluorescence Spectra for Thick Oil Film of Diesel in Vancouver Island.....	74
Figure 5.3: Observed Fluorescence Spectra for Thin Film of	74
Diesel in Vancouver Island Area	74
Figure 5.4: Fluorescence Spectra of Water (Gelbstoff) in Vancouver Island Area.....	75
Figure 5.5: Fluorescence Spectra of Turbid Water in Vancouver Island Area.....	75
Figure 5.6: Fluorescence Spectra of Water (Gelbstoff) in East Coast of Canada.....	76
Figure 5.7: Georeferenced and Processed SLEAF Data in East Coast of Canada	79
Figure 5.8: Oil Spill Detected around Vancouver Island.....	79
Figure 5.9: Oil Slick Extracted from SLEAF Data around Vancouver Island	80
Figure 5.10: Emergency Response Map for Oil Spill at Vancouver Island.....	81
Figure 5.11: Oil Spill Trajectory Map with Assumed Parameters for Trajectory Modeling.....	82
Figure 5.12: ESI map for the Shoreline of Southern California (Source: NOAA).....	83
Figure 6.1: Use Case Scenerio for Integrated System for Oil Spill Response.....	88

Figure 6.2: System Architecture of Integrated System for Oil Spill Response	88
Figure 6.3: SLEAF Data Processing and Analysis Flow Chart	91
Figure 6.4: Hawth's Analysis Tool for Creating Vector Grids.....	92
Figure 6.5: Software Tool Providing General Information about the Prototype System .	93
Figure 6.6: Laser Fluorosensor Data Processing Part of the System.....	93
Figure 6.7: Dialog Box Showing that Processing of Laser Fluorosensor Data is Complete	94
Figure 6.8: Tool for Oil Spill Incident Reporting	94
Figure 6.9: Oil Spill Trajectory Modeling Tool Showing Options for Selecting Different Oil Types	95
Figure 6.10: Oil Spill Trajectory Modeling Tool Showing Options for Selecting Different Measurement Type for Oil	95
Figure 6.12: Trajectory of Oil Spill after Time Interval of 150 Minutes.....	96
Figure 6.13: GUI for GIS Analysis Component of the System	97
Figure 6.14: Oil Spill Emergency Response Map Displayed in GIS Analysis Tool	97
Figure 6.15: Oil Spill Trajectory Map Displayed in GIS Analysis Tool	98
Figure 6.16: ESI Map Displayed in GIS Analysis Tool	98

List of Symbols, Abbreviations and Nomenclature

Abbreviation	Definition
AISA	Airborne Imaging Spectrometer for Applications
APIs	Application Programming Interfaces
AVIRIS	Airborne Visible/Infrared Imaging Spectrometer
CA	Cellular Automaton
CAs	Cellular Automata
CDOM	Coloured Dissolved Organic Matter
DSS	Decision Support System
EMS	Enterprise Message Service
ENEA	Ente per le Nuove tecnologie, l'Energia e l'Ambiente
ESB	Enterprise Service Bus
ESI	Environmental Sensitivity Index
ESRI	Environmental Systems Research Inc.
ESTD	Emergency Science and Technology Division
GIS	Geographic Information Systems
GNOME	General NOAA Operational Modeling Environment
GNSS	Global Navigation Satellite System
GPS	Global Positioning System
GUI	Graphical User Interface
IDE	Integrated Development Environment
INS	Inertial Navigation System
IR	Infrared
IROE-CNR	Istituto di Ricerca sulle Onde Elettromagnetiche del Consiglio Nazionale delle Ricerche
ISTOP	Integrated Satellite Tracking of Oil polluters
LBS	Location Based Services
LDI	Laser Diagnostic Instruments
LEAF	Laser Environmental Airborne Fluorosensor
LiDAR	Light Detection and Ranging
LIF	Laser Induced Fluorescence
LURSOT	Laser-Ultrasonic Remote Sensing of Oil Thickness
MIR	Mid-band Infrared
MWR	Microwave radiometer
NOAA	National Oceanic and Atmospheric Administration
PMIS	Positioning and Mobile Information Systems
PCA	Principal Component Analysis
PCs	Principal Components

RDBMS	Relational Database Management System
SAR	Synthetic Aperture Radar
SDSS	Spatial Decision Support System
SLAR	Side- Looking Airborne Radar
SLEAF	Scanning Laser Environmental Airborne Fluorosensor
TIR	Thermal Infrared
UV	Ultraviolet
VMR	Variance-to-Mean Ratio

Chapter One: Introduction

Petroleum products play an important role in modern society, particularly in the transportation, plastics, and fertilizer industries. There are typically ten to fifteen transfers involved in moving oil from the oil field to the final consumer. Oil spills can occur during the transportation or storage of the oil, and the spillage can happen in water, ice or on land. Marine oil spills can be highly dangerous given that the wind, waves and currents can scatter an oil spill over a wide area within just a few hours in the open sea (Fingas, 2001). Between 1988 and 2000, there were 2,475 spills which released over 800,000 litres of oil in Toronto and surrounding regions (Li, 2002). An oil spill can occur due to a number of reasons, including transportation accidents. Grüner (1991) mentions that in addition to accidents, the controlled release of oil by shipping operators and oil production platforms are major sources of oil spill. Many oiled birds have been found in the east and west coast of Canada due to illegal oil discharges (Brown et al., 2004a and Brown et al., 2006b). Various measures such as firm legislations and strict operating procedures have been imposed to prevent oil spills, but these measures cannot completely eliminate the risk of oil spills (Fingas, 2001).

1.1 Damages Caused by Oil Spill

Once oil is spilled, it quickly spreads to form a thin layer on the water surface, known as an “oil slick”. As time passes, the oil slick becomes thinner, forming a layer known as “sheen” which has a rainbow like appearance. Light oils are highly toxic but evaporate quickly. Heavy oils are less toxic but persist in the environment for a long time. Heavy oils can get mixed with pebbles and sandy beaches and remain there for years (Environment Canada, 2007). Fuels and crude oil contribute to 48% and 29% of

total spilled oil into the sea worldwide, respectively (Brekke and Solberg, 2005). The environmental impacts of oil spills can be considerable. Oil spills in water may severely affect the marine environment causing a decline in phytoplankton and other aquatic organisms. Phytoplankton is at the bottom of the food chain and can pass absorbed oil on to higher levels in the food chain. Oiled birds display behavioural changes leading to loss of eggs and even death (Figure 1.1). The livelihood of many coastal people can be impacted by oil spills, particularly those whose livelihood is based on fishing and tourism (NOAA, 2009). The movement of oil on land depends on various factors such as oil type, soil type and moisture content of the soil. Oil spilled on agricultural land can impact soil fertility and pollute ground water resources (Fingas, 2001).



Figure 1.1: Sea Birds Affected by the Exxon Valdez Oil Spill (Photo Courtesy of the Exxon Valdez Oil Spill Trustee Council)

1.2 Oil Spill Surveillance

Oil spill surveillance constitutes an important component of oil spill disaster management. Advances in remote sensing technologies can help to identify parties potentially responsible for oil spill incident and to identify minor spills before they cause widespread damage (Jha et al., 2008a). Remote sensing data can be very useful input for an oil spill detection and decision support system (DSS). Fingas (2001) describes the guidelines for estimating oil thickness using visual surveillance as shown in Table 1.1. The appearance of oil varies from silvery-sheen to dark brown.

Table 1.1: Appearance of Oil on a Calm Water Surface

Oil Appearance	Approximate Film Thickness (μm)
Silvery sheen	0.05
Rainbow sheen	0.15
Reddish-brown sheen	0.50
Brownish	2.00
Dark	10.00
Dark Brown	50.00

Visual detection of an oil spill is not reliable as oil can be confused with other substances, e.g. sea weeds and fish sperm. Moreover, oil on the surface cannot be observed clearly through fog and darkness (Fingas, 2001). Remote sensing can be used

for detecting and monitoring oil spills. Sensors can provide the following information for oil spill contingency planning (Grüner, 1991):

- The location and spread of an oil spill over a large area
- The thickness distribution of an oil spill to estimate the quantity of spilled oil
- A classification of the oil type in order to estimate environmental damage and to take appropriate response activities
- Timely and valuable information to assist in clean-up operations

Remote sensing technologies for oil spill surveillance have been reviewed by many authors. Goodman (1994) notes that the operational use of remote sensing for oil spill contingency planning is limited although simple systems, such as UV/IR systems and radar, have been used to some extent for responding to oil spills. Brown and Fingas (1997) found that no single sensor can give all the information required for oil spill contingency planning. Currently, many coastal nations have proper maritime surveillance systems in place to detect and monitor oil spill (Brown and Fingas, 2005). Due to the large number of sensors currently available for oil spill surveillance, there is a need for a comprehensive overview and comparison of the existing sensors. A better understanding of the oil spill surveillance sensor characteristics will help improve the effectiveness and operational use of these sensors for oil spill response and contingency planning. Laser Fluorosensors can detect oil under the water surface and on various backgrounds including snow or ice (Brown and Fingas, 2003a). The operational use of laser fluorosensors is expected to increase with time since it is the most useful instrument for oil spill detection (Jha et al., 2008b). Accordingly, it is important to analyze the reliability

and robustness of various oil spill detection algorithms. In this thesis, an in-depth analysis of existing algorithms for oil spill detection and classification is provided, further to which, a novel method is developed.

1.3 Oil Spill Trajectory Modeling

Once oil is spilled in an oceanic environment, it is important to know the movement of oil spill from the start of the incident to its removal from the sea due to various processes. Moreover, the knowledge about the oil state such as density, viscosity, emulsion state and chemical composition is also needed at all stages of oil spill for choosing the appropriate response actions. Oil spill modeling in the oceanic environment is a complicated process as the behaviour and spread of the spilled oil depends on various processes including evaporation, drift, spreading, emulsification, dispersion, dissolution and entrainment (Figure 1.2). These processes are described briefly here.

- **Drift:** Drift is the horizontal and vertical transport of centre of the oil slick by wind and sea currents.
- **Spreading:** The oil slick area increases and oil slick thickness decreases with time in the spreading process. Spreading is an important aspect in understanding its role in the weathering process and containment operations.
- **Natural dispersion:** Dispersion is the process by which wind-driven waves split the surface oil layer into water droplets and propel them into the water column.
- **Emulsification:** Water comes into the oil and forms water-in-oil emulsions. The main effect of emulsification is the increase in the

viscosity and the volume of the oil spill. This makes clean up operations more difficult.

- **Evaporation:** The volatile components in the oil go from their liquid state into vapours. Light oil evaporates quicker than heavy oils. Evaporation can cause loss of petroleum hydrocarbons upto 25% in short term and 40% in the long term.
- **Dissolution:** Dissolution is the process in which the soluble components of crude oil dissolve into water. It is more active when spill first occurs.
- **Sedimentation and shoreline stranding:** Sedimentation is the process when spilled oil reaches a coastline and returns to the marine environment
- **Photo-oxidation:** Oil undergoes oxidation in presence of sunlight. This is a long term process.
- **Biochemical degradation:** Micro-organisms break petroleum hydrocarbons into simpler products. Biochemical degradation is also a long term process.

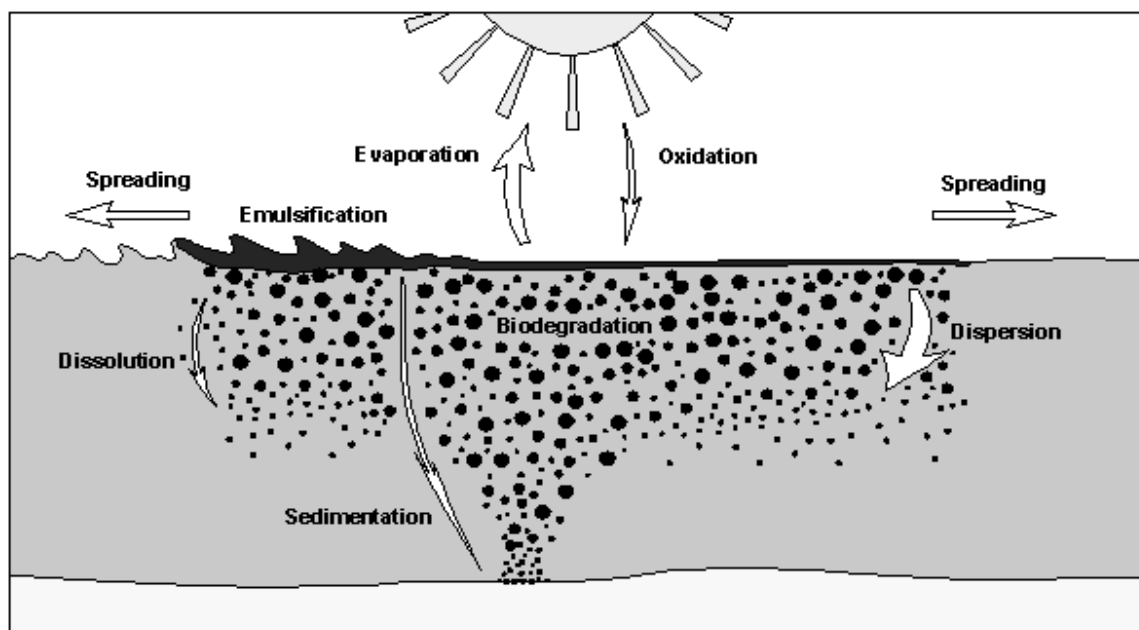


Figure 1.2: Processes Involved In Determining Fate and Behaviour of Oil Spill (Graph Courtesy Of ITOP. © International Tanker Owners Pollution Federation Limited (ITOPF)

A detailed analysis of the current techniques available for oil spill modeling can be found in Reed et al. (1999), Brebbia (2001) and Fingas (2001). Cellular Automata (CAs) are simple but useful technique to model complicated physical processes in discrete space and time. It was introduced by Ulam and Von Neumann in 1951. Fate of oil spill in oceanic environment can be successfully modeled using cellular automata (Karafyllidis, 1997; Rusinovic and Bogunovic, 2006). Karafyllidis (1997) has proposed a simple method to model oil spill trajectory using CAs which has been applied in this thesis to develop a tool for oil spill trajectory modeling. The details of the method developed by Karafyllidis (1997) for oil spill trajectory modeling using Cellular Automata is provided in section 4.5.

1.4 Oil Spill Response and GIS

Contingency planning refers to establishing some plan of action to counter emergencies. The purpose of contingency planning is to minimize economic and environmental damages in case of an oil spill. Fingas (2001) has described that response action for an oil spill can be divided into various phases such as alerting and reporting, evaluation and mobilization, containment and recovery, disposal and remediation. However, traditional methods suffer from the lack of updated information and situational awareness. Hugh (1977) developed an oil spill contingency plan for oil spill response in marine environment. His plan emphasized on resources at risk such as aquatic organisms and public beaches. Green (1996) notes that effective response planning should include timely acquisition of data and information in a cost-effective manner. Geographic information systems (GIS) with comprehensive storage and analysis capability can be an effective tool for oil spill response (Howlett and Bradstreet, 1996). Moreover, GIS is designed to solve spatial problems and many issues related to oil spill contingency planning and any emergency management are spatial.

The response time is crucial for an oil spill in the open ocean as wind and current can rapidly spread the oil over a large area in a short time. GIS can facilitate rapid response and thereby mitigate environmental and economic damages caused by an oil spill. The timeframe for collecting and processing the data is important for oil spill surveillance and monitoring. Real time remote sensing data is essential for oil spill response so that resources can be immediately directed to sensitive areas for cleaning and containment operations. The integration of a remote sensing data processing component with GIS can greatly assist decision makers. Environmental sensitivity index (ESI)

describes the susceptibility of shorelines due to damages caused by oil pollution (Fingas, 2001). ESI is commonly used for evaluating potential risks due to an oil spill. ESI map as a GIS tool can be useful for oil spill decision support system. In addition to having shorelines ranked in terms of their susceptibility to damage caused by an oil spill, it also includes the areas which are environmentally or economically sensitive to an oil spill. ESI map has information about location of fishes, birds, human facilities, any relevant natural feature, types of shoreline etc. ESI maps for USA shorelines are freely available at National Oceanic and Atmospheric Administration (NOAA) website which can be combined with oil spill models to predict the impact of an oil spill. ESI maps for Canada are maintained by oil spill responding agencies, but are not freely available for public use. The list of agencies that need to be notified about an oil spill should be part of any oil spill contingency plan. There should also be a procedure to inform the public about the oil spill incident. A GIS system can contain a list of individuals and agencies who need to be notified in case of an oil spill, and they can be automatically notified in event of an oil spill. Oil spill emergency response typically utilizes an extensive set of resources, equipment and multiple agencies and the coordination between them is a difficult and complex task. Effective communication is crucial to any emergency response (Cova, 1999). A GIS based oil spill detection and decision support system can facilitate communication between various agencies and any relevant data about oil spill incident can be shared quickly among them.

A knowledge-based spatial decision support system (SDSS) for oil spill response can resolve the problems ingrained in the traditional oil spill response decision making. GIS is still mostly used as a spatial database or mapping tool for the oil spill response

(Ranger and Cassas, 1995). The problem is attributed to the lack of modeling capability in the GIS system. Armstrong and Densham (1990) have mentioned that a spatial decision support system (SDSS) consists of the following components:

1. A database management system
2. Analysis routines
3. Display and report generators
4. A user interface

There is a need for an oil spill decision support system, which can use available data and information to tackle oil spill response in a better way. There are components available for the various parts of oil spill response but an integrated comprehensive GIS system is required to quickly respond to an oil spill. For example, General NOAA Operational Modeling Environment (GNOME) is the oil spill trajectory model used by oil spill responders in event of an oil spill but the environmental risk associated with an oil spill can not be estimated using GNOME. The available expert knowledge can be put together to build an expert system with GIS capabilities. A combination of GIS and an expert system can provide significant advantages to decision makers. The unavailability of an expert system for oil spill contingency planning despite significant advancement in technologies acts as a hindrance in effective oil spill response (Graham, 2004; Ornitz and Champ, 2002). A web-based GIS system can resolve the problem of accessibility. The oil spill responders and responsible agencies can access the up-to-date information about an oil spill from anywhere in the world if an internet connection is accessible.

1.5 Research Objectives

The primary objective of this research is to develop a scheme for oil spill detection and classification. Laser fluorosensor data processing will be discussed in detail due to the ability of laser fluorosensors in detecting and classifying oil on various backgrounds in real time. This research also aims to develop additional tools including oil spill trajectory modeling tool and oil spill disaster products which can help personnel involved in oil spill response in taking quick and better decisions. The research objectives of the thesis are:

- To evaluate various remote sensing sensors for oil spill detection and classification. State-of-the-art sensors technology for oil spill surveillance will be discussed and various sensors will be studied based on their ability to detect and classify oil.
- To analyze issues associated with processing laser fluorosensor data for oil spill detection and classification. The algorithms to process laser fluorosensor data will be discussed and analyzed.
- To develop a scheme for oil spill detection and classification using laser fluorosensor data. Reliable oil spill detection is important for oil spill response.
- To develop software which can act as an integrated system for oil spill response and will include components for oil spill detection, oil spill trajectory modeling and oil spill disaster products. System architecture for conceiving a GIS system for oil spill response will be discussed. The developed software will demonstrate that a system can be realized which can handle requirements of oil spill disaster management.

1.6 Thesis Outline

Chapter 1 presents introduction, the problem statement and research objectives for this thesis.

Chapter 2 contains review of the state-of-the-art sensors technology for oil spill surveillance. Various remote sensing sensors available for oil spill surveillance are discussed and compared based on several criteria.

Chapter 3 discusses the issues associated with processing laser fluorosensor data. The advantages and disadvantages of various existing algorithms for laser fluorosensor data are discussed.

Chapter 4 explains the oil spill detection and classification scheme that has been developed in this research. Scanning Laser Environmental Airborne Fluorosensor (SLEAF) data format is described. The procedure of geo-referencing SLEAF data is explained as well. The use of Cellular Automata (CAs) for oil spill trajectory modeling is described.

Chapter 5 provides the analysis of real world laser fluorosensor data based on oil spill detection and classification scheme developed in this research. Oil spill disaster products are discussed.

Chapter 6 explains development of a software tool for oil spill detection and response. The system architecture for realizing an integrated system for oil spill response is discussed. The technologies used for developing the software tool are explained in detail.

Chapter 7 builds on the observations and conclusions drawn from this research as well as recommendations for the future work.

Chapter Two: State-of-the-Art Sensors Technology for Oil Spill Surveillance

There are many sensors available to detect oil spills on various kinds of surfaces. Oil spill location, extent as well as thickness distribution can be obtained by using remote sensors. Multi-temporal imaging captured by remote sensing sensors can provide important information required to model the spread of an oil spill (Natural Resources Canada, 2009). Oil spill models may be useful for cleanup operations and controlling the oil spill. Remote sensing devices for oil spill detection include infrared video and photography, thermal infrared imaging, airborne laser fluorosensors, airborne and space-borne optical sensors, and airborne and space-borne SAR (Natural Resources Canada, 2009). Satellite remote sensing suffers from low spatial and temporal resolution although it provides a synoptic view and a more cost effective system than an airborne platform, which is typically used for oil spill surveillance (Brown and Fingas, 2001a). The usefulness of various sensors with regard to oil spill surveillance is described in this chapter.

2.1 Remote Sensing for Oil Spill Surveillance

Remote sensing bands and related instruments for oil spill detection are shown in Table 2.1. Infrared, visible and UV sensors will not be able to detect oil in inclement weather such as heavy rain or fog (Goodman, 1994). Visible sensors are generally used to create a base map for the oil spill. Active sensors use their own energy source to capture information whereas passive sensors do not have their own energy source and rely on other energy sources. A brief description of sensors useful for oil spill detection is given in the following sections.

Table 2.1: Remote Sensing Bands and Related Instruments used for Oil Spill Detection (Adapted from Goodman, 1994)

Band	Wavelength	Type of Instruments
Radar	1-30 cm	SLAR/SAR
Passive microwave	2-8 mm	Radiometers
Thermal infrared (TIR)	8-14 μm	Video cameras and line scanners
Mid-band infrared (MIR)	3-5 μm	Video cameras and line scanners
Near infrared	1-3 μm	Film and video cameras
Visual	350-750 nm	Film, video cameras and spectrometers
Ultraviolet	250-350 nm	Film, Video cameras and line scanners

2.1.1 Visible Sensors

Thermal and visible scanning systems as well as aerial photography were commonly used airborne remote sensing sensors at the start of 1970 (Wadsworth, 1992). Visible sensors (passive sensors operating in the visible region of the light) are still widely used in oil spill remote sensing despite many shortcomings. The reflectance of oil is higher than that of water but oil also absorbs some radiation in the visible region. These sensors are not good for oil detection as it is difficult to distinguish oil from the background (Figure 2.1). Water surface may have shining effect due to the blowing wind. Sun-glint and wind sheen may create an impression similar to oil sheen. Moreover, sea weeds and a darker shoreline may be mistaken for oil. Visible sensors can not normally

operate at night as they are based on the reflectance of sunlight. Visible sensors are widely available and can be easily mounted on an aircraft. Video cameras possess a lower resolution than still cameras but are still in widespread use for oil spill remote sensing. Visible sensors are inexpensive and simple in operation; therefore, they are often used to create the basic data in coastal areas (Brown and Fingas, 1997; Goodman, 1994).

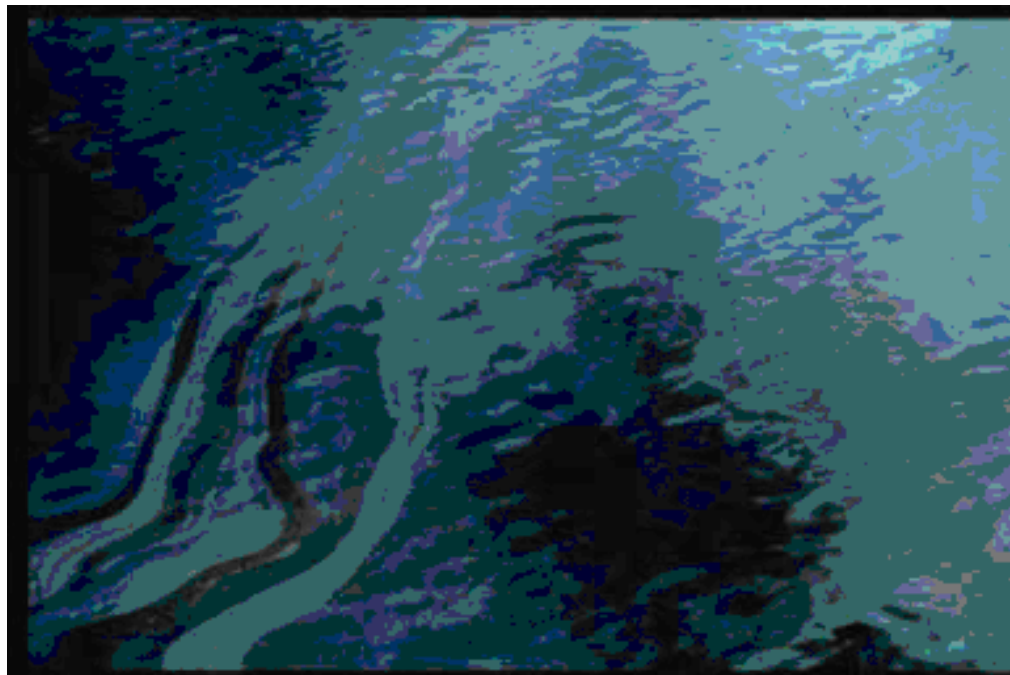


Figure 2.1: Image of Exxon Valdez Oil Spill Captured by a Sensor in the Visible Range (Source: NOAA, 2007)

Improvements in sensor technologies have led to the development of hyperspectral sensors such as Airborne Visible/Infrared Imaging Spectrometer (AVIRIS) and Airborne Imaging Spectrometer for Applications (AISA). A hyperspectral image consists of ten to hundreds of spectral bands and can provide a spectral signature for an object. Plaza et al. (2001) and Salem and Kafatos (2001) have reported the use of hyperspectral data for oil spill detection. Extensive spectral information can be used to

discriminate between light and crude oil. Hyperspectral data has very high spatial and spectral resolution, hence data analysis is little difficult and computationally intensive. Hyperspectral sensors can not detect oil in emulsions formed by water and oil.

2.1.2 Infrared Sensors

Infrared sensors are passive sensors. The oil absorbs solar radiation and emits some part of it as the thermal energy mainly in the thermal infrared region (8-14 μm). Oil has a lower emissivity than water in the thermal infrared region (TIR) and therefore oil has a distinctively different spectral signature in the thermal infrared region compared to the background water (Salisbury et al., 1993). TIR is typically used for oil spill detection in the IR region. Infrared sensors can provide some information about the relative thickness of oil slicks. These sensors are unable to detect emulsions of oil in water as emulsions contain 70% of water and thermal properties of emulsion are similar to the background water (Brown and Fingas, 1997).

Thermal radiation from sea weeds and the shoreline appear similar to the radiation arising from the oil which may lead to a false positive result. The infrared sensors are relatively inexpensive remote sensing technologies which can be used to detect oil spills and are hence widely used systems for oil spill surveillance (Brown and Fingas, 2005).

2.1.3 Ultraviolet Sensors

UV scanners capture the ultraviolet radiation reflected by the sea surface. A UV sensor is a passive sensor as it uses reflected sunlight in the ultraviolet region (0.32-0.38 micron) for detecting oil spills. Oil has stronger reflectivity than water in the UV region. Even a very thin oil film has a strong reflectance in the UV region. Very thin sheens of thickness (less than 0.1 micron) can be detected using a UV sensor. However, UV

sensors cannot detect oil thickness greater than 10 micron. UV images can only give information about the relative thickness of the oil slick (Grüner, 1991).

False detection may occur due to the wind sheen, sun glint and sea weeds. Interferences in UV are different from IR and a combination of these two techniques can provide improved results for oil spill detection (Brown and Fingas, 1997; Goodman, 1994). The ultraviolet images can be overlaid with infrared images to generate an oil spill relative thickness map. UV images are based on the reflected sunlight and hence cannot operate in the night.

2.1.4 Radar

Radar is an active sensor and operates in radio wave region. Radar waves are reflected by capillary waves on the ocean and therefore, a bright image is obtained for ocean water. Oil diminishes capillary waves and as a result, if oil is present in the ocean then reflectance is reduced. Hence, the presence of oil can be detected as dark part in the bright image for the ocean (Brown et al., 2003). Radar is useful as it can be used to detect oil over a large area. Thus, it can be used as a first assessment tool to detect the possible location of an oil spill. Radar can work in both inclement weather and at night. SAR (Synthetic Aperture Radar) and SLAR (Side Looking Airborne Radar) are the two most common types of Radar which can be used for oil spill remote sensing. SAR has superior spatial resolution and range than SLAR (Brown and Fingas, 1997). However, SLAR is less expensive and predominantly used for airborne remote sensing. A SAR image captured by RADARSAT-1 of an oil spill caused by Hurricane 'Katrina' is shown in Figure 2.2. The darker region in Figure 2.2 can be an oil spill, but sophisticated algorithms and expert guidance are needed to find the actual extent of the oil spill.

The major problem with this technology is false detection. The interference in detecting oil may be due to the presence of organic substances other than oils which produce films on the sea surface. Seaweed creates this type of film and may lead to a false alarm in the radar image. Both low and high wind speeds influence oil spill detection (Jones, 2001). SAR is the most widely used sensor on space-borne platforms for oil spill detection.

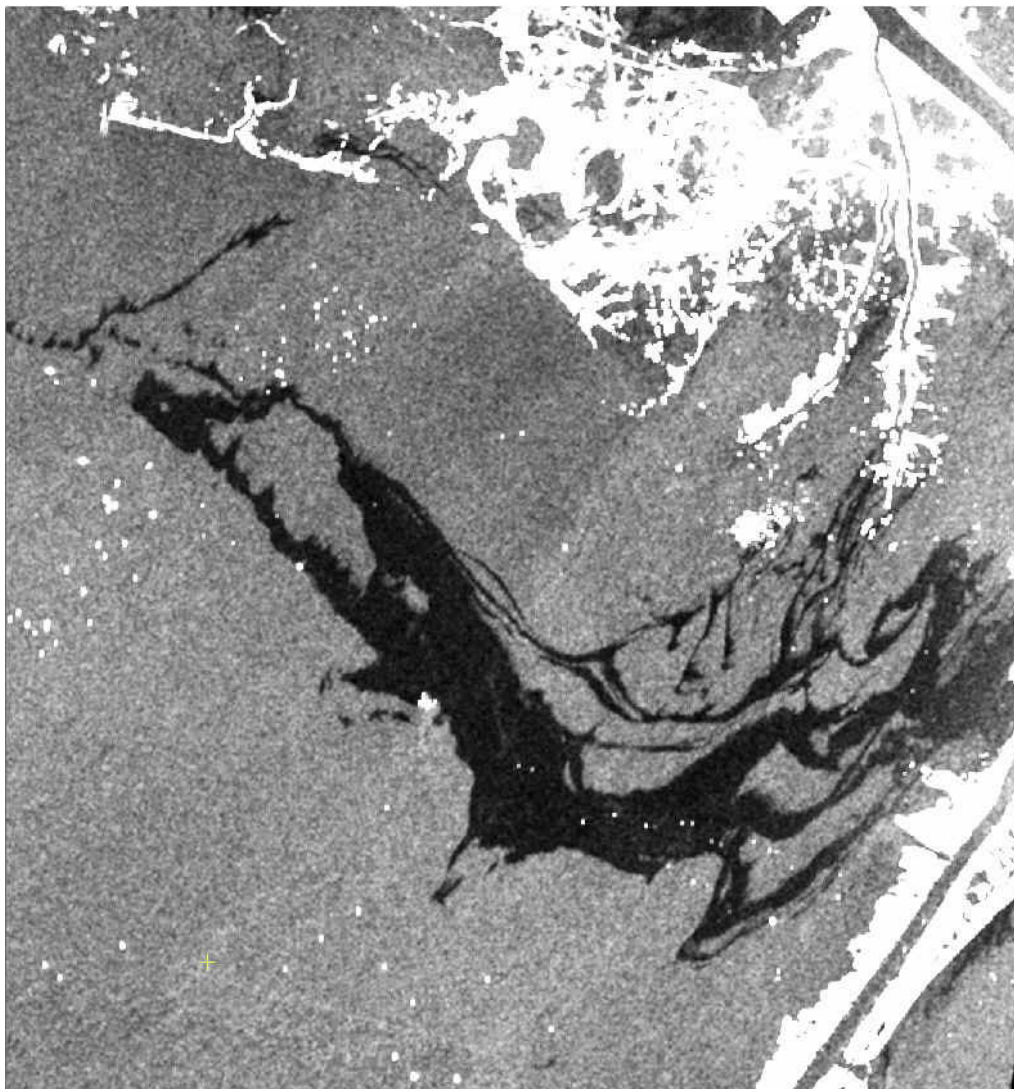


Figure 2.2: SAR Image (RADARSAT-1) of Oil Spill Caused by Katrina Hurricane (2005) in the Gulf of Mexico

2.1.5 Microwave

MWR (Microwave radiometer) is a passive sensor and is used for oil spill detection and oil thickness measurements. Oil emits stronger microwave radiation than water and appears brighter than the water (which is dark in the background). Measuring oil thicknesses with MWR involves the interference of radiation from the upper and lower boundaries of the oil film (Brown and Fingas, 1997). Biogenic materials can produce similar signals to oil which may lead to a false alarm. This sensor can work well in adverse weather conditions and in both, day and night settings. MWR sensors are expensive and complicated in operation. MWR sensors require information about many environmental characteristics and oil properties in order to accurately detect the oil. The main disadvantage of using the MWR sensor is its low spatial resolution.

2.1.6 Laser fluorosensor

Laser fluorosensor is an active sensor and uses characteristic fluorescence properties of oil for oil spill detection. Some aromatic hydrocarbon compounds in petroleum oils absorb laser-induced UV light to become electronically excited. The excitation is released through fluorescence emission by the compound mainly in the visible region. A multi-channel receiver is used to record the fluorescence spectrum (Goodman, 1994). Fluorescence spectrum of gelbstoff and phytoplankton look different from that of petroleum oils. Different types of oils have distinct fluorescence emission signature which allows for oil classification. Water Raman scattering signal occurs due to the energy transfer between water molecules and incident light. Water Raman scattering signal is discussed in detail in section 3.1. An oil film on the water surface suppresses the water Raman scattering signal which can be also used as a distinguishing feature. A

schematic diagram depicting operation of a typical laser fluorosensor is shown in Figure 2.3. A laser scanner mounted on the aircraft hits the targets with laser pulses of some specified excitation wavelength. The induced fluorescence spectra is recorded and stored. Every laser target point in the flight path has a fluorescence spectra associated with it.

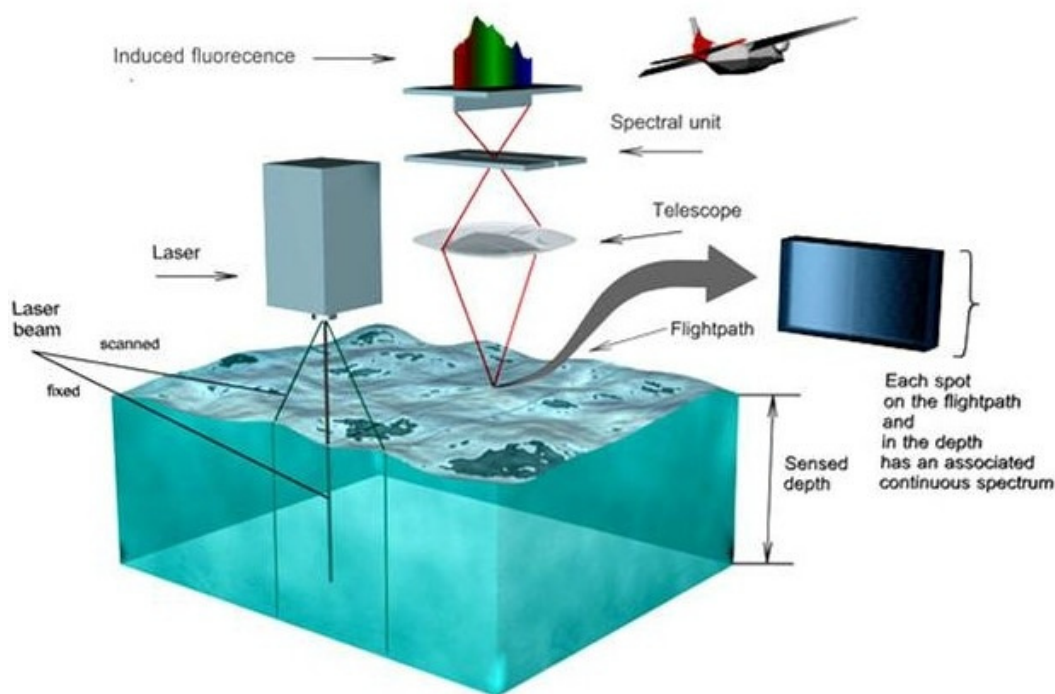


Figure 2.3: Schematic Diagram of the Laser Fluorosensor (source: Laser Diagnostic Instruments AS (LDI))

The laser fluorosensor is the most useful and reliable instrument to detect oil on various backgrounds including water, soil, weeds, ice and snow. They are the only reliable sensors to detect oil in the presence of ice or snow (Zielinski et al., 2001 and Brown and Fingas, 2003a). The laser fluorosensor signals also contain information about some ecologically relevant properties including seawater attenuation coefficients; phytoplankton and gelbstoff concentrations (i.e. coloured dissolved organic matter). These parameters are useful in describing the ecological state of coastal waters (Brown

and Fingas, 2003a). Laser fluorosensor was found to successfully detect water-in-oil emulsions whereas other sensors including UV, IR, and MWR have problems in detecting these emulsions (Brown et al., 2004b). Laser fluorosensors can be used for day and night operations. The atmosphere should be reasonably clear for the operational use of laser fluorosensors. The excitation wavelength for the laser is typically chosen as 308 or 355 nm (Grüner, 1991). The U.S. Coast Guard tested three laser fluorosensor systems for subsurface oil spill detection (Fant and Hensen, 2006) and found them to be successful in detecting surface and subsurface refined oils but the results were not encouraging for the real time detection of crude oils. This may be attributed to the poor performance of the algorithms for detecting heavy oils. Laser fluorosensors are discussed in more detail in the next chapter.

2.1.7 Laser-acoustic oil thickness sensor

This sensor detects the oil based on its acoustic or mechanical properties rather than its optical and electromagnetic properties and can be used to measure the absolute oil thickness. The laser-acoustic sensor is an active sensor and can operate day and night (Goodman, 1994). The time taken by ultrasonic waves to travel in oil is measured by three lasers and the oil thickness can be computed by using this time of flight. Brown and Fingas (2003b) found that results of laboratory tests of measuring oil thickness using LURSOT sensor indicate great potential. In 2006, the LURSOT system was successfully tested for oil slick thickness measurements from an aircraft by Environment Canada (Brown et al., 2006a). LURSOT uses CO₂ laser in infrared region to create thermal pulse. This thermal pulse leads to creation of acoustic pulse and time of travel of this acoustic pulse is measured by Nd:YAG laser in infrared region and HeNe laser (~630 nm).

However, laser-acoustic sensors are bulky and expensive and cannot work in fog and cloud.

2.2 Comparison of Remote Sensing Systems for Oil Spill Surveillance

Sensors can be compared based on various oil spill surveillance criteria. Specifically, the spatial resolution of the sensors can be important factor. Brown and Fingas (2001a) note that the width of a typical oil spill window is less than 10 meters and hence the spatial resolution of sensors should be at least 10 meters. The timeframe for collecting and processing the data is important for oil spill surveillance and monitoring. Time is particularly critical for an oil spill occurring in the open ocean as wind and current can rapidly spread the oil over a large area in a short time. Goodman (1994) notes that any remote sensing data available only after 2-3 hours of oil spill is of little use. Brown et al. (2003) mention that remote sensing data should be available within an hour of the spill. The minimum spatial resolution and time requirement for various tasks in oil spill monitoring are given in Table 2.2. The large oil spill is defined as any oil spill where volume of the spilled oil is greater than 10, 000 gallons. The small oil spills are generally due to the illegal oil discharges and not due to accidents. The width of a typical oil spill window is greater than 10 meters and, hence spatial resolution should be greater than 10 meters. Spatial resolution requirement is higher for oil spill detection than that for the oil spill mapping in case of large oil spill. Oil spill disaster managers are looking for very small amounts of oil, sometimes less than visible amounts in case of oil spill detection. However, for oil spill mapping the spatial resolution requirement depends on the actual scale of the oil spill and the scale of the map. The existing airborne sensors have greater spatial and temporal resolution than the space-borne sensors. Since time is a critical

factor (due to dynamic nature of oil spills) airborne sensors are currently used for tactical response. Visible sensors are the best in terms of having a high spatial resolution. Sensors capturing a synoptic view of the area are desirable and will help in monitoring the oil spill over a large area. Radar sensors (SAR and SLAR) can capture a large area and are useful for providing general view of affected area. While satellite remote sensing can capture a large area it suffers from low spatial resolution.

Table 2.2: Requirements for Oil Spill Detection (Adapted from Fingas et al., 1998)

Minimum Resolution Requirements (<i>m</i>)			Maximum Time During Which Useful Data Can Be Collected (Hours)
Task	Large Spill	Small Spill	
Detect oil on water	6	2	1
Map oil on water	10	2	12
Map oil on land/shore	1	0.5	12
Tactical water cleanup	1	1	1
Tactical support land/shore	1	0.5	1
Thickness/volume	1	0.5	1
Legal and prosecution	3	1	6
General documentation	3	1	1
Long-range surveillance	10	2	1

Sensors should be operational in day and night in order to constitute an effective surveillance system, since it may be required any time of the day. Visible and UV sensors cannot work at night and this is the great disadvantage associated with using them. The effect of weather conditions such as rain and fog should be limited. Radar sensors are the best sensors for oil spill surveillance in case of cloud and fog. However, oil spill detection from radar images are affected by wind speeds and these images are useful for only a small wind window. The cost and size of sensors can also play significant role in using sensors for oil spill surveillance. IR sensors are inexpensive and this has led to their widespread use for oil spill surveillance. Advanced sensors such as laser fluorosensors are expensive which makes their operational use difficult. Moreover, most of the advanced sensors require a dedicated aircraft which makes them even more expensive to operate. The major problem with most of the sensors used for oil spill is false detection (due to sea weed, sun sheen etc). The detection of oil slicks by laser fluorosensors is unaffected by sea weed, sun sheen and other factors that can yield a false positive result. Laser fluorosensors are also the only sensor which can detect oil on various backgrounds including ice or snow. Detecting an oil spill on the shoreline is extremely important for cleaning operations and the laser fluorosensor is the only sensor which can positively detect oil on shorelines.

Oil can be classified into heavy, medium crude and light crude or refined oil. Once classified, it is easier to respond to the oil spill and to model the oil spill drift and spreading. For example, light oil such as diesel evaporates quickly whereas the evaporation rate of heavy oil is slow. Laser fluorosensor has capability to classify oil. Hyperspectral sensors also have some limited ability to classify oil.

Measuring oil thickness is important in modeling the spread of an oil spill. However, simply detecting and mapping the relative thickness of an oil spill is not sufficient for oil spill contingency planning. The measurement of oil thickness on the water surface can provide information about the oil quantity. If the surface area of the spill is known, the total volume of the oil can be calculated from this information. Moreover, oil spill countermeasures such as dispersant application can be directed to the thicker portion of the oil slick. The composite image created by combining IR and UV images can give some idea of the relative thickness of an oil slick. Laser fluorosensors are limited in their ability to measure oil slick thickness as an oil slick of thicknesses greater than 10-20 μm cannot be measured. MWR can measure oil slick thickness between 50 μm to a few millimetres but suffer from coarse spatial resolution. The LURSOT sensor developed by Environment Canada is the only sensor available for measuring absolute oil slick thickness (Brown and Fingas, 2006a). A comparison of various remote sensing technologies for oil spill surveillance is shown in Table 2.3. The cost information is from Fingas and Brown (2005) and the horizontal range information is from Trieschmann et al. (2001). As Laser acoustic oil thickness sensor is still under research and development, no concrete information is provided about the price.

Table 2.3: Comparison of Various Sensors for Oil Spill Detection

	Visible	Infrared	UV	Radar	Microwave Radiometer	Laser Fluorosensor	Laser-acoustic oil thickness sensor
Cost (K\$)	0.25-20	1-200	100-300	1200-8000	400-2000	300-2000	Expensive
False Detection	Sea weed, darker shoreline	Sea weed, shoreline	Wind sheen, sun glint and sea weed	Many interferences	No significant interferences	Can identify oil on any background	Low
Thickness Information	No	Relative thickness	No	Relative thickness under some conditions	50 μ m-few mm	< 20 μ m	Measures Absolute thickness
Spatial Resolution	High	High	High	High	Low	High, line profile	High, line profile
Weather Requirement	Cloudless, Clear	Absence of cloud and heavy fog	Requires clear atmosphere	All weather. Detection dependent upon wind speed	All weather except heavy rain	Can not penetrate cloud and fog	Can not penetrate cloud and fog
24 hour operation	No	Yes	No	Yes	Yes	Yes	Yes
Horizontal Range (300m Altitude)	Medium	\pm 250m	\pm 250m	\pm 30 km	\pm 250m	\pm 75m	Small
Dedicated Aircraft	No	No	No	Yes	Yes	Yes	Yes
Oil Classification	No	No	No	No	No	Yes	No

From the above discussion it can be concluded that there is currently no single sensor available which can give an accurate estimate for all the parameters required for oil spill contingency planning. However, laser fluorosensors are the most useful sensors for real time oil spill detection and response. They are sensitive to sheens of oil which can not be seen in the visible region. Laser fluorosensors can also detect oil in emulsions (while other sensors may have difficulty detecting oil in emulsions). The U.S. Coast Guard conducted a cost benefit analysis for the operational use of laser fluorosensor in oil spill detection and found that the high cost of operating laser fluorosensors hinders their operational use. They also concluded that a low cost multi-sensor system is needed for

the Coast Guard since no single sensor can provide all information for oil spill response (Fant and Hensen, 2006). Lennon (2006) discusses the combined use of hyperspectral imagery and laser fluorosensor data for oil spill surveillance. The Emergency Science and Technology Division (ESTD) of Environment Canada conducts oil spill surveillance in the event of major oil spills in Canada. Environment Canada has a combination of sensors including SLEAF, UV, IR and SAR sensors (Brown and Fingas, 2005).

Chapter Three: Existing Methods for Laser Fluorosensor Data Processing

As per the discussion in Chapter 2, laser fluorosensors are one of the best sensors for oil spill surveillance. Since the laser fluorosensor data can be processed and transferred in real-time due to the advancement in technology, laser fluorosensors can be useful for the development of real-time oil spill detection and decision support systems. This chapter describes the issues associated with processing laser fluorosensor data for oil spill detection and classification. A literature review of algorithms which are being used to process laser fluorosensor data is presented. SLEAF data is provided by Environment Canada for this research.

3.1 Oil Spill Detection using Laser Fluorosensors

Laser fluorosensor was first used for airborne surveillance in 1970. Most of the laser fluorosensors use laser for excitation in the ultraviolet wavelength range of 300 and 355 nm. These wavelengths are in some way a compromise as these can excite all types of oils with reasonably good efficiency. Shorter wavelengths are good for exciting light oils, but not appropriate for crude and heavy refined oils whereas larger wavelengths are appropriate for crude and heavy refined oils and not for light oils. Laser Environmental Airborne Fluorosensor (LEAF) was the early system developed by Barringer Research Limited for the Canadian Government. Now, the development work for laser fluorosensor in Canada is under the aegis of the Emergencies Science and Technology Division (ESTD) of Environment Canada. Currently, Environment Canada uses SLEAF for oil spill surveillance. SLEAF has a 308 nm XeCl excimer laser for excitation. The detector has 64 spectral channels (328-664 nm) and collects only laser induced fluorescence, thereby discarding most of the background solar radiation. The

fluorescence reference spectra have been collected in laboratory conditions using a telescope at a distance of 39 meters in such a way that it simulates the SLEAF operation at a distance of 300 meters. The raw output from SLEAF had been calibrated against few targets. This calibration is being used for recording fluorescence spectra in all SLEAF data collection processes. Hence the fluorescence spectra recorded during SLEAF data collection process denote relative intensity rather than absolute intensity. The scanner has the facility to operate in narrow or wide swath coverage which is 1/3 to 1/6 of the operating altitude (300-600 m). SLEAF has been tested successfully by Environment Canada in oil spill situations (Brown et al., 2004a and Brown et al., 2006b). The SLEAF data is used as laser fluorosensor data in this research. Some other prominent research centers working on laser fluorosensors are following:

- University of Oldenburg, Germany
- Ente per le Nuove tecnologie, l'Energia e l'Ambiente (ENEA), Italy
- Istituto di Ricerca sulle Onde Elettromagnetiche del Consiglio Nazionale delle Ricerche (IROE-CNR), France
- NASA Oceanographic LIDAR project, USA
- Laser Diagnostic Instruments AS, Estonia

Table 3.1 describes the technical specifications for various laser fluorosensors (Adapted from Brown and Fingas, 2003a).

Table 3.1: Technical Specifications for some Laser Fluorosensors

System	Excitation wavelength (nm)	Spectral Channels	Repetition rate (Hz)
LEAF, Canada	308	64	100
SLEAF, Canada	308	64	400
F-LIDAR IROE-2, France	308	512	Unknown
ENEA, Italy	308	1024	200
LFS, Germany	308	12	200

A thin oil film on the water surface is characterized by the broad fluorescence spectrum and the water Raman scattering signal. Some aromatic hydrocarbon compounds in petroleum oils absorb UV laser light to become electronically excited. The excitation is released through fluorescence emission by the compound mainly in the visible region. A multi-channel receiver is used to record the fluorescence spectrum (Brown and Fingas, 2003a). For practical purposes it may be sufficient to classify oil into heavy refined, medium crude and light refined oil. The reference fluorescence spectra for various oil types and background materials are collected by Environment Canada in laboratory conditions. It can be clearly observed that the fluorescence spectra of different oil types and background materials appear distinct from each other (Figure 3.1, 3.2 and 3.3). Light oils such as Diesel has its peak fluorescence emission in the UV region (Figure 3.1). Crude oils have large variation in their fluorescence spectra, but still appear distinguishable from other oil types (Figure 3.2). The peak fluorescence emission of crude oils lies in the visible range (410-500 nm) and the fluorescent emission from heavy

refined oils is considerably lower than others (Figure 3.3). Oil spills in coastal areas are damaging and difficult to detect. An oil spill in an open sea tends to reach the coastal regions due to various factors including wind and current. Possible background materials include water, sand and stone. Figure 3.4 shows the fluorescence spectra of background materials.

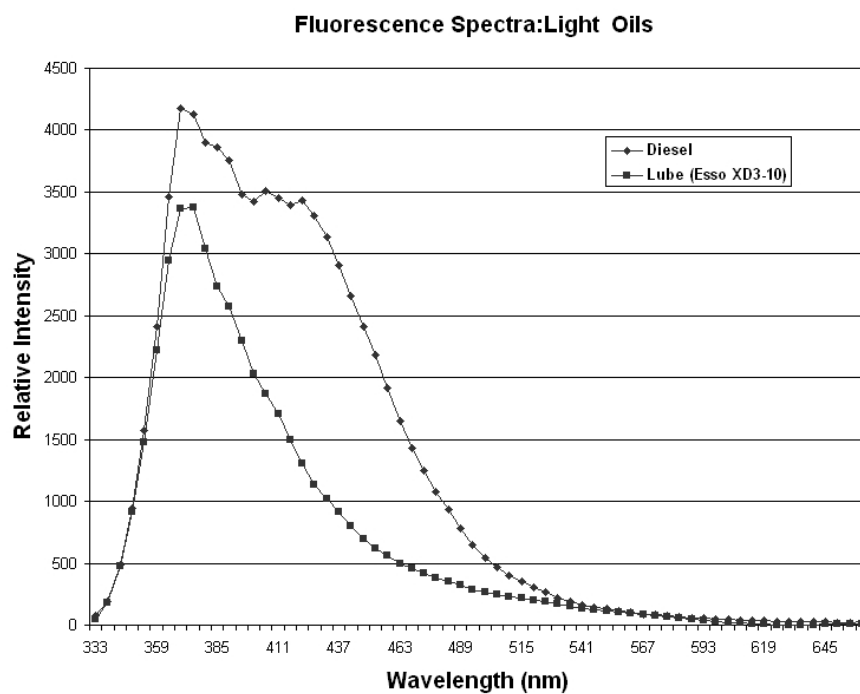


Figure 3.1: Fluorescence Spectra of Light Oils. Data Source: Environment Canada

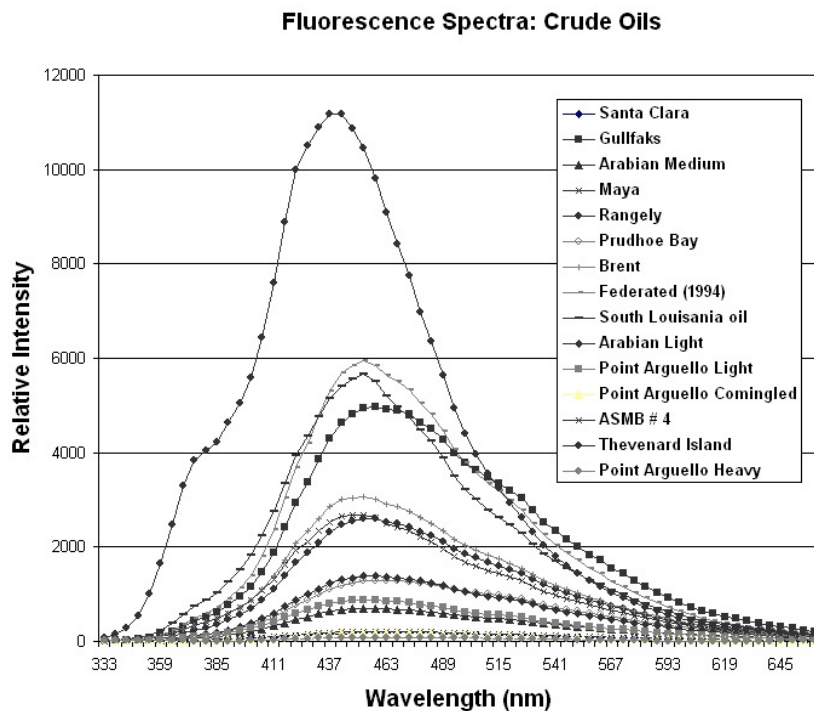


Figure 3.2 Fluorescence Spectra of Crude Oils (Data Source: Environment Canada)

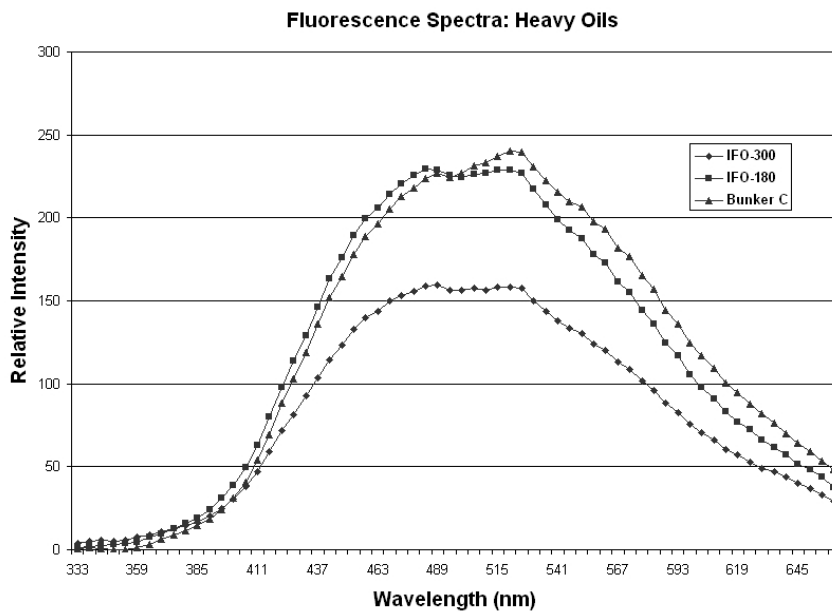


Figure 3.3: Fluorescence Spectra of Heavy Oils (Data Source: Environment Canada)

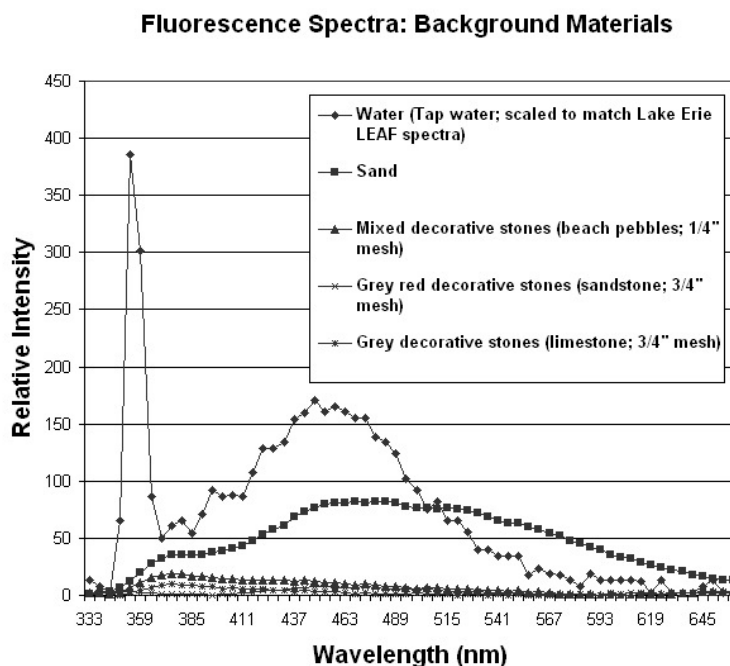


Figure 3.4: Fluorescence Spectra of Background Materials (Data Source: Environment Canada)

Light can be scattered due to an atom or molecule and most of the photon undergoes Rayleigh scattering in which scattered photons have the same energy as the incident photons. Nevertheless, few scattered photons have frequency lower or higher than the incident photon and this is called Raman scattering. The energy transfer between incident light and water molecules is known as water Raman scattering. The position of the water Raman scattering signal is governed by the excitation wavelength and the fluorescence emission (Grüner, 1991). Natural water contains yellow organic matter called gelbstoff and some amount of chlorophyll. The fluorescence response of natural water is shown in Figure 3.5.

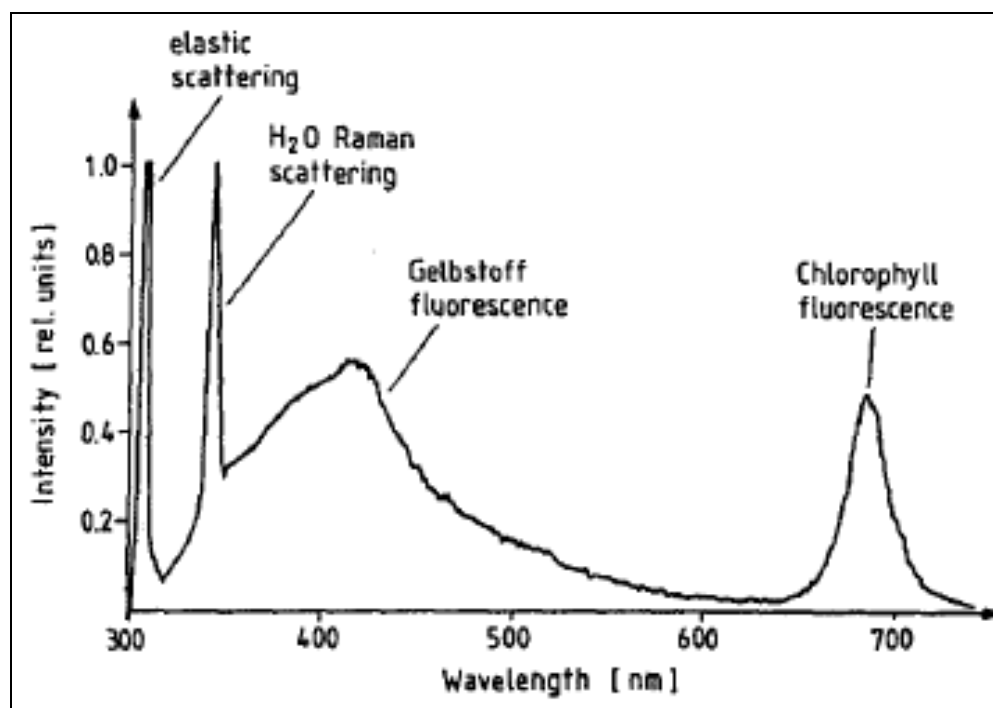


Figure 3.5: Fluorescence Spectra of Natural Water for Excitation Wavelength as 308 nm (Adapted from Grüner, 1991)

The oil film on the water suppresses the water Raman scattering signal corresponding to the absorption coefficient of the oil (Hoge and Swift, 1980). If the excitation wavelength is 308 nm (XeCl laser) then the water Raman scattering signal is observed at 344 nm. The water Raman scattering signal is useful for fluorescence calibration as well as for estimating oil thickness to some extent (Brown and Fingas, 2003a). To obtain the oil thickness from the Raman signal depression data, the following data must be known (Figure 3.6):

- (1) Seawater background fluorescence from organic materials
- (2) Oil fluorescence

The ratio of the Raman intensity measured above the oil slick and the Raman intensity measured outside the oil slick is a function of thickness d of the oil film and the

attenuation coefficient of the oil film. The attenuation coefficient of a material is its ability to reduce intensity of energy beam passing through it. The attenuation coefficient of the oil depends upon the oil type. The relation can be represented in Equation 3.1 (Hoge and Swift, 1980).

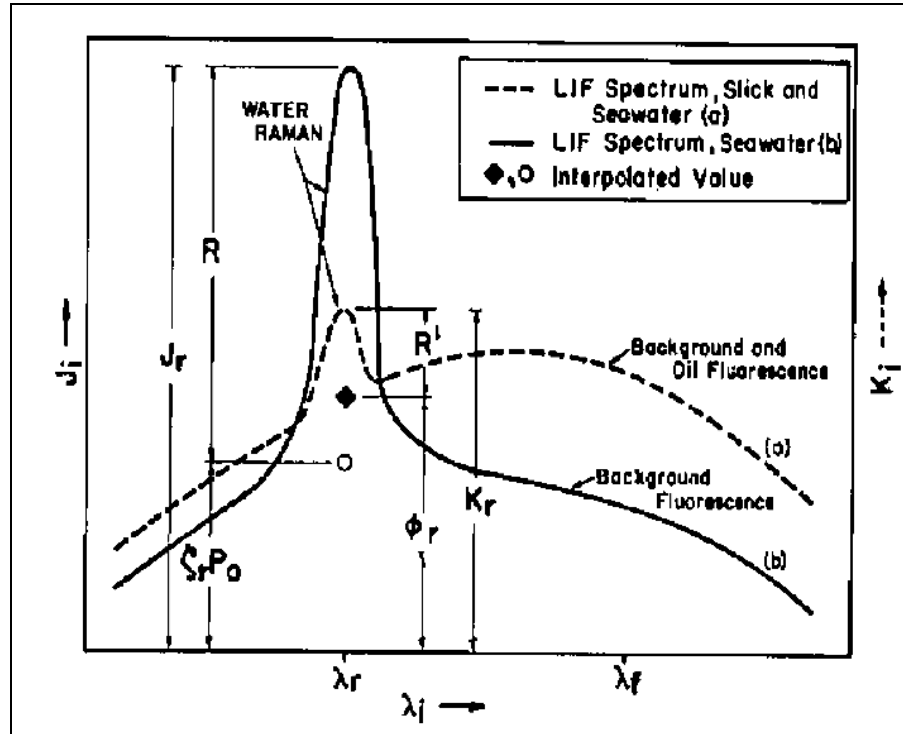


**Figure 3.6: Laser Induced Fluorescence (LIF) spectrum for Oil Slick and Sea Water
(Adapted from Hoge and Swift, 1980)**

$$d = -1/(k_e + k_r) \ln(R^*/R) \quad (3.1)$$

where d is the thickness of oil spill, R^* is the Raman Intensity measured above the oil slick, R is the Raman Intensity measured outside the oil slick in background water, k_e is the attenuation coefficient of oil at the excitation wavelength, k_r is the attenuation coefficient of oil at the Raman wavelength. Raman intensity is also used for correcting

the fluorescence signal for optical penetration depth in the water column. A fluorescence signal normalized by Raman intensity indicates the concentration of fluorescent substances. Laser fluorosensors cannot measure oil thickness greater than 10-20 microns as UV laser light is completely absorbed by oil and cannot reach the underlying water (Brown and Fingas, 2003b).

Various characteristics can be used for oil identification such as spectral shape, the fluorescence decay time, the position of the fluorescent peak, the fluorescence yield, the depression of water Raman scattering signal, and the variation of these parameters with the excitation wavelength (Quinn et al., 1994). Fluorescence yield is the total fluorescence emission for a given substance. The time at which the intensity becomes $1/e$ of the original value is known as Fluorescence decay time. Fluorescence decay time can be useful for the identification of oil in laboratory conditions, but its practical application may be limited by a variety of factors in the field (Camagni, 1991). When oil undergoes weathering due to environmental factors, its fluorescence properties also change. However, the spectral shape changes are not significant and oils can still be distinguished as light refined, crude and heavy refined oils (Jha et al., 2008b). The life time of the oil can be significantly affected by natural weathering and consequently the fluorescence decay time may not be able to classify weathered oil. The peak of the fluorescence return for crude oils is centered between 420-490 nm while the peak of the fluorescence return from chlorophyll is centered on 680 nm and hence the fluorescence emission from chlorophyll can be easily distinguished from that from oil (Patsayeva et al., 2000). The peak of fluorescence return from gelbstoff or yellow matter is centered on 420 nm and, hence it may be difficult to detect crude oils on water rich with gelbstoff. Gelbstoff can

be present in high amounts in coastal areas. However, the fluorescence return from oil is much larger in magnitude than water with high amount of CDOM and this can be useful in differentiating oil from the water (Dick and Fingas, 1992). Hence, if the fluorescence emission peak exceeds a threshold set for water then it can be used as the first indicator for the presence of oil. The fluorescence emission peak depends on the target distance, type of the oil, oil thickness and the amount of oil dispersed in water (Patsayeva et al., 2000).

3.2 Oil Spill Detection Methods and Algorithms

The primary goal in oil spill detection is to positively distinguish oil from the background, i.e. water, ice etc. Once oil is detected, it can be further classified into various oil types. Once classified, actions can be taken to respond to the oil spill and to model the oil spill drift and spreading. For example, light oil such as diesel evaporates quickly whereas the evaporation rate of heavy oil is slow and this information about oil type can help in knowing the fate and behaviour of oil spill with time. Fluorescence signatures of different materials are distinct and may serve as a primary feature for classification. The Pearson Correlation Coefficient is found to be a suitable statistical parameter for oil detection and classification (O'Neil et al., 1980; Dick et al., 1992). A sample can be classified as belonging to a petroleum product if the correlation of the sample exceeds a threshold level and is greater than its correlation with the background materials. Babichenko et al. (2004) observed how pollution led to a change in the spectral shape of the fluorescence spectra of the water and suggested using this asymmetry as the basis for oil pollution identification. Dick and Fingas (1992) have also suggested the use of skewness as an asymmetry parameter to determine relative ages of crude oils. Oil spill

detection and classification can also be carried out based on the ratio of values of the relative intensity of various spectral bands in the fluorescence spectra (Alaruri et al., 1995; Quinn et al., 1994). Quinn et al. (1994) note that the emission spectra obtained using a single excitation wavelength cannot be used to classify the oil into specific oil types but it can classify the oil into three broad categories: light refined, medium crude and heavy refined oil. Quinn et al. (1994) consider a number of parameters, including the spectral and temporal characteristics of the fluorescence spectra of the material and use Principal Component Analysis (PCA) to reduce the feature space (to a few significant PCs). PCA has been widely used for oil classification (James and Dick, 1996; Alaruri et al., 1995). For example, James and Dick (1996) discuss the advantages of using PCA over the Pearson Correlation Coefficient. They note that PCA involves less computation and can help in separating the mixed pixels, although it is assumed that materials are optically thick which can be valid for littoral oil spills but may not be applicable for open ocean spills. Moreover, they did not address the classification problems for dealing with in-situ data which may require more than simply adding Gaussian noise. The Pearson Correlation Coefficient and PCA have been widely used for oil spill detection and classification, and the theory is described below. The Pearson Correlation Coefficient (ρ) yields the quantitative value of the correspondence between observed and reference spectra (Equation 3.2).

$$\rho = \frac{N \sum_i X_i Y_i - \sum_i X_i \sum_i Y_i}{\sqrt{\left[N \sum_i X_i^2 - \left(\sum_i X_i \right)^2 \right]} \sqrt{\left[N \sum_i Y_i^2 - \left(\sum_i Y_i \right)^2 \right]}} \quad (3.2)$$

where X_i and Y_i are the intensity values for the i th spectral band in reference and observed spectra respectively and N is the number of spectral bands used in finding the correlation. A correlation value of +1 indicates perfect correlation; a value of 0 indicates no correlation; and a correlation value of -1 indicates perfect anti-correlation between the reference and observed spectra (O'Neil et al., 1980).

The PC transformation is a linear transformation which produces uncorrelated and noise segregated components. The data is transformed such that first few PCs have the most variances. Accordingly, later components can be ignored. The Principal Component Transformation (Y) may be expressed as in Equation 3.3.

$$Y = A^T X \quad (3.3)$$

where A is the matrix of eigenvectors which diagonalizes the covariance matrix Σ_x of original data (X) as expressed by Equations 3.4 and 3.5.

$$\Sigma_y = A^T \Sigma_x A \quad (3.4)$$

$$\Sigma_y = \begin{bmatrix} \lambda_1 & 0 & 0 & 0 & 0 \\ 0 & \lambda_2 & 0 & 0 & 0 \\ \cdot & 0 & \cdot & \cdot & \cdot \\ \cdot & \cdot & \cdot & \cdot & 0 \\ 0 & 0 & 0 & 0 & \lambda_N \end{bmatrix} \quad (3.5)$$

where $\lambda_1, \lambda_2, \dots, \lambda_N$ are the eigenvalues of the matrix Σ_x and $\lambda_1 > \lambda_2 > \dots > \lambda_N$. The choice of the matrix to find eigenvectors depends upon the application as second moment matrix and correlation matrix can also be used instead of covariance matrix Σ_x . Comprehensive details about PCA can be found in Jackson (1991).

Chapter Four: A Scheme for Oil spill Detection and Trajectory Modeling

The SLEAF data format is first described to support the following sections that present the processing schemes for the data. As per discussion in Chapter 3, some methods are reported in literature as suitable for oil spill detection and classification using laser fluorosensor data. In this thesis, the algorithm reliability has been tested using simulated oil spill data. The idea is to find the most effective approach for identifying and classifying oil from the simulated data. The appropriate approach can then be used to detect and classify oil based on real world SLEAF data. The SLEAF data must be geo-referenced to get spatial distribution of the oil spill. The procedure to geo-reference SLEAF data is explained. The oil spill trajectory modeling is important for devising appropriate response strategy and directing resources to the critical places, and hence the oil spill trajectory modeling tool is an integral part of an oil spill detection and decision support system. An oil spill trajectory model based on the CA technique has been developed for this work.

4.1 Description of Dataset

The data files for SLEAF consist of a repeating set of 128-sample blocks. The data format for a set of 128-sample block is specified below.

[altitude for the sample] \t [scan angle for the sample] \n

[shortest wavelength channel] \t [next channel] \t... \t [longest wavelength channel] \n

[altitude for the sample] \t [scan angle for the sample] \n

[shortest wavelength channel] \t [next channel] \t... \t [longest wavelength channel] \n

.

.

[altitude for the sample] \t [scan angle for the sample] \n
[shortest wavelength channel] \t [next channel] \t..... \t [longest wavelength channel] \n
[time of first sample] \t [latitude] \t [longitude] \t [heading] \t [pitch] \t [roll] \t [course
over ground] \t [ground speed] \n

The scan angle is given in degrees and the scanning pattern is elliptic with major axis along the flight direction (7.6 x 5.3 degrees). The sampling rate is 350 Hz. The minimum wavelength specified is 332.6 nm and the maximum wavelength is 662.8 nm. The last line for the block which contains time, latitude and longitude applies to the preceding 128-sample block. This sequence repeats until the *End of File*. “Time of first sample” applies to the first sample of the 128-sample block and remaining time references have been interpolated for the other samples.

4.2 Comparative Evaluation of Existing Methods for Oil Spill Detection

The reference laser fluorescence spectra for various petroleum products and background materials provided by Environment Canada are used. The summary statistics for various kinds of oils and background materials provide more insight into data characteristics (Table 4.1, 4.2, 4.3, 4.4). The summary statistics is generated using Microsoft excel for the reference laser fluorescence spectra data provided by Environment Canada. Sum denotes the summation of intensity values over all the bands and range denotes the difference between maximum and minimum intensity values for a given material. Skewness is the measure of symmetry of dataset. It is zero for normal distributions. If distribution has an asymmetric tail stretching towards more positive values then skewness is positive otherwise skewness is negative. Skewness is positive for light oils, crude oils and all background materials except sand whereas it is negative for

heavy oils. Kurtosis denotes the flatness of a distribution relative to a normal distribution. Kurtosis is positive for a relatively peaked distribution whereas it is negative for a relatively flat distribution (Rogerson, 2001). Heavy oils have their peak fluorescence values (maximum) relatively lower than other oils. Crude oils have huge variation in terms of statistical properties such as mean, maximum, sum, range and standard deviation. Though they have similar properties if skewness and kurtosis are considered as skewness is positive and kurtosis is negative for all these oils. The values of kurtosis for oils and background materials do not follow any specific pattern. Conclusively, these statistical properties are good for understanding data, but they do not provide any concrete features for oil spill identification and classification.

Table 4.1: Summary Statistics for Light Oils (Data Source: Environment Canada)

	<i>Diesel</i>	<i>Lube (Esso XD3-10)</i>
Mean	1246.87	648.88
Median	352.19	216.64
Standard Deviation	1479.19	929.32
Kurtosis	-1.02	2.00
Skewness	0.83	1.73
Range	4157.28	3369.39
Maximum	4178.79	3370.41
Sum	71071.52	36986.01

Table 4.2: Summary Statistics for Heavy Oils (Data Source: Environment Canada)

	IFO-300	IFO-180	Bunker C
Mean	93.86	132.61	137.65
Median	95.88	136.28	144.30
Standard Deviation	50.22	74.55	75.79
Kurtosis	-1.45	-1.46	-1.34
Skewness	-0.13	-0.12	-0.23
Range	149.11	220.03	233.61
Maximum	159.71	229.59	239.97
Sum	5349.82	7558.56	7845.77

Table 4.3: Summary Statistics for Some Crude Oils (Data Source: Environment Canada)

	Santa Clara	Gullfaks	Arabian Medium	Maya	Rangely
Mean	94.29	2202.82	335.88	105.74	1124.96
Median	88.63	1836.72	298.07	97.70	876.01
Standard Dev	54.52	1637.62	219.04	66.84	840.99
Kurtosis	-1.44	-1.33	-1.35	-1.43	-1.25
Skewness	0.18	0.40	0.30	0.20	0.45
Range	160.11	4753.68	650.42	195.75	2504.43
Maximum	177.83	4961.90	701.16	210.60	2612.02
Sum	5374.37	125560.71	19145.28	6027.06	64122.49

Table 4.4: Summary Statistics for Background Materials (Data Source: Environment Canada)

	Water	Sand	Beach Pebbles	Sandstone	Limestone
Mean	66.33	52.35	7.18	3.08	2.75
Median	55.40	53.21	6.06	2.45	1.63
Standard Deviation	55.42	22.20	5.61	2.21	2.65
Kurtosis	-1.13	-1.31	-1.06	-0.80	0.95
Skewness	0.51	-0.17	0.50	0.63	1.38
Range	168.97	68.97	18.68	7.22	9.75
Maximum	170.95	81.76	18.75	7.34	9.75
Sum	3780.56	2983.98	409.15	175.54	156.59

For each reference material, 20 simulated fluorescence spectra are generated by adding 10% white Gaussian noise to the reference fluorescence spectra. Some sample fluorescence spectra generated from the reference spectra of light oil are shown in Figure 4.1. As there are 25 reference materials, the total number of simulated fluorescence spectra is 500.

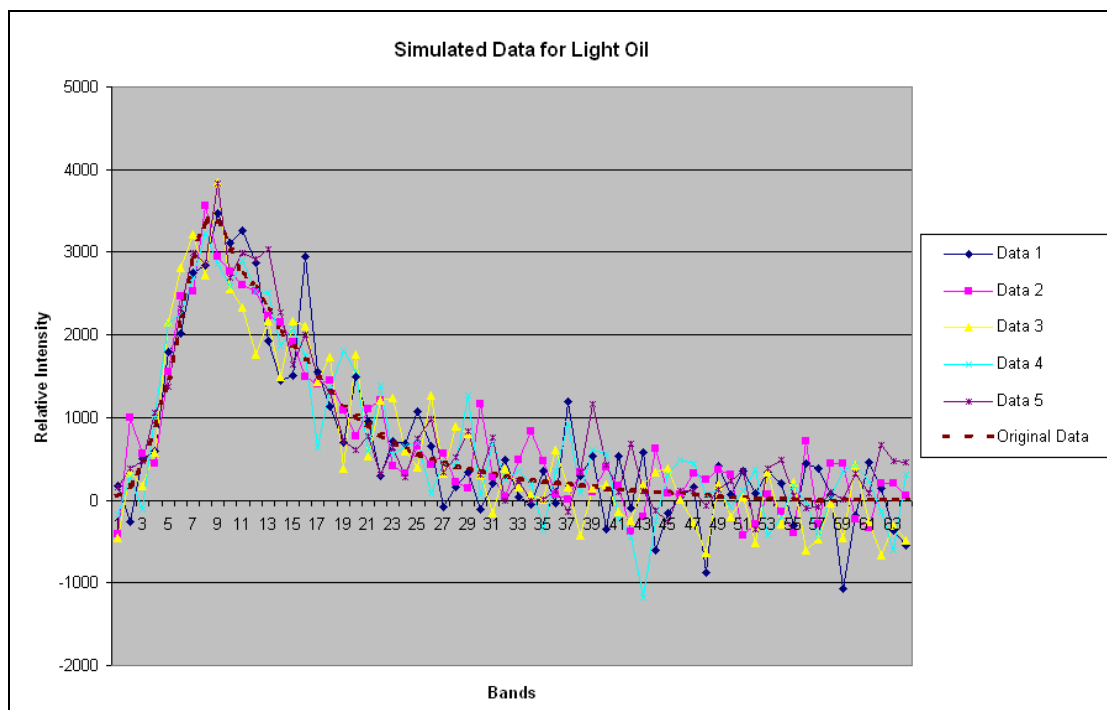


Figure 4.1: Sample Simulated Data Generated for Light Oil by adding 10% Gaussian Noise

The Raman scattering bands are not considered for the classification since this feature commonly occurs in fluorescence spectra over the water surface. The most general approach to classify and detect oil involves the determination of the spectral distance between the simulated and the reference spectra. The observed spectra can be labelled as that reference material for which this spectral distance is minimum. In the second approach, PCA is applied to the collection of the reference spectra and only those PCs which contribute significantly to the variance in the reference data are considered for creating the PC space. The oil classification is based on the spectral distance between the observed fluorescence spectra and the reference spectra in the PC space. The third approach is based on Pearson Correlation Coefficient for classifying and detecting oil. In the fourth approach, the ratios of the relative intensities in different spectral bands (for

each pair) are used as a distinguishing feature. When considering 58 spectral bands, the number of ratio combinations will be 1653 (${}^{58}C_2$), the idea therefore is to regard the distinguishing combinations as relevant. For this purpose, the variance-to-mean ratio (VMR) is calculated to find variability for each ratio combination for all the reference materials. The six ratio combinations with the highest VMR ratio were considered and then PCA was applied to find the only significant components. The spectral distance between observed and reference spectra was used as the basis for the classification in this newly formed PC space. A scheme has been developed for the classification of the observed SLEAF data based on the results of algorithms applied to simulated data.

The PCs for all the reference spectra were computed. The plot of eigenvalues depicting variance contained in their corresponding PCs is shown in Figure 4.2. Only the first three PCs contribute significantly to the data's variance and hence the classification is based on only these PCs. The PC loading plot explains the contribution of the original bands in forming the PCs. As mentioned earlier, the minimum wavelength for data acquisition is 332.6 nm and the maximum wavelength is 662.8 nm. There are 64 receiver channels to capture the fluorescence spectrum. This implies that the band 1 corresponds to the wavelength of 332.6 nm whereas the band 64 corresponds to the wavelength of 662.8 nm. The approximate difference between two consecutive bands is 5.2 nm. For the first PC, it can be observed that the contribution of bands increases with the band increase till the band 24 and then the contribution starts decreasing (Figure 4.3). The second and third PCs have more uniform contribution from all original bands than the first PC. The scatter plot for all reference materials in the PC space is shown in Figure 4.4. The light oils are shown in blue; the heavy oils are shown in green; the crude oils are shown in red,

the water is shown in cyan; the sand is shown in black and stone is shown in magenta. The used legend remains the same for Figure 4.5 and 4.7. The light oils and the crude oils are well separated from background materials, but the heavy oils seem closer to the background materials in the PC space. The identification of the heavy oil on the background materials can be problematic. The 2D scatter plot is then created to check the separability more closely in the PC space created by PC1 and PC2 (Figure 4.5). The reference materials are found to be well separated in the 2D space as well.

The six ratio components having the highest VMR were identified and PCA was applied to find the significant components. The plot of eigenvalues for the covariance matrix is determined for these six ratio components (Figure 4.6). It can be observed that only the first PC is significant. The 3D scatter plot for reference materials in PC space for the ratio components is shown in Figure 4.7. The reference materials are closely placed in this PC space except the heavy oils. Thus, the oil spill identification and classification results using this PC space can give incorrect results. Moreover, the technique based on the ratio components can be sensitive to noise in data. This can work well if the effect of noise is uniform over the whole fluorescence spectrum as in that case the ratios will not be affected. Ratio Components can be useful in case of real SLEAF data as this technique only considers the ratios of relative intensities in different bands and not the actual values of the relative intensities of the target materials. The classification results based on the simulated data using PCs for ratio components were not satisfactory. Accordingly, it was concluded that the ratio components are not a reliable feature for oil spill detection and classification. As previously mentioned, the classification process should successfully classify the oil into the following three broad categories: light refined, crude and heavy

refined oil. Hence, the results are categorized into specific and aggregate (broad) categories. The successful specific classification implies that a particular oil remains classified in the same category after adding 10% white Gaussian noise. The results of classification using the other algorithms with the simulated data are shown in Table 4.5. The background materials are successfully classified with 100% accuracy by all three approaches. All algorithms are highly successful in classifying oil into the three broad categories of light refined, crude and heavy refined oil with classification accuracy around 100%. This implies that all these three approaches can detect and classify oils into the broad categories even if the data is noisy. The classification accuracy for all three approaches in specific categories for light oils is 100%. The reference sample set of the light oils only consists of two oils namely “Diesel” and “Lube (Esso XD3-10) and specific classification into these two oils are possible by all three approaches. The classification accuracy for specific classification in case of the heavy oils is around 95% when General and PCA approach is used. On the other hand, classification accuracy is only 83% when Pearson Correlation Coefficient is used. Hence, General and PCA approach can be more reliable than Pearson Correlation Coefficient for classification into specific categories in case of the heavy oils. The classification accuracy for the classification into specific categories for the crude oils is around 90% when using General and PCA approach. The performance of Pearson Correlation Coefficient is the worst for specific oil classification among all the methods used. The results are particularly bad in case of classifying the crude oils into specific categories as the accuracy is only 42%. The low specific oil classification accuracy in case of crude oils when using Pearson Correlation Coefficient can be due to high correlation among the oils

belonging to crude oils. As it is sufficient to classify oils into broad categories for practical applications, all three approaches can be considered for developing a scheme for oil spill detection and classification. Though Pearson Correlation Coefficient can give erroneous results in case of classification into specific categories, it can be still considered as a good statistical parameter for oil spill detection and classification.

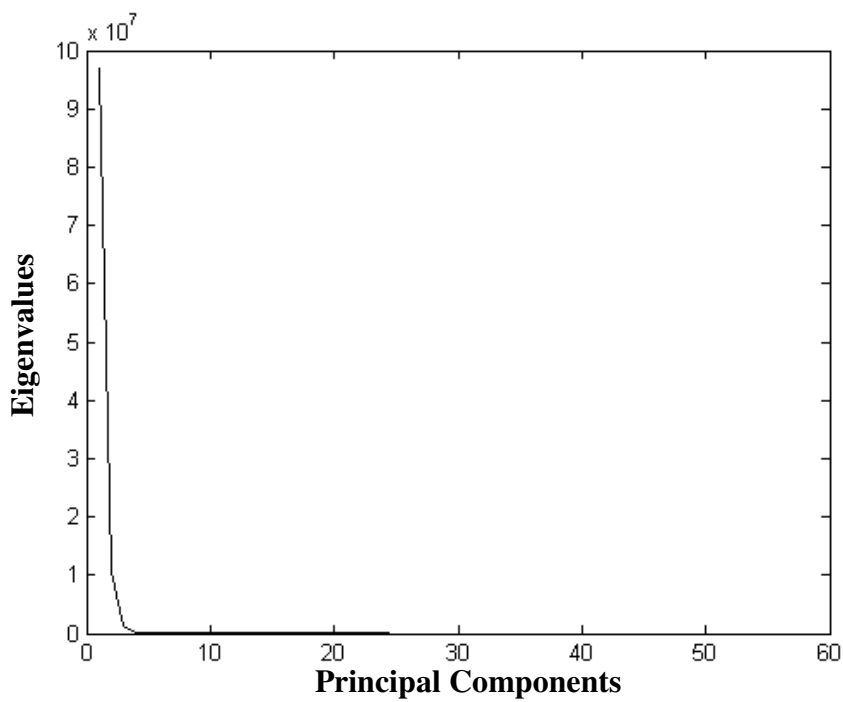


Figure 4.2: Eigenvalues for the PCs Computed for Reference Spectrum

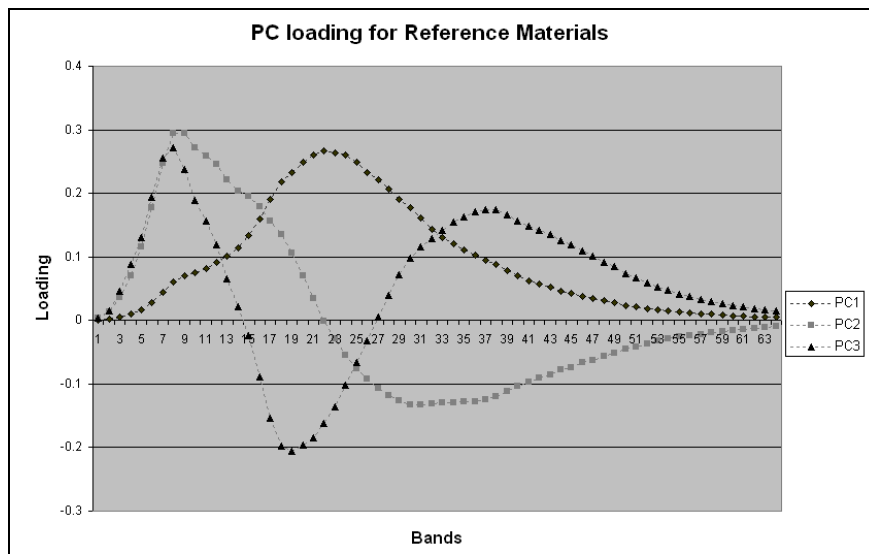


Figure 4.3: PC Loading for Reference Materials

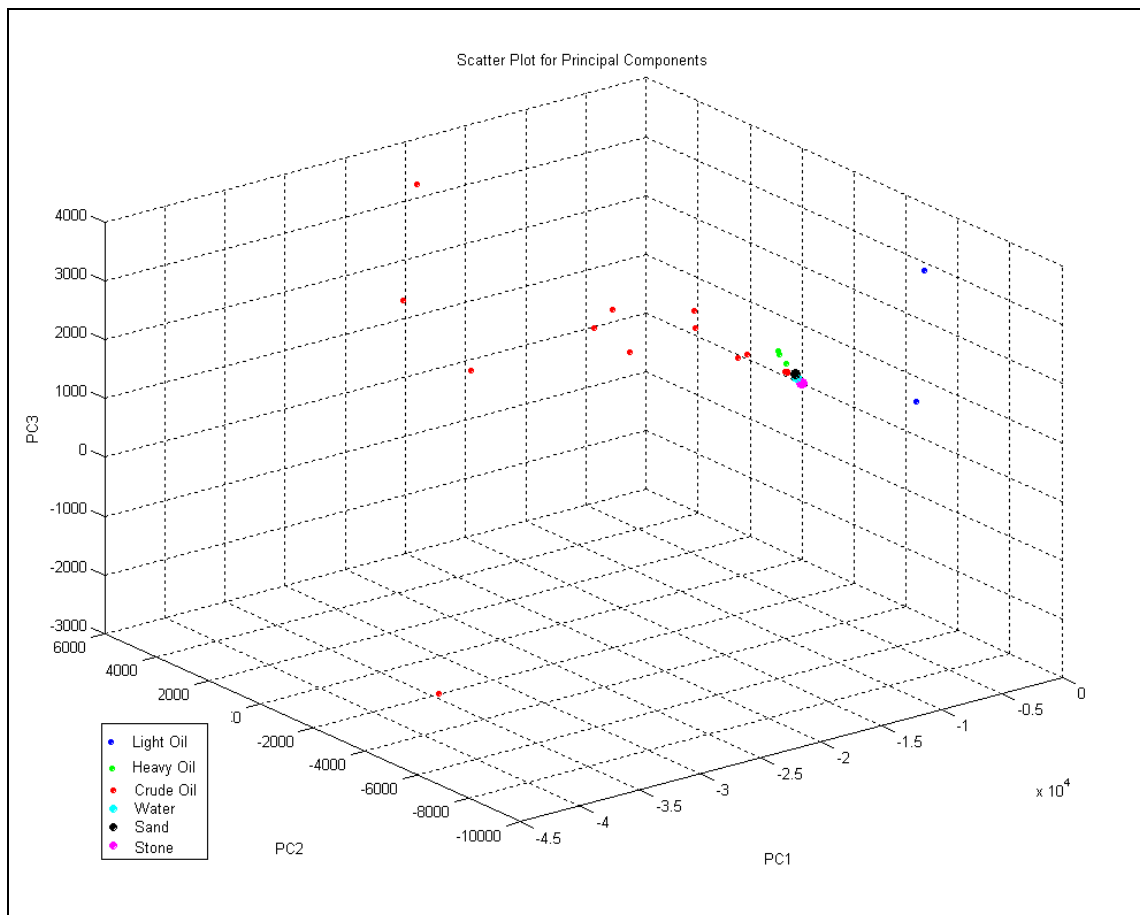


Figure 4.4: 3D Scatter Plot of Reference Materials in the PC Space

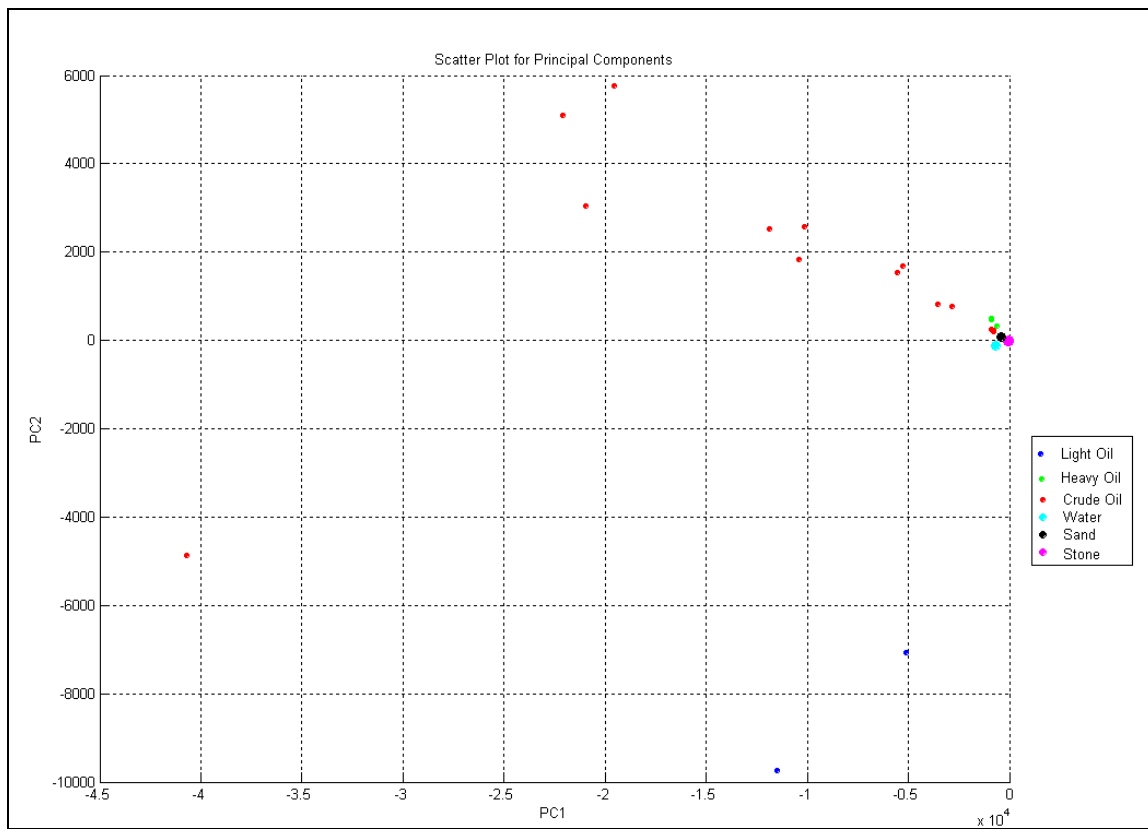


Figure 4.5: 2D Scatter Plot of Reference Materials in the PC Space (PC1 and PC2)

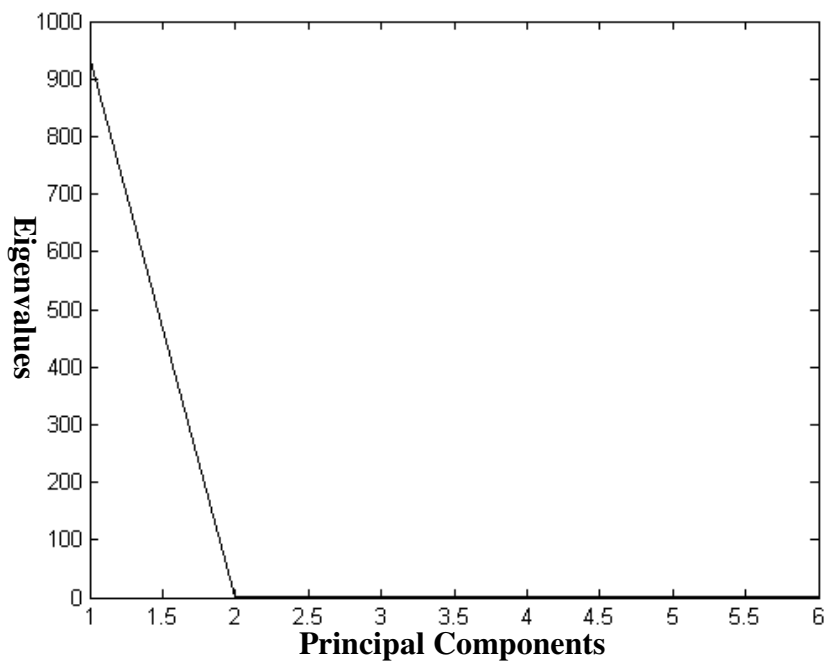


Figure 4.6: Eigenvalues for the PCs Computed for Ratio Components

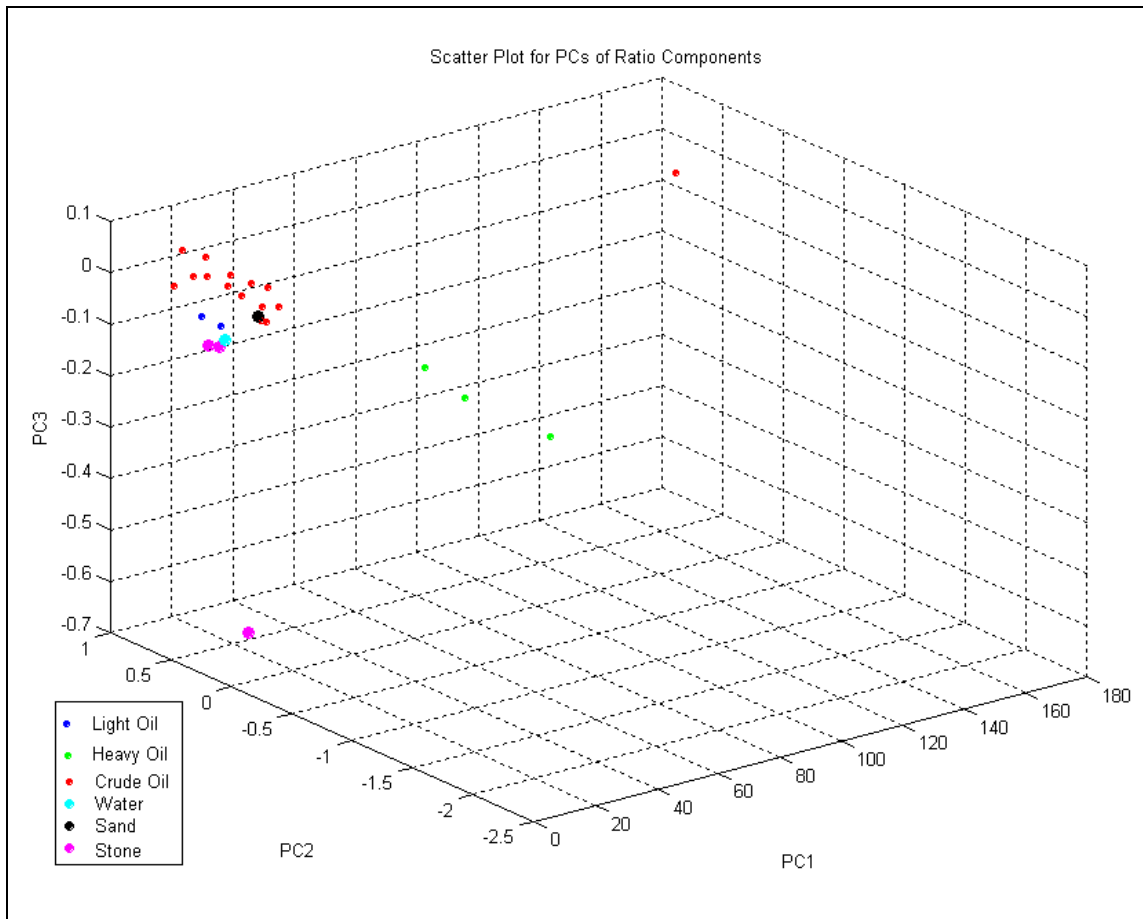


Figure 4.7: 3D Scatter Plot of Reference Materials in the PC Space for Ratio Components

Table 4.5: Classification Results using Various Algorithms for Simulated Data

Type		General (%)	PCA (%)	Correlation (%)
Light Oil	Broad	100	100	100
	Specific	100	100	100
Crude Oil	Broad	100	100	99.7
	Specific	90.7	90	42
Heavy Oil	Broad	100	100	100
	Specific	95.8	95	83.3
Water		100	100	100
Sand		100	100	100
Stone		100	100	100

4.3 A Proposed Oil Spill Detection and Classification Scheme

Oil's fluorescence emission depends on various factors such as the oil thickness, the distance from the target and atmospheric conditions. If PCA or General approach is used, the observed SELAF data has to be normalized so that it can be compared to the reference spectra collected in the laboratory (Almhdi, 2007). The data normalization is a difficult process as the information about the oil thickness, the distance from the target and atmospheric conditions are needed. It is difficult to model effect of these conditions on the fluorescence spectra. Moreover, these information are often not available in the field conditions. Classification of data using Pearson Correlation Correlation depends only on the shape of the fluorescence spectra and not the total fluorescence emission. Pearson Correlation Correlation is used to classify the data in the case of the actual

SLEAF data due to the erroneous nature of data normalization. Classification based on the correlation coefficient will not yield reliable results if high correlations between reference materials exist. Accordingly, it is imperative to investigate the correlation between various reference materials. The correlation map for different materials is shown in Figure 4.8. This correlation map is generated using MATLAB. Features 1-2 belong to light oil, features 3-5 belong to heavy oil, features 6-20 belong to crude oils, feature 21 is water and features 22-25 are other background materials. The oil spill detection and classification scheme is shown in Figure 4.9. High correlation between petroleum products and background materials is the primary challenge for accurate oil spill detection. If maximum correlation between reference and observed spectra is greater than threshold 'th0' then classification can be reliable otherwise the observed point can be labelled as 'unknown'. Light oils have a high correlation with the stones, but the fluorescence emission from stones are significantly lower than that from light oils and this can be a distinguishing factor (see Figure 3.1 and Figure 3.4). A threshold 'th1' can be selected. Heavy oils (IFO 180 and IFO 300) and some crude oils (e.g. Arabian Medium) have a high correlation with sand, but the fluorescence emission from sand is significantly lower than those for these oils (Figure 3.3 and Figure 3.4). A threshold (th2) of fluorescence emission may be used to distinguish sand from oils. If fluorescence emission of the observed material is greater than this threshold (th2) it may belong to heavy oils or some crude oils. As peak of fluorescence emission from crude oils are significantly higher than heavy oils a threshold 'th 3' can be chosen. Some crude oils such as Thevenard Island, ASMB#4 and South Louisiana Oil have a high correlation with the water. Marine oil spills can cause serious environmental degradation, and hence it is

important that a reliable mechanism is established to distinguish oil from the water. Compared to the fluorescence emissions of water, those from the correlated crude oils are high (Figure 3.2), and thus a threshold 'th4' can be set for the minimum peak fluorescence emission. If the peak fluorescence emission is less than this threshold, we consider it to be water. Oceanic water may contain gelbstoff and the amount of gelbstoff can be considerably high in coastal regions. The fluorescence emission from gelbstoff may also be high. The Raman suppression can be a useful parameter to assist in distinguishing the fluorescence spectra from oil and gelbstoff. Oil suppresses the water Raman scattering signal considerably in comparison to the gelbstoff and, therefore the ratio of the peak fluorescence emission and the water Raman scattering signal for oil will be much higher than that of water containing gelbstoff. An appropriate threshold 'th4' can be selected such that the material will be assumed to be oil if the ratio is higher than the threshold and as water otherwise. Selection of the values of the six thresholds indicated in the scheme i.e. th0, th1, th2, th3, th4 and th5 should be done with great care as this can affect the oil spill detection and classification results. The ground truth is required to get the appropriate values of these thresholds. The developed oil spill detection and classification scheme can be used for finding oil from the area where ground truth is available. The thresholds can be adjusted to get the correct results. This process can be repeated for other areas where ground truth is available to get the suitable values of these thresholds. The ground truth could not be obtained for this research and hence initial values of these thresholds are obtained by carefully analysing reference fluorescence spectra. These values are later adjusted based on the results obtained by applying developed oil spill detection and classification scheme on real world SLEAF

data and feedback from ESTD, Canada. The set of thresholds which are used for the oil spill detection and classification scheme in this research is shown in Table 4.6.

Table 4.6: Typical Values of Thresholds for Oil Spill Detection and Classification Scheme

Thresholds	th0	Th1	th2	th3	th4	th5
	0.9	200	130	250	500	3

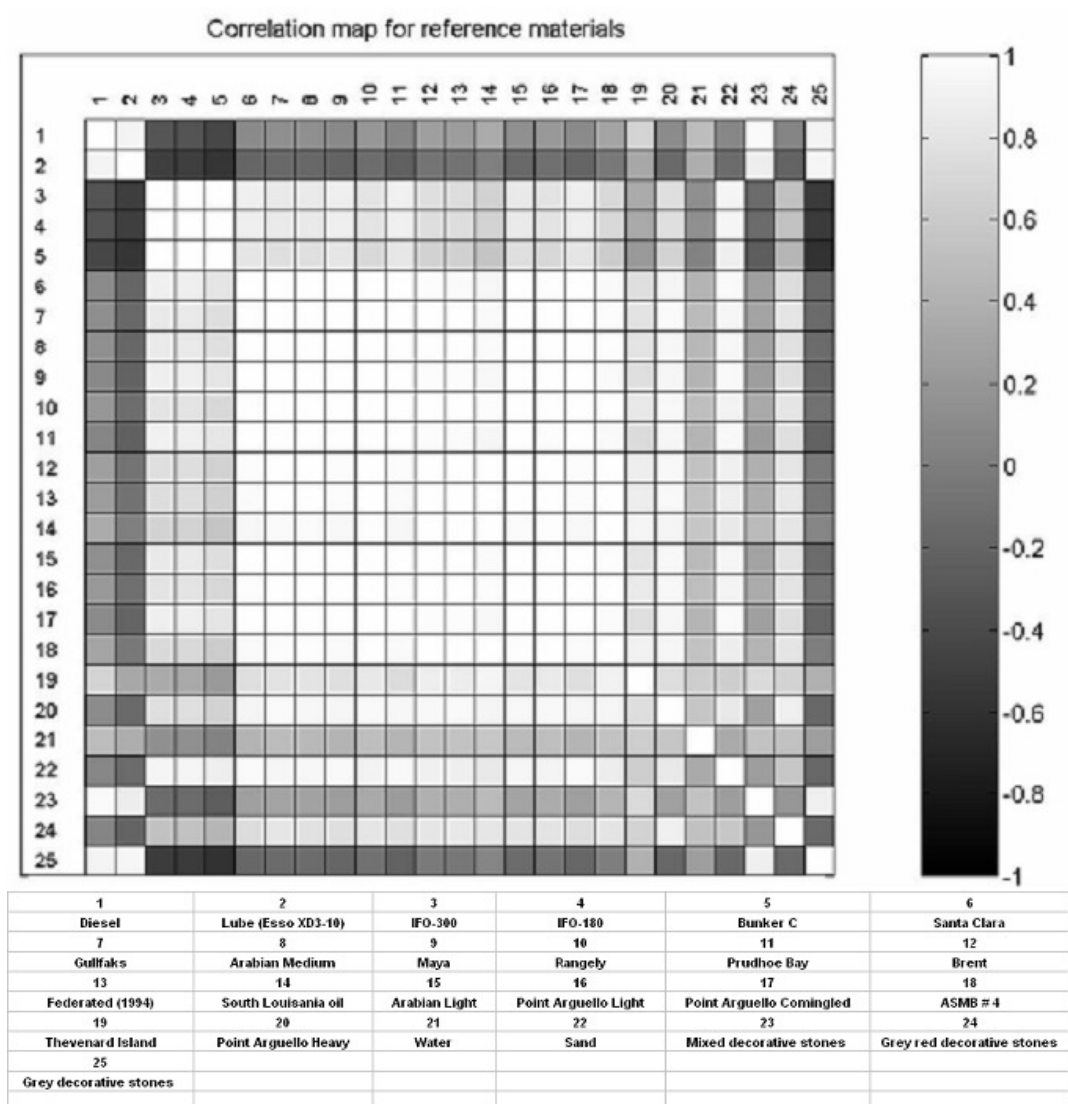


Figure 4.8: Correlation Map for Reference Fluorescence Spectra

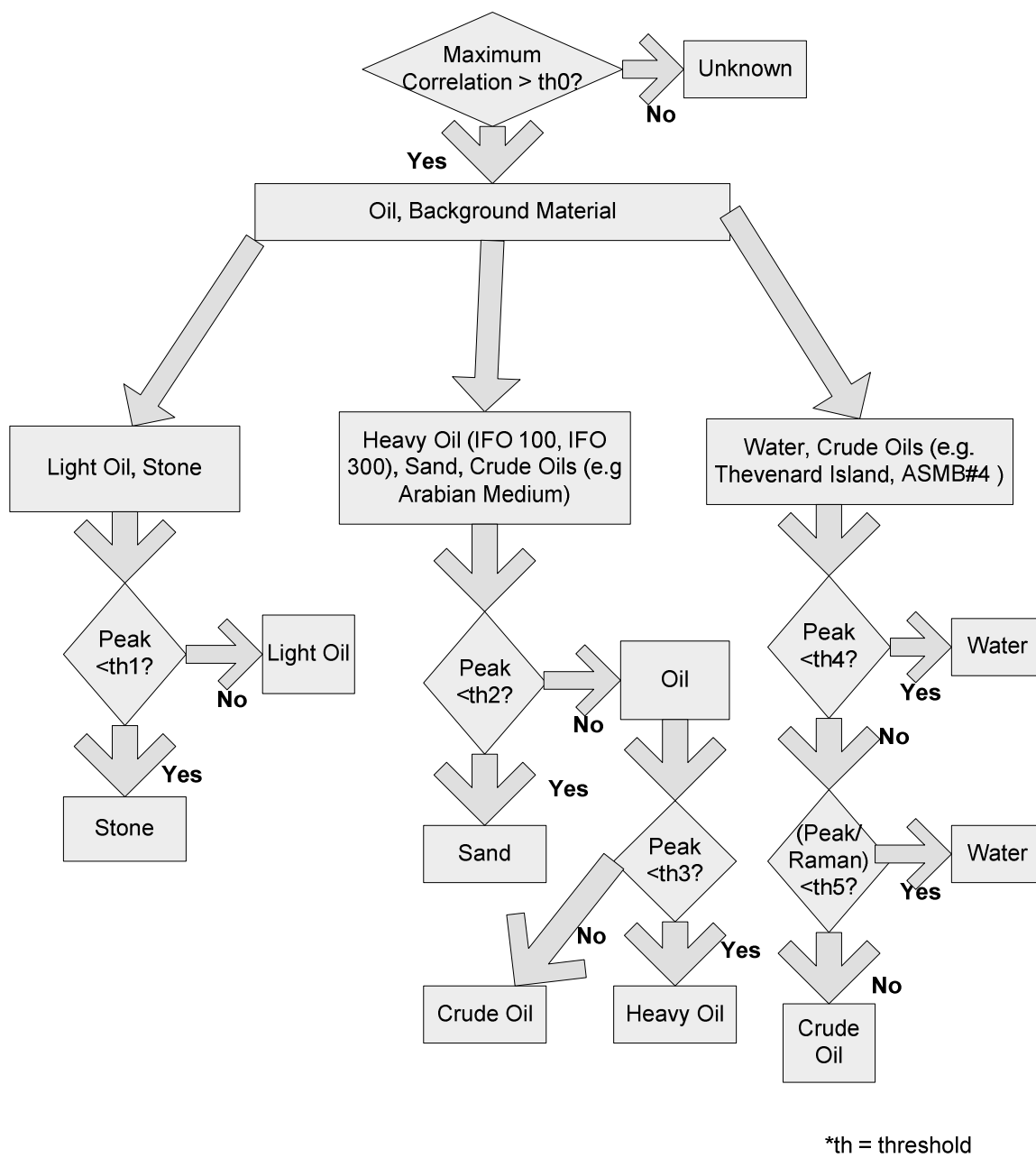


Figure 4.9: Scheme for Oil Spill Detection and Classification

4.4 Geo-referencing of SLEAF Data

The SLEAF data needs to be geo-referenced before it can be analyzed in a GIS system. The GPS/INS (Global Positioning System/Inertial Navigation System) onboard the aircraft provides latitude, longitude, altitude and attitude of the aircraft while collecting SLEAF data, in addition the scan angle for each laser pulse is also known. The SLEAF data is geo-referenced using the techniques of Light Detection and Ranging (LiDAR) geo-referencing. A detailed description of LiDAR geo-referencing techniques can be found in Wehr and Lohr (1999). The LiDAR geo-referencing method used in this research is based on the geo-referencing technique discussed by Habib et al. (2007). A software tool has been developed using C#.Net to automatically geo-reference and process the SLEAF data. The details about the software tool are provided in Chapter 6.

A typical LiDAR system consists of three major components: Global Navigation Satellite System (GNSS), Inertial Navigation System (INS) and a laser unit (Habib et al., 2007). There are four coordinate systems involved in geo-referencing process namely ground coordinate system, GNSS/INS coordinate system, laser unit coordinate system and laser beam coordinate system (Figure 4.10). The origin of GNSS/INS coordinate system is defined by the position of the phase center of the Antenna which is provided by GNSS. The INS provides attitude of the aircraft which is used to determine the orientation of the GNSS/INS coordinate system with respect to the Ground Coordinate System. Yaw, pitch and roll define the attitude of the aircraft. Yaw is rotation about the Z axis, pitch is the rotation about the X axis (across flight direction) and roll is the rotation about the Y (flight direction) axis. The rotation matrix R_{INS} is derived from yaw, pitch and roll and applied to the ground coordinate system for making it parallel to the laser

unit coordinate system. The procedure of deriving the rotation matrix can be found in detail in Habib (2009).

The laser unit has a laser scanner which measures distance to the ground points and scans angles. The origin of the laser unit coordinate system is at the laser firing point. The Y direction for the laser unit coordinate system is assumed to be in the flight direction and the X axis is considered across the flight direction. The Z direction is assumed to be in the vertical direction and perpendicular to the XY plane. The laser beam coordinate system share same origin as the laser unit coordinate system. The scan angles define the rotational offset between the laser unit coordinate system and the laser beam. There is spatial and rotational offset/boresighting between the GNSS/INS unit and the laser unit. The spatial offset between the GNSS/INS system and the laser unit can be denoted by a vector \vec{P}_G with respect to the GNSS/INS coordinate system. The rotational offset is the orientation of the laser unit with respect to the GNSS/INS system. The rotation matrix ΔR is applied to the GNSS/INS coordinate system for making it parallel to the laser unit coordinate system. R_{scan} is the rotation matrix derived using scan angles and it is applied to laser unit coordinate system to make it parallel to the laser beam coordinate system. The range vector $\vec{\rho}$ denotes the coordinates of target point in laser beam coordinate system.

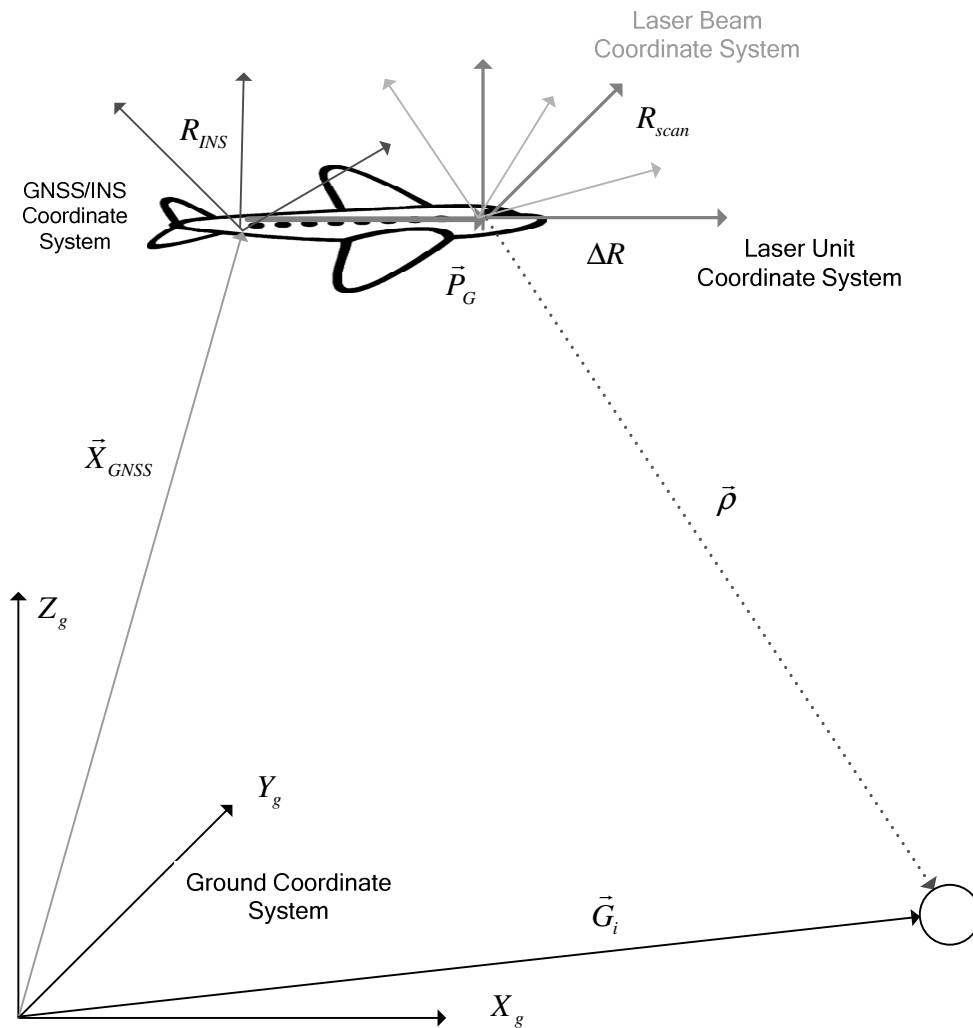


Figure 4.10: Components and Coordinate Systems for a Typical LiDAR System

\vec{X}_{GNSS} refers to ground coordinates of GNSS antenna phase centre and \vec{G}_i denotes desired ground coordinates of target point. The general equation for ground coordinates of target point can be expressed in terms of combination of three vectors ($\vec{X}_{GNSS}, \vec{P}_G, \vec{\rho}$) as defined in their respective coordinate system and rotation matrices as in Equation 4.1 (Habib et al., 2007).

$$\vec{G}_i = \begin{bmatrix} X_i \\ Y_i \\ Z_i \end{bmatrix} = \vec{X}_{GNSS} + R_{INS} \vec{P}_G + R_{INS} \Delta RR_{scan} \begin{bmatrix} 0 \\ 0 \\ -\rho \end{bmatrix} \quad (4.1)$$

The general Equation 4.1 can not be used for geo-referencing SLEAF data due to the limitation in the acquired SLEAF dataset. There is no range (ρ) information provided for SLEAF dataset. No information is provided in the dataset about spatial and rotational boresighting/offset. Considering that spatial accuracy is not so critical in this application, the effect of spatial and rotational boresighting/offset will be ignored. Thus, the GNSS/INS coordinate system will be identical to the laser unit coordinate system with respect to the ground coordinate system. (Figure 4.11).

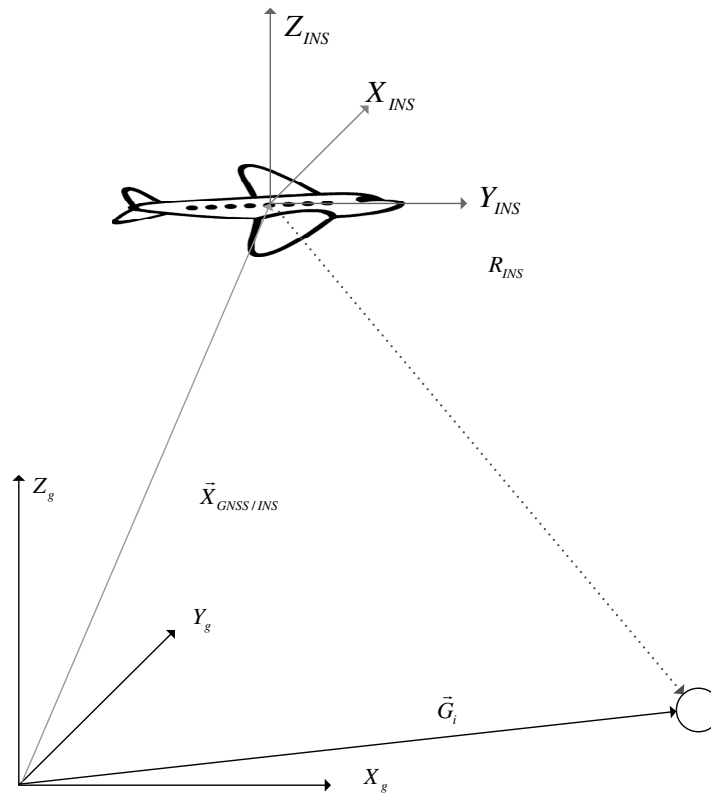


Figure 4.11: Coordinate Systems for SLEAF

As explained in section 4.1 for SLEAF dataset description, the dataset consists of repeating sets of 128-sample block. The position provided by the GNSS system \vec{X}_{GNSS} belongs to the first sample for that sample block, but the aircraft moves forward and a term \vec{P}_{speed} is added to \vec{X}_{GNSS} to compensate for the movement because of the speed of the aircraft. The position of the target in the laser unit coordinate system can be measured using scan angle θ_t at time 't' and total field of views α_T and β_T (Figure 4.12 and Figure 4.13). As SLEAF is used for detecting oil in ocean, we can assume that the surface for a given set of sample block has no significant variation in elevation from the reference. \vec{P}_{speed} and \vec{P}_{laser} are defined in the GNSS/INS coordinate system or laser unit coordinate system as in Equation 4.2 and Equation 4.3.

$$\vec{P}_{speed} = \begin{bmatrix} 0 \\ speed * time \\ 0 \end{bmatrix} \quad (4.2)$$

$$\vec{P}_{laser} = \begin{bmatrix} X \\ Y \\ -H \end{bmatrix} \quad (4.3)$$

where X , Y , $-H$ are the coordinates of target point observed in laser unit coordinate system. The position of the object in the ground coordinates system \vec{G}_i is a combination of three vectors $\vec{X}_{GNSS}^{t_0}$, \vec{P}_{speed} and \vec{P}_{laser} defined in the coordinate systems specified above (Equation 4.4).

$$\vec{G}_i = \begin{bmatrix} X_i \\ Y_i \\ Z_i \end{bmatrix} = \vec{X}_{GNSS}^{t_0} + R_{INS}^t * \vec{P}_{speed} + R_{INS}^t * \vec{P}_{laser} = \vec{X}_{GNSS}^{t_0} + R_{INS}^t \begin{bmatrix} 0 \\ V * \Delta t \\ 0 \end{bmatrix} + R_{INS}^t \begin{bmatrix} X \\ Y \\ -H \end{bmatrix}$$

$t = t_0 + \Delta t$

(4.4)

where,

\vec{G}_i : Ground coordinates of the object point under consideration

$\vec{X}_{GNSS}^{t_0}$: Ground coordinates of the GNSS antenna phase center at time t_0

\vec{P}_{speed} : Aircraft movement in GNSS/INS coordinate system in time Δt

\vec{P}_{laser} : The position of the target object in laser unit coordinate system.

$\vec{X}_{GNSS}^{t_0}$ is originally given in terms of latitude and longitude which must be transformed into a suitable projected coordinate system to facilitate further calculation. A projected coordinate system is based on a geographic coordinate system and locations are specified by x, and y coordinates in a grid (ArcGIS Desktop Help, 2009). Any projection system would introduce certain distortion. The conical projection system is suitable for mid-latitude region. The Lambert conformal conic projection is commonly used conical projection system for USA and Canada and has been used in this research. The latitude and longitude derived from the onboard GPS are projected into Lambert conformal conic projection and hence \vec{X}_{GNSS} denotes the transformed coordinates. R_{INS}^t can be derived by using the values of yaw, pitch and roll provided in the dataset. Altitude H is also provided in the dataset. The only problem is to derive expression for X and Y in terms of altitude of the aircraft, two total angular field of views (α_T and β_T) and scan angle θ_i at time t

(Figure 4.12). SLEAF uses an elliptical scanner to capture the data. A nutating mirror is part of the elliptical scanning system which is used to form elliptical footprints on the ground. α_T is the total angular field of view with respect to the flight direction, and β_T is the total angular field of view with respect to the across flight direction (Figure 4.12). As specified in the data description section of this chapter, values of α_T and β_T are 7.6 and 5.3 degrees respectively.

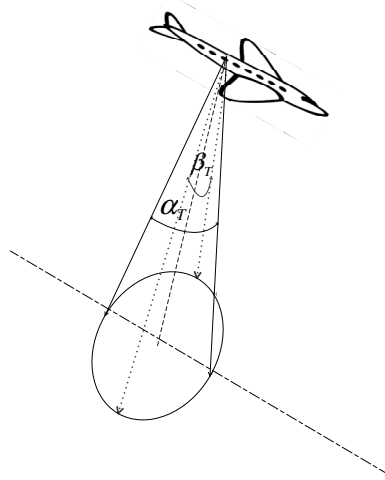


Figure 4.12: Angular Field of Views for Elliptical Scanner

The major axis is along the flight direction as specified in SLEAF data description. The equation of ellipse can be expressed by Equation 4.5.

$$\frac{x^2}{a^2} + \frac{y^2}{b^2} = 1 \quad (4.5)$$

where, 'a' is the semi-minor axis and 'b' is the semi-major axis of the ellipse. The relationship between the angular field of views α_T , β_T and a , b can be evaluated using principles of trigonometry as expressed by Equation 4.6 if altitude of aircraft is assumed as l .

$$\begin{aligned} a &= \tan(\beta_T / 2) \\ b &= \tan(\alpha_T / 2) \end{aligned} \quad (4.6)$$

Putting values of a and b in Equation 4.5, we get Equation 4.7 (Habib et al., 2007).

$$\frac{x^2}{\tan^2(\beta_T / 2)} + \frac{y^2}{\tan^2(\alpha_T / 2)} = 1 \quad (4.7)$$

A typical laser foot print at time ' t ' can be represented as in Figure 4.13. x_t and y_t are the position of target point with respect to the laser unit coordinate system. x_t and y_t can be expressed in term of scan angle θ_t and r_t as follows

$$\begin{aligned} x_t &= r_t \cos \theta_t \\ y_t &= r_t \sin \theta_t \end{aligned} \quad (4.8)$$

Now, (x_t, y_t) point lies on the ellipse and will satisfy Equation 4.5. Equation 4.9 can be obtained by substituting x and y with x_t and y_t in Equation 4.7.

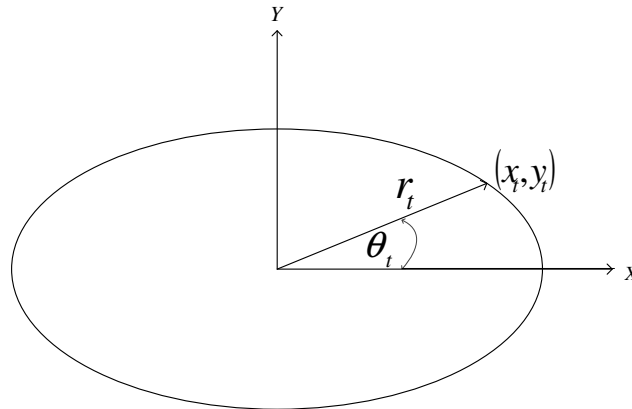


Figure 4.13: Angular Position of a Point in Elliptical Footprint

$$\frac{r_t^2 \cos^2 \theta_t}{\tan^2(\beta_T / 2)} + \frac{r_t^2 \sin^2 \theta_t}{\tan^2(\alpha_T / 2)} = 1 \quad (4.9)$$

After solving Equation 4.9, the radius r_i can be given as in Equation 4.10 (Habib et al., 2007).

$$r_i = \frac{\tan(\beta_T / 2) \tan(\alpha_T / 2)}{\sqrt{\cos^2 \theta_i \tan^2(\alpha_T / 2) + \sin^2 \theta_i \tan^2(\beta_T / 2)}} \quad (4.10)$$

The values of (x_i, y_i) can be obtained from Equation 4.8. Now if the altitude of aircraft is H , X and Y for Equation 4.3 can be obtained as follows (Equation 4.11 and Equation 4.12).

$$X = x_i * H \quad (4.11)$$

$$Y = y_i * H \quad (4.12)$$

The ground coordinates of target points can now be estimated using Equation 4.4.

As described earlier, the SLEAF data set is composed of sets of 128-samples. Each sample consists of two lines. The first line of each sample contains altitude, scan angle; these values are stored in an Array say 'dataArray'. The second line contains fluorescence spectra for that sample. The scheme developed for oil spill detection and identification is used for assigning material type to that sample. This information is stored as feature type 'dataArray'. This 'dataArray' is added to an arraylist say 'data'. This process is repeated till we reach 128th sample or 256th line in the SLEAF text file. Now, we have scan angle, altitude and feature type stored for each sample as 'dataArray' in the arraylist 'data'. At the 257th line for the set of 128-samples, the latitude, longitude, attitude and speed are provided corresponding to the first sample. Based on the geo-referencing process discussed here, the ground coordinates of each 128-samples is

obtained and stored. The whole process is repeated for all set of 128-samples in the SLEAF data file until we reach the end of file.

4.5 Oil Spill Trajectory Modeling using Cellular Automata

CA is made up of identical n-dimensional cells. The value of the physical quantity under consideration at a cell denotes the local state of that cell. The interactions between cells are assumed to be local and the neighbourhood of a cell is defined by adjacent and diagonal cells. The state at a particular cell is calculated from states of neighbouring cells and the state of that cell in previous time step based on a CA local rule, which is typically the same for all cells in the CA. A two dimensional CA can have four bordering cells (von Neumann neighbourhood) or eight bordering cells (Moore neighbourhood) as shown in Figure 4.14 and 4.15 respectively.

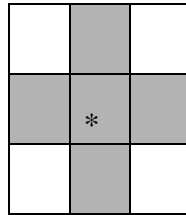


Figure 4.14: The Von Neumann Neighborhood

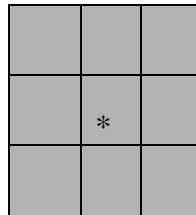


Figure 4.15: The Moore Neighborhood

If Moore neighbourhood is considered, the cell state $C_{i,j}^{t+1}$ at time $t+1$ can be defined as function of eight neighbourhood cells as in Equation 4.13.

$$C_{i,j}^{t+1} = F(C_{i-1,j-1}^t, C_{i-1,j}^t, C_{i-1,j+1}^t, C_{i,j-1}^t, C_{i,j}^t, C_{i,j+1}^t, C_{i+1,j-1}^t, C_{i+1,j}^t, C_{i+1,j+1}^t) \quad (4.13)$$

where, $C_{i,j}^t$ and $C_{i,j}^{t+1}$ are the states of the (i, j) cell at time steps t and $t+1$, respectively.

There are various processes involved in oil spill modeling, but only drifting, spreading and evaporation are considered in this thesis. The area of interest for simulating the oil spill is divided into a matrix of uniform square cells. Each square cell represents a CA cell and has many physical properties associated with it. The mass of oil in a cell at a time step is denoted by $M_{i,j}^t$ and its value in next time step $t+1$ is dependent on various factors such as the mass of oil in neighbouring cells, wind speed, and current speed. The state of the cell (i, j) at time t , $C_{i,j}^t$ can be expressed by Equation 4.14.

$$C_{i,j}^t = \{LF, M_{i,j}^t, CD_{i,j}^t, CV_{i,j}^t, WD_{i,j}^t, WV_{i,j}^t\} \quad (4.14)$$

LF indicates land or water areas. $CD_{i,j}^t$ and $WD_{i,j}^t$ denote the current direction and wind direction whereas $CV_{i,j}^t$ and $WV_{i,j}^t$ indicate current speed and wind speed respectively. Given the mass distribution of oil, wind speed and direction, current speed and direction, the geography at time step t , the task is to find the mass distribution at next time step $t+1$. The neighbourhood of cell (i, j) and cell masses at time step t is shown in Figure 4.16.

$M_{i-1,j-1}^t$	$M_{i-1,j}^t$	$M_{i-1,j+1}^t$
$M_{i,j-1}^t$	$M_{i,j}^t$	$M_{i,j+1}^t$
$M_{i+1,j-1}^t$	$M_{i+1,j}^t$	$M_{i+1,j+1}^t$

Figure 4.16: Oil Masses in Neighbourhood of Cell (i,j) at Time t

The oil mass gradient among two cells is the main driving force for oil mass transport and is directly proportional to the mass difference between the cells as a first

order approximation. For example, the oil mass at cell (i, j) due to oil mass in cell $(i-1, j)$ can be given as in Equation 4.15.

$$M_{i,j}^{t+1} = M_{i,j}^t + m(M_{i-1,j}^t - M_{i,j}^t) \quad (4.15)$$

where, m is a constant and governs the portion of the mass difference transferred to the neighbouring cell. The mass transport between diagonal cell will be less than the mass transport between adjacent cells and it can be modeled by introducing an additional diagonal factor ' d '. Therefore, considering all eight neighbouring cells $M_{i,j}^{t+1}$ can be given by Equation 4.16 (Karafyllidis, 1997).

$$\begin{aligned} M_{i,j}^{t+1} = & M_{i,j}^t + m(M_{i-1,j}^t - M_{i,j}^t) + m(M_{i,j-1}^t - M_{i,j}^t) + m(M_{i,j+1}^t - M_{i,j}^t) \\ & + m(M_{i+1,j}^t - M_{i,j}^t) + md(M_{i-1,j-1}^t - M_{i,j}^t) + md(M_{i-1,j+1}^t - M_{i,j}^t) + \\ & md(M_{i+1,j-1}^t - M_{i,j}^t) + md(M_{i+1,j+1}^t - M_{i,j}^t) \end{aligned} \quad (4.16)$$

No oil transport between cells is possible if a neighbouring cell represents a land. The 'LF' flag for a cell indicates whether a cell represents land or not. An additional term to take care of evaporation can be added (Equation 4.17), where T^t is the temperature of environment, t_m is the model time step and p is a constant (Karafyllidis, 1997).

$$\begin{aligned} M_{i,j}^{t+1} = & M_{i,j}^t + m(M_{i-1,j}^t - M_{i,j}^t) + m(M_{i,j-1}^t - M_{i,j}^t) + m(M_{i,j+1}^t - M_{i,j}^t) \\ & + m(M_{i+1,j}^t - M_{i,j}^t) + md(M_{i-1,j-1}^t - M_{i,j}^t) + md(M_{i-1,j+1}^t - M_{i,j}^t) + \\ & md(M_{i+1,j-1}^t - M_{i,j}^t) + md(M_{i+1,j+1}^t - M_{i,j}^t) - pt_m T^t \end{aligned} \quad (4.17)$$

Direction coefficients are defined to take wind and current effects into consideration. For example, direction coefficient for south direction can be represented as in Equation 4.18 (Karafyllidis, 1997).

$$\begin{aligned}
S_{i,j}^t &= S_{w_{i,j}^t} + S_{c_{i,j}^t} \\
\left| S_{c_{i,j}^t} \right| &= \frac{CV_{i,j}^t}{CV_{\max}} \\
\left| S_{w_{i,j}^t} \right| &= R \frac{WV_{i,j}^t}{WV_{\max}}
\end{aligned} \tag{4.18}$$

$S_{w_{i,j}^t}$ is called wind direction constant and $S_{c_{i,j}^t}$ is called current direction constant. $WV_{i,j}^t$ and $CV_{i,j}^t$ are wind and current speeds in the cell (i, j) at time step t . R is wind-current transformation factor and used to transform wind speed to wind-driven current speed. Typical values of R lie between 0.03 to 0.16. WV_{\max} and CV_{\max} are the maximum wind and current speed in that area. The final equation considering all the factors can be written as expressed by Equation 4.19 (Karafyllidis, 1997).

$$\begin{aligned}
M_{i,j}^{t+1} &= M_{i,j}^t + m((1 + N_{i,j}^t)M_{i-1,j}^t - M_{i,j}^t) + m((1 + W_{i,j}^t)M_{i,j-1}^t - M_{i,j}^t) + \\
& m((1 + E_{i,j}^t)M_{i,j+1}^t - M_{i,j}^t) + m((1 + S_{i,j}^t)M_{i+1,j}^t - M_{i,j}^t) + md((1 + NW_{i,j}^t)M_{i-1,j-1}^t - M_{i,j}^t) \\
& + md((1 + NE_{i,j}^t)M_{i-1,j+1}^t - M_{i,j}^t) + md((1 + SW_{i,j}^t)M_{i+1,j-1}^t - M_{i,j}^t) + \\
& md((1 + SE_{i,j}^t)M_{i+1,j+1}^t - M_{i,j}^t) - pt_m T^t
\end{aligned} \tag{4.19}$$

The value of m and d for the time step of 30 minutes was found to be 0.0014 and 0.18 respectively (Karafyllidis, 1997).

Chapter Five: Results and Discussion

The methodology for oil spill detection and classification was discussed in Chapter 4. Many existing algorithms used for oil spill detection and classification may work well for simulated data with additive noise, but they have been found to be ineffective for real world data, which can be attributed to a number of reasons. The fluorescence emission captured in the actual data acquisition process may get affected by various factors including the distance of the sensor from the target and oil thickness. SLEAF data from 2004 and 2006 Environment Canada flights are used for testing methods for oil spill detection. The data collected in 2004 was acquired on the east coast of Canada and the data collected in 2006 is from the area around Vancouver Island. Figure 5.1 shows the location of the study area. These data were collected by Environment Canada to check for illegal oil discharges in the ocean. As laser fluorosensors can detect even the sheen of oil from the background materials, SLEAF data is expected to detect even small traces of any small oil discharge. Data collection and the methods have been elaborated in Brown et al. (2004a) and Brown et al. (2006b). The identification of oil in coastal areas can be challenging due to various factors such as the presence of large amounts of suspended materials and the lower depth of the water column.

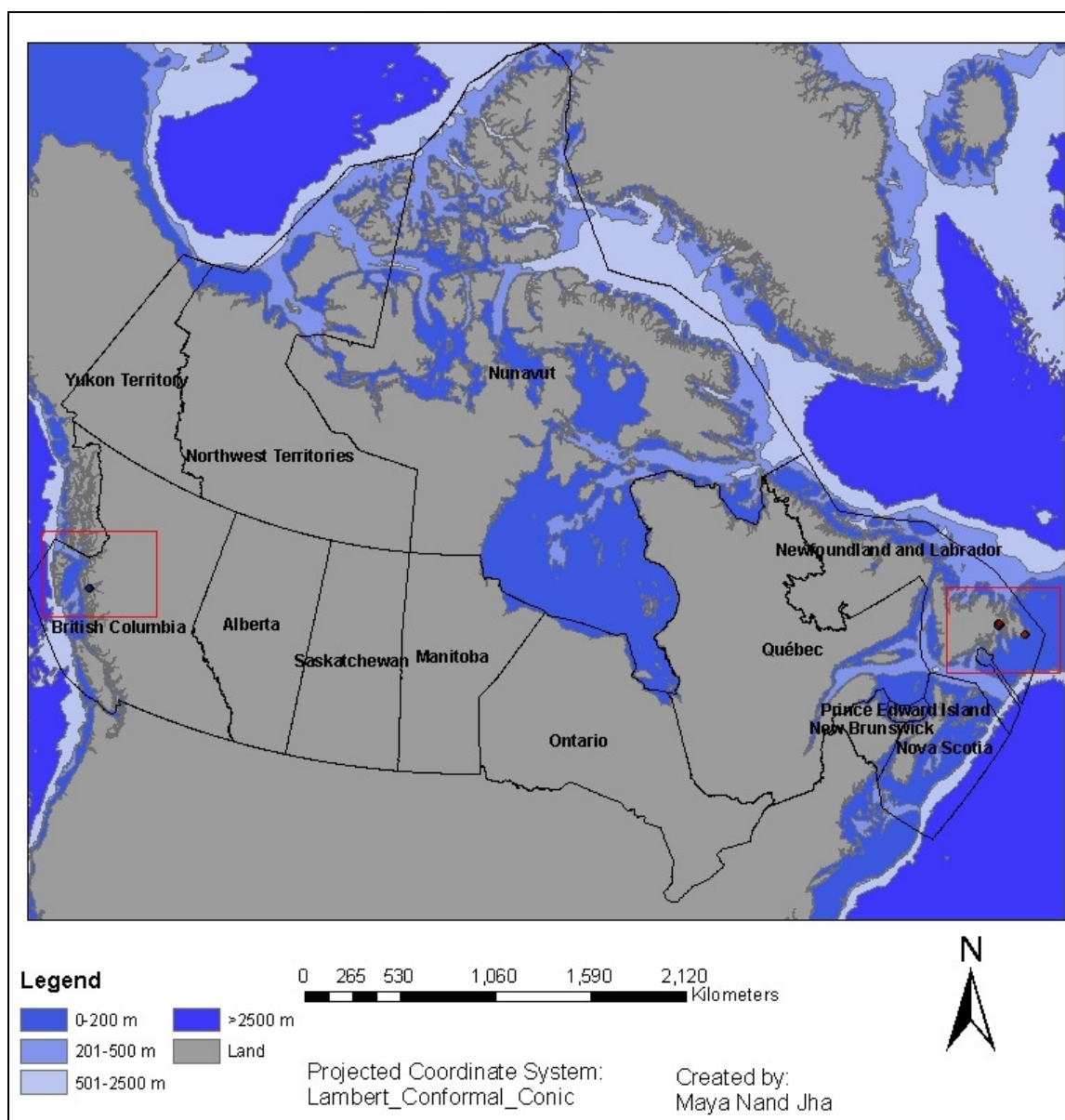


Figure 5.1: Study Area Displaying Locations of SLEAF Test Flights Conducted by Environment Canada

5.1 Results of using Proposed Scheme on SLEAF Data

The simulated data was classified according to the proposed scheme and 100% classification accuracy was achieved (for broad classification). The scheme was then employed for oil spill detection and classification from the real world data. The program generates a report in 'text' file format which summarizes the results of the analysis. The

sample from the 'text' file is provided below. The results are saved in a personal geodatabase which also facilitates further GIS analysis.

X: -2104601.22966204, Y: 2043406.30789842 Max Correlation is: 0.983976865895914 This spectra belongs to Material 0 Diesel
X: -2104601.41274777, Y: 2043406.28800501 Max Correlation is: 0.974989134340548 This spectra belongs to Material 0 Diesel
X: -2104601.59583349, Y: 2043406.2681116 Max Correlation is: 0.971220277558307 This spectra belongs to Material 0 Diesel
X: -2104601.77891921, Y: 2043406.24821819 Max Correlation is: 0.956692802038031 This spectra belongs to Material 20 Water
X: -2104601.96200493, Y: 2043406.22832478 Max Correlation is: 0.971905956257307 This spectra belongs to Material 20 Water
X: -2104602.14509066, Y: 2043406.20843137 Max Correlation is: 0.957579084095699 This spectra belongs to Material 20 Water
X: -2104602.32817638, Y: 2043406.18853796 Max Correlation is: 0.951878238195994 This spectra belongs to Material 20 Water

Light oil slick (diesel) is detected in the area around Vancouver Island which is consistent with Environment Canada observations. Observed fluorescence spectra containing thick and thin oil films are shown in Figure 5.2 and Figure 5.3, respectively. The spectra showing water rich with gelbstoff and turbid water are shown in Figure 5.4 and Figure 5.5, respectively. The oil was not found in the SLEAF Canadian east coast data. East coast regions contain high doses of gelbstoff as evident from the high fluorescence emissions of water in that area (Figure 5.6).

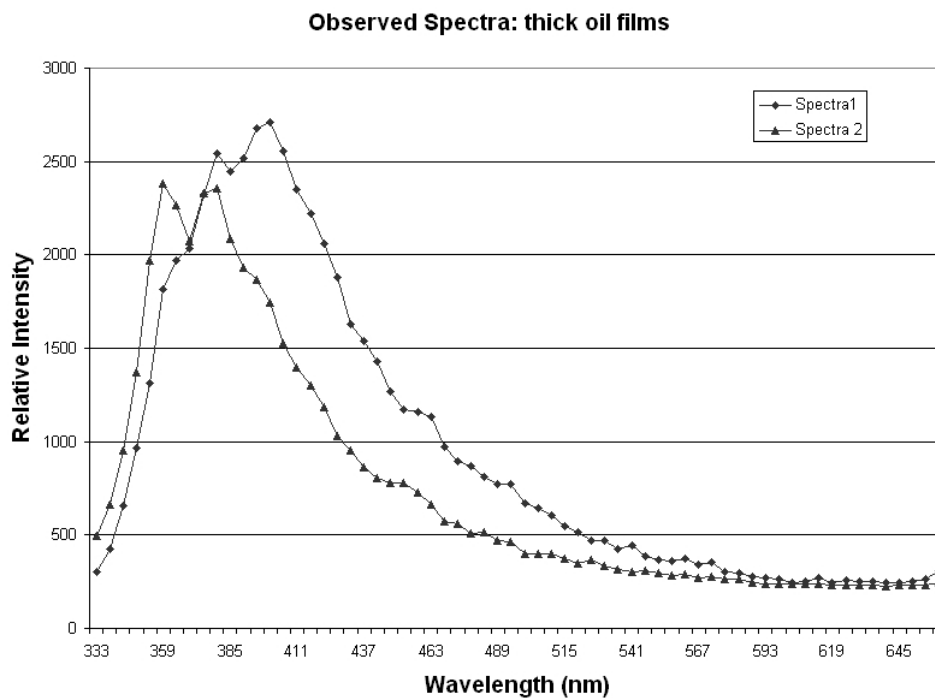


Figure 5.2: Observed Fluorescence Spectra for Thick Oil Film of Diesel in Vancouver Island

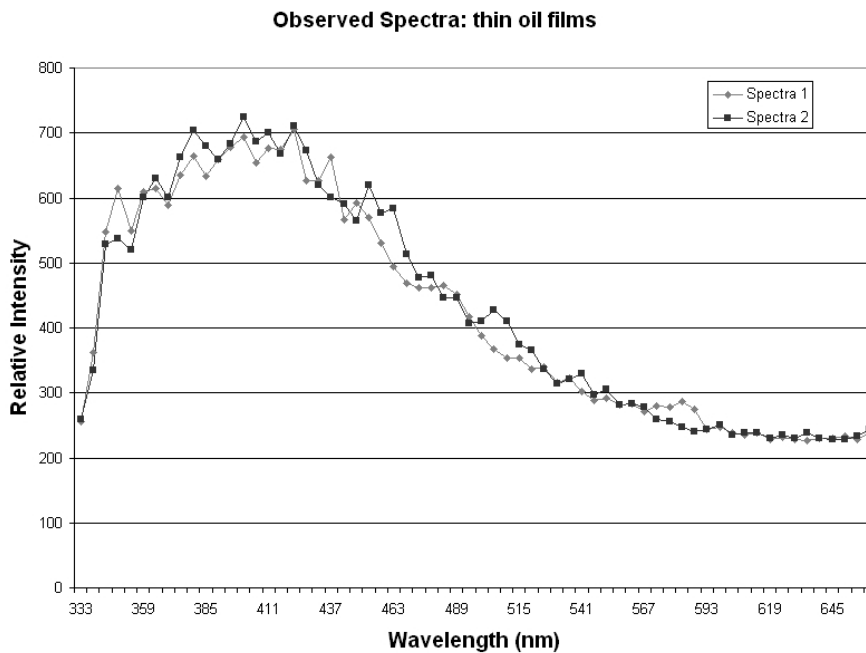


Figure 5.3: Observed Fluorescence Spectra for Thin Film of Diesel in Vancouver Island Area

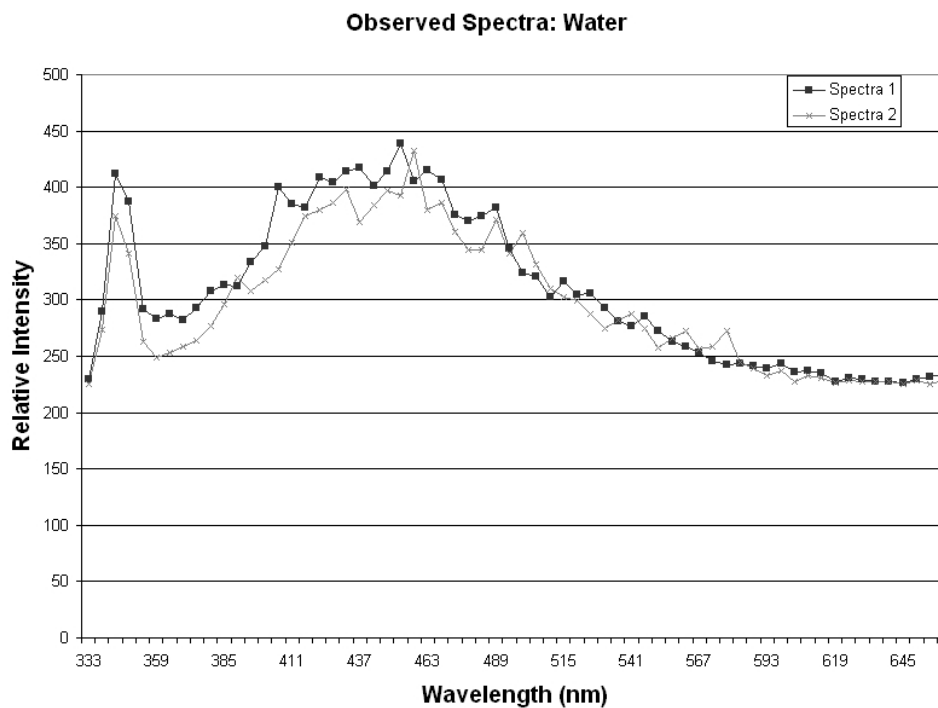


Figure 5.4: Fluorescence Spectra of Water (Gelbstoff) in Vancouver Island Area

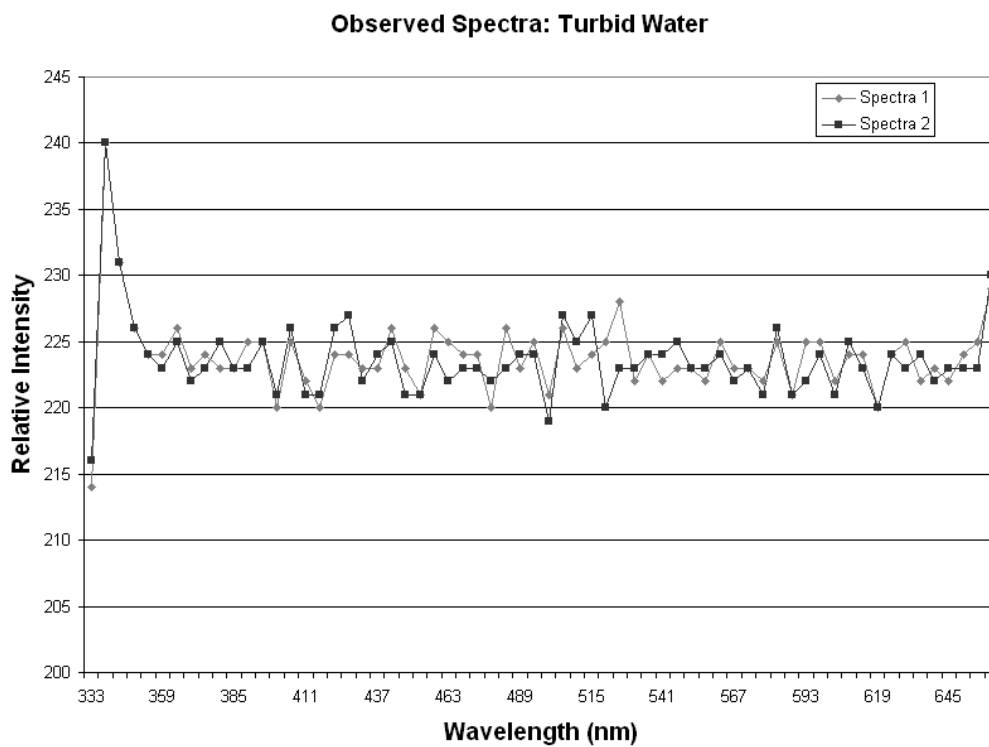


Figure 5.5: Fluorescence Spectra of Turbid Water in Vancouver Island Area

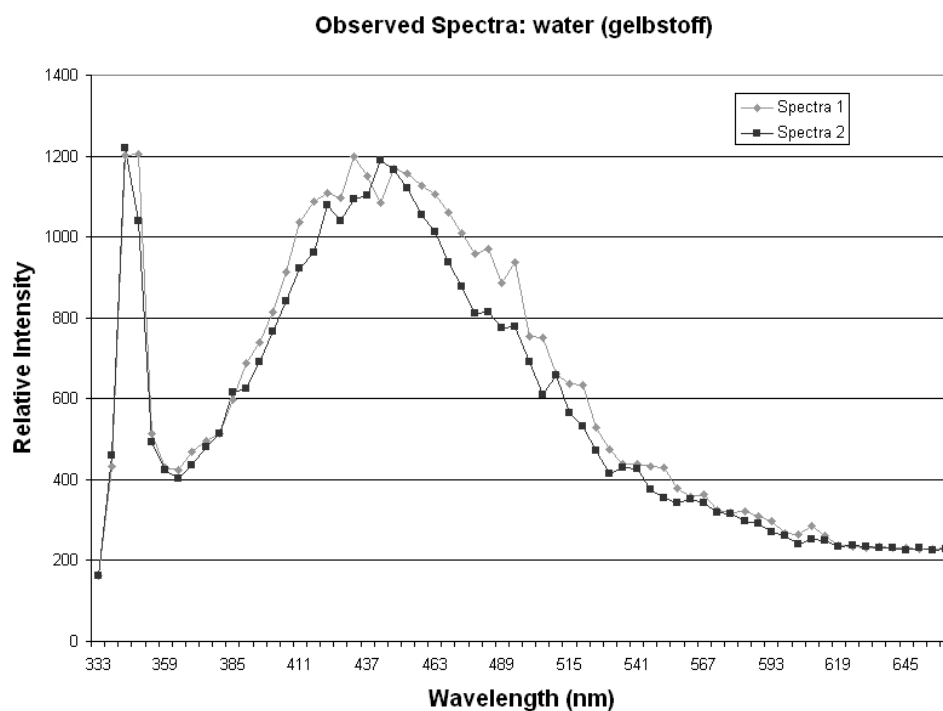


Figure 5.6: Fluorescence Spectra of Water (Gelbstoff) in East Coast of Canada

5.2 Oil Spill Disaster Products

Oil spill disaster products in map format can be a useful tool for oil spill responders and decision makers. Maps can present enormous information in a conceptually simple way. Maps are an essential component of planning and management of an oil spill. The system can integrate the spill locations and trajectory vectors with additional data from the database to provide utilities such as the oil spill location map, oil spill trajectory map, oil spill risk map, oil spill affected area map and oil spill emergency response maps. These maps can be used in managing the equipment and resources such as booms, skimmers and chemicals for oil spill clean up and containment operations. A base GIS map is first created based on common features required for all oil spill disaster products. Base GIS map includes bathymetry layer, layer containing street network, layer

having provinces, layer containing major cities etc. Oil spill information can be combined with base map to create oil spill location map. Oil spill trajectory map is created using prediction of trajectory of oil spill along with the base map. The Oil Spill Risk Map explains the risk associated with an oil spill. The estimated trajectory of oil spill can be combined with infrastructure and environmental data to evaluate the risk with respect to a particular oil spill. Oil Spill Affected Area Map can be derived by using the actual extent and spread of an oil spill. The actual damage caused by an oil spill can be estimated using this map. Oil Spill Emergency Response Map provides the locations important to the emergency response for the oil spill. For example, GIS layers indicating police stations, emergency response centers, government agencies oil spill access points, road networks, etc can be combined to formulate an effective response mechanism.

The geo-referenced SLEAF data from the Canadian east coast is shown in Figure 5.7. Many SLEAF flight lines can be seen around this area, but no oil discharge is detected. Diesel discharge is detected around Vancouver Island area as shown in Figure 5.8. Elliptical footprints of SLEAF can be seen in this Figure. Diesel points are separated from these elliptical foot prints and are combined with appropriate GIS layers to get oil spill location map (Figure 5.9). Oil spill location map gives general information about an oil spill and its surroundings. Oil Spill Emergency Response Map serves as important tool for oil spill responder as it can help in taking quick and informed decisions (Figure 5.10). Any information which can be useful for oil spill emergency response agencies such as police stations, emergency response centers, can be a part of this map. The exact information about locations of police stations, hospitals, disaster support centers, oil spill response agencies are not freely available and, hence some arbitrary locations are

assumed for the sake of this work. Oil spill trajectory is generated based on an imaginary oil spill incident specified in oil spill trajectory modeling tool. Oil spill trajectory is modeled based on assumed wind and current magnitude and direction. Oil spill trajectory map is created combining predicted oil spill trajectory with base map (Figure 5.11). Environmental information presented in map form can be useful for estimating damages due to an oil spill as well as directing resources to proper locations. ESI map is a crucial part of the system and can greatly assist disaster managers in taking decisions. ESI maps for Canada is not freely available and, hence for illustration purposes ESI map for Southern California, USA is shown in Figure 5.12. This ESI map is based on the data provided by NOAA. The ESI map has coastal shorelines graded from 1 to 10, where 1 indicates the least environmental sensitivity and 10 indicates the highest environmental sensitivity. ESI map also has other information useful for oil spill response planning such as locations of biological resources and human-use resources.

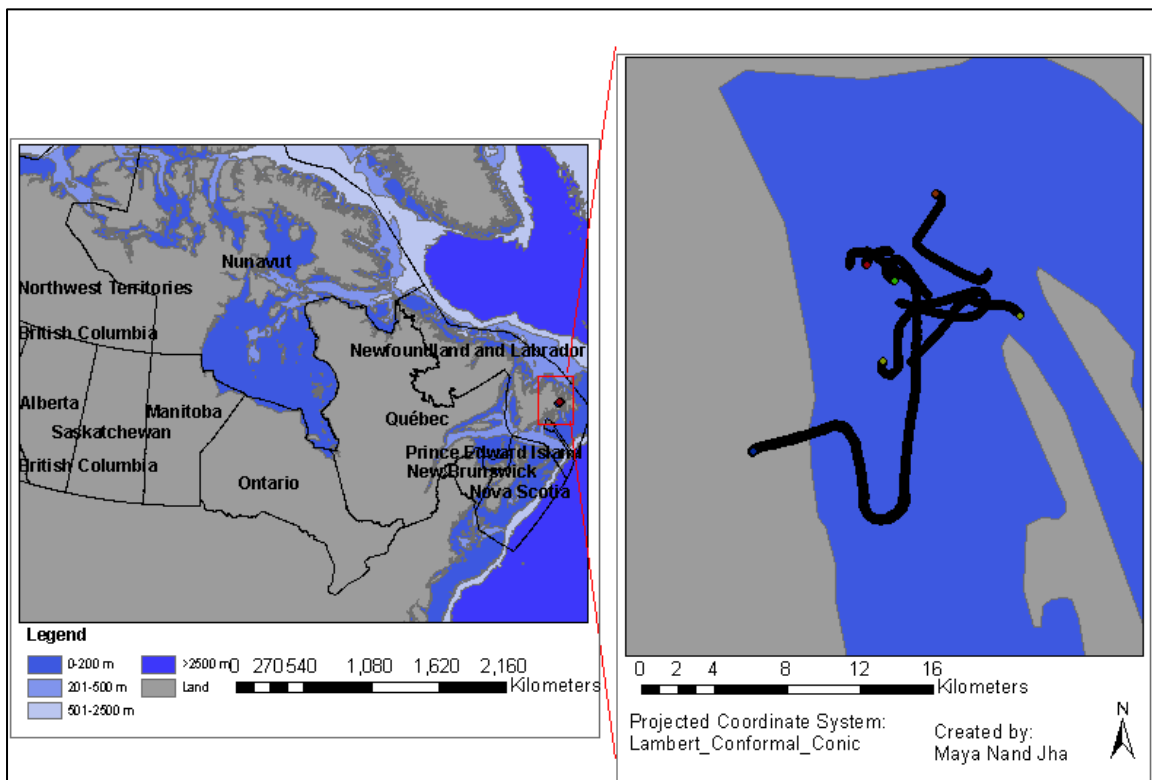


Figure 5.7: Georeferenced and Processed SLEAF Data in East Coast of Canada

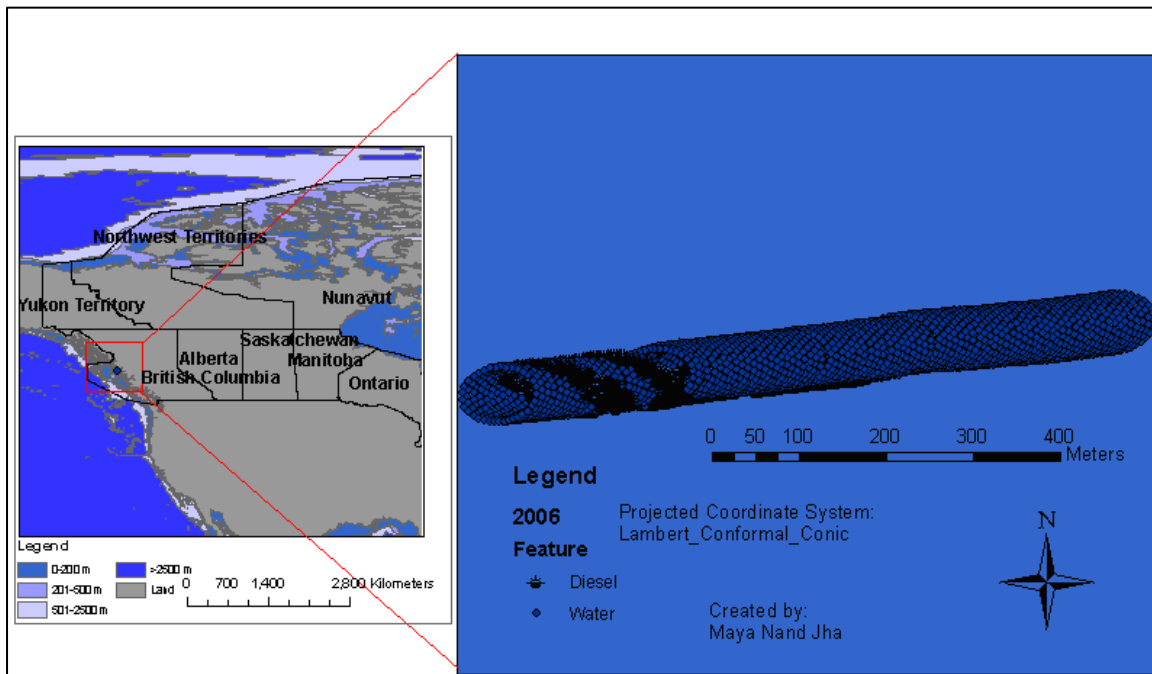


Figure 5.8: Oil Spill Detected around Vancouver Island

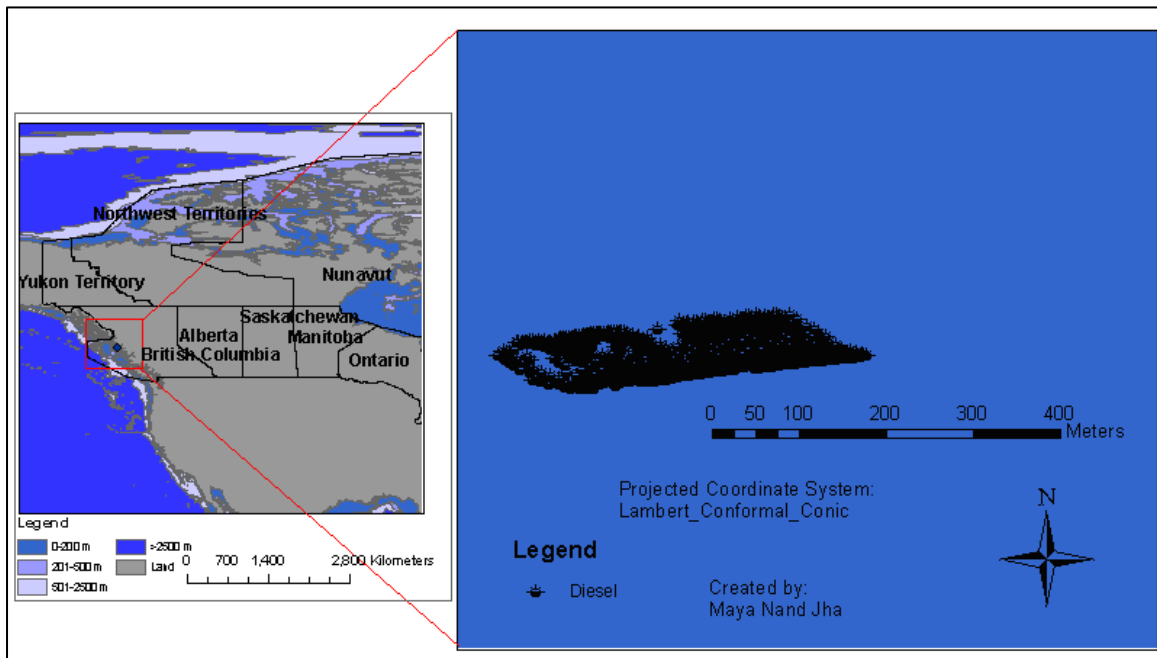
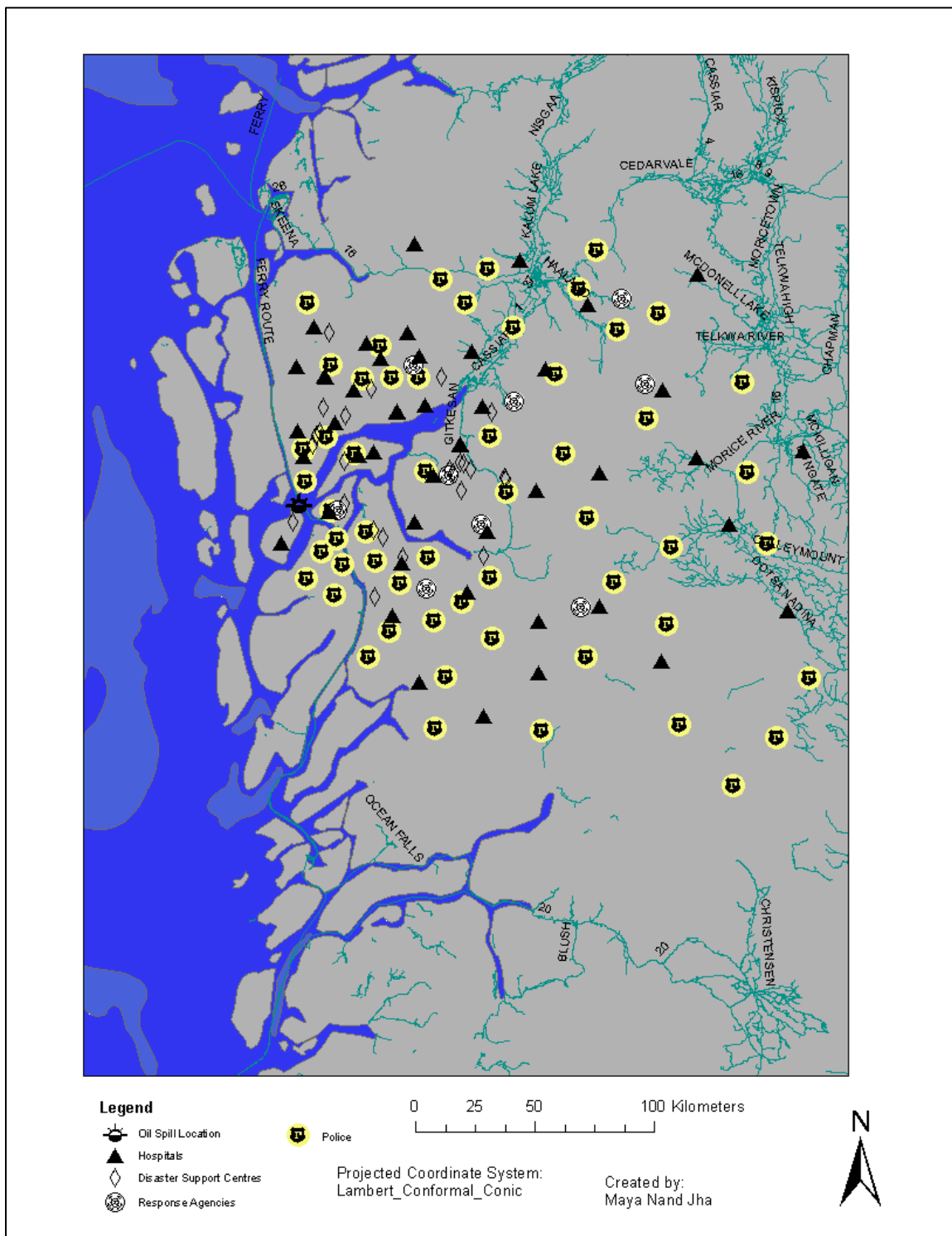


Figure 5.9: Oil Slick Extracted from SLEAF Data around Vancouver Island



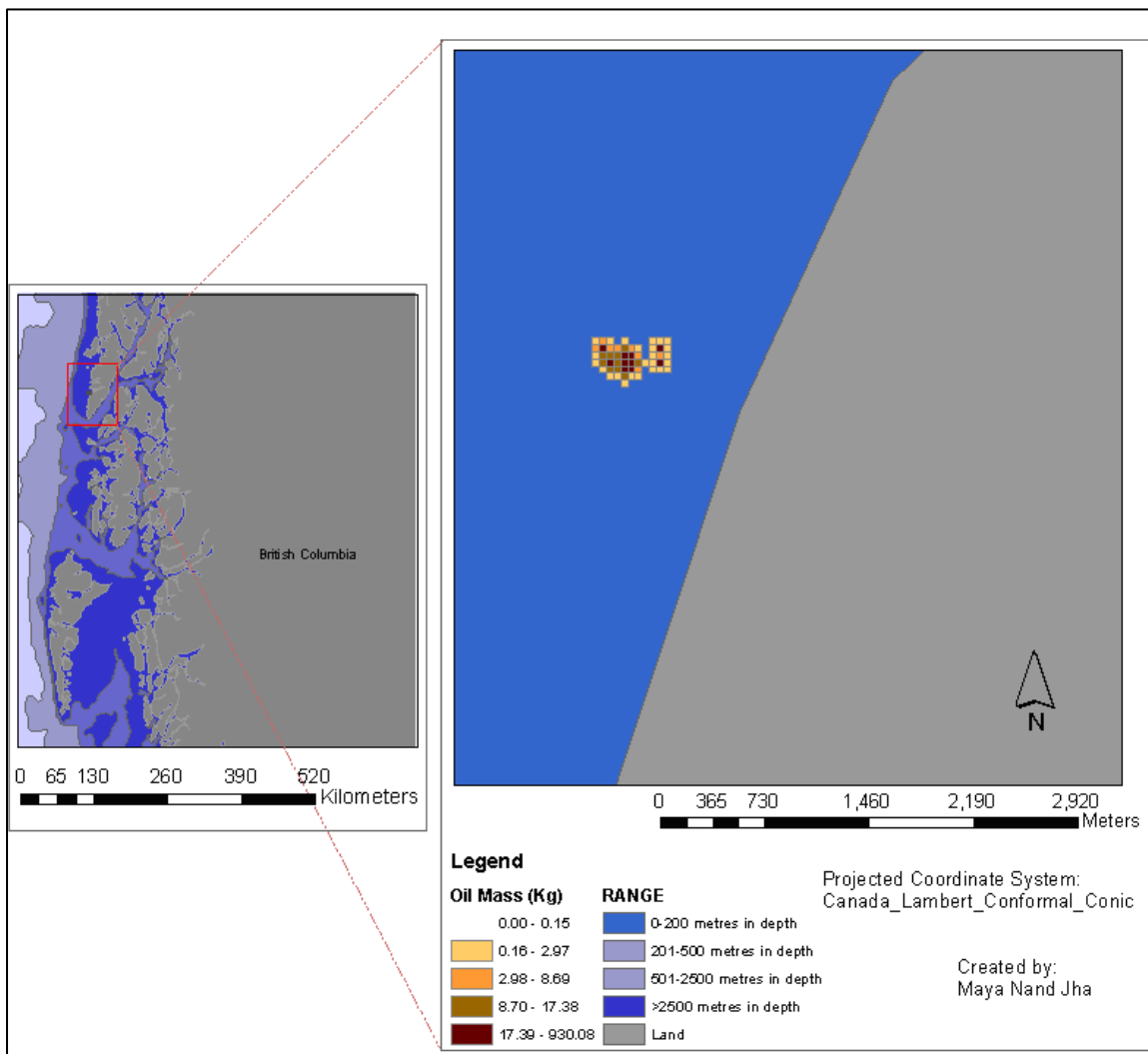


Figure 5.11: Oil Spill Trajectory Map with Assumed Parameters for Trajectory Modeling

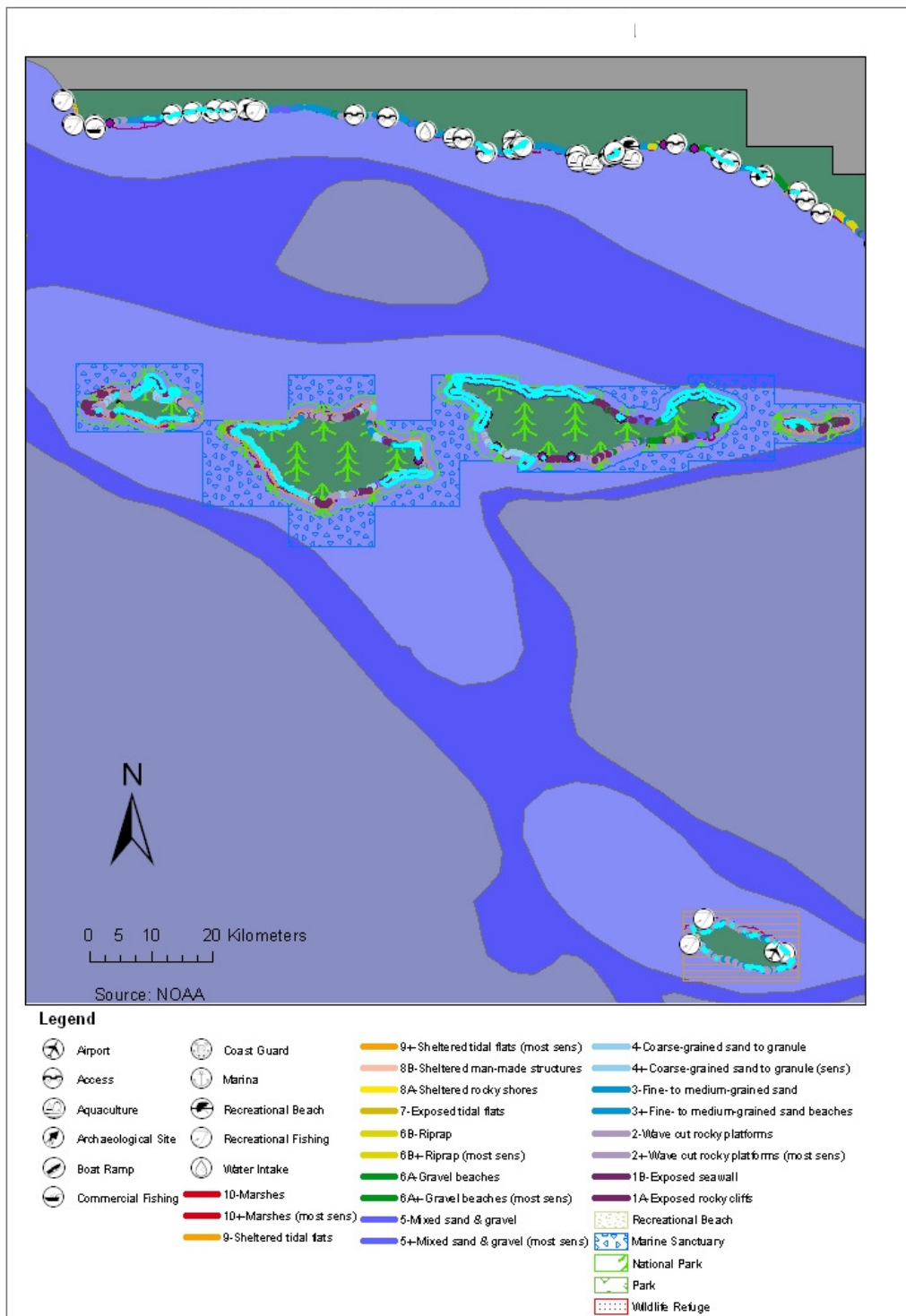


Figure 5.12: ESI map for the Shoreline of Southern California (Source: NOAA)

Chapter Six: Development of a Tool for Oil Spill Detection and Response

There are various challenges in developing an integrated system for oil spill decision support. The system architecture is proposed as a result of extensive discussion among members of Positioning and Mobile Information Systems (PMIS) research group at University of Calgary. A software tool is developed as an integrated system for oil spill detection and decision support. It is important to describe system architecture in this thesis as the software tool developed is based on the proposed system architecture. The detailed description of software tool development is presented in this chapter.s

6.1 System Architecture

There are many challenges in building an oil spill detection and decision support system. One important factor is user accessibility i.e. the disaster managers should have easy access to all the relevant information regarding an oil spill. A web-based system can be accessed from anywhere in the world. A portal can be designed to provide a single access point to diverse types of information coming from different data sources. Real time communication between the system components is another major consideration. A real time GIS system should be able to respond quickly by handling dynamic data and it should have situational awareness. PMIS research group has proposed system architecture to meet these challenges in this research (Liu et al., 2008; Jha and Gao, 2008). Most of the GIS systems are designed to handle static spatial data. An event-driven GIS system has the situational awareness functionality and it can quickly ‘sense and respond’ to events. An event can be anything which is of interest to the system ranging from business transactions to various kinds of disasters such as an oil spill incident. Event sensors should be able to capture the event and then generate an even

object which can be further processed in the system (Liu et al., 2008). Event driven GIS system can be understood as similar to nervous system in our body. The basic components of an event-driven GIS system are events, services, orchestration (event processes) and the Enterprise Service Bus (ESB). ESB is a crucial part of an event-driven GIS system as it facilitates a robust environment for accessing events and processes. Any system can attach to ESB with built-in “publish and subscribe” facilities without interfering with other existing systems attached to ESB. Another advantage of ESB is that applications developed in multiple programming languages can interact with each other via ESB. Various system components are described below.

- Sensors that generate events: These may include call centers, satellites or airborne images, CCTV etc for oil spill accidents.
- Internet portal: It provides a centralized service for oil spill detection and decision support.
- Web-GIS services: These services can generate oil spill disaster products including oil spill location and trajectory maps, risk map and emergency response maps. Location based services (LBS) can be also part of Web-GIS services.
- Orchestrations (Event Processes): These event processes include business logic for oil spill disaster response such as oil spill image analysis, laser fluorosensor data processing, trajectory analysis, risk analysis and emergency response analysis.
- Other systems that are interested in receiving/exchanging advanced events generated from Web-GIS or oil spill management system can be registered into the system. Potential system components can be following:

- Fleet management system
 - Other emergency systems
 - Hospital management systems
 - Government service system
 - Applications in police department
 - Other applications developed for oil spills by other departments
- Database Management System: All output results and relevant input data will be stored in database. A robust database is needed to facilitate easy retrieval and manipulation of information.
 - Enterprise Service Bus: ESB provides the environment to access events and services. TIBCO Enterprise Message Service by TIBCO software Inc is popular software to facilitate real time flow of information and this will be used as ESB in our system.

The use case diagram for the integrated system for oil spill response developed for this research is shown in Figure 6.1. There can be two primary users for this system. The first kind of users can be laser fluorosensor (SELAF) data providers. They can use this system to check if SLEAF dataset captured for a particular area has any oil. The other important user can be oil spill disaster manager. Oil spill disaster manager can also have access to the SLEAF datasets and he/she can use the laser fluorosensor data processing tool to analyse SLEAF data for oil. The oil spill reporting tool is available which can be used to report an oil spill at a given location. GIS analysis tool can be used for detailed spatial analysis and can be useful for directing appropriate resources to the oil spill incident location. The system can be defined for more use cases if low-level design

is available. Different system components can be made available to different users based on their responsibility and role. The system design as proposed by PMIS research group is shown in Figure 6.2. The laser fluorosensor data source processing system, oil spill reporting tool, oil spill trajectory modeling tool, GIS analysis tool and any other system components can communicate with each other using ESB. Laser fluorosensor data processing system is developed in this thesis utilizing the oil spill detection and classification scheme developed in this research. The software tool developed in this research can generate a personal geodatabase containing oil spill information when SELAF data and the reference spectra files are provided. This personal geodatabase can be then published to ESB. Oil spill reporting tool can be used to report an oil spill incident and this event can be published to ESB. Any application interested in getting information about a new oil spill can be subscribed to ESB. GIS components have been developed to report an oil incident and model oil spill trajectory. The development of software tool is explained in detail in the next section.

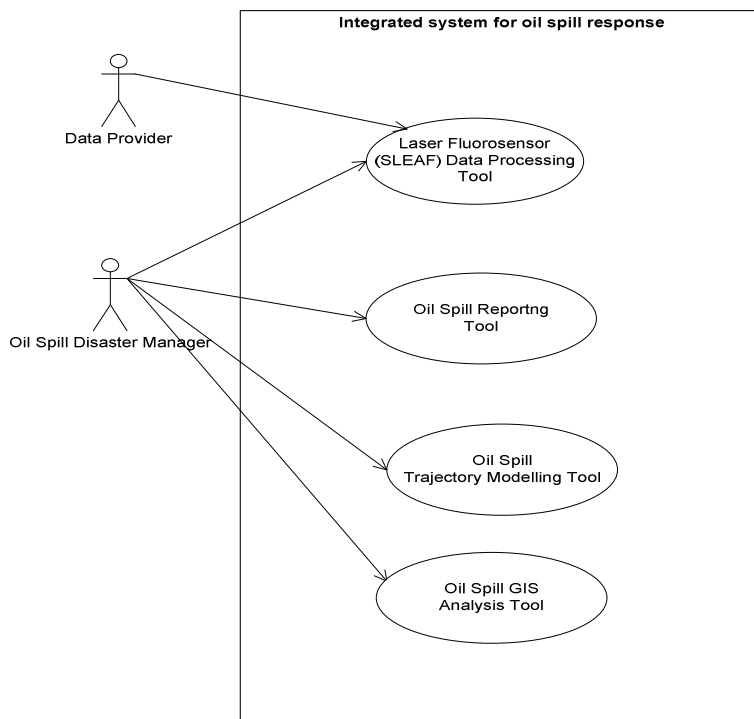


Figure 6.1: Use Case Scenario for Integrated System for Oil Spill Response

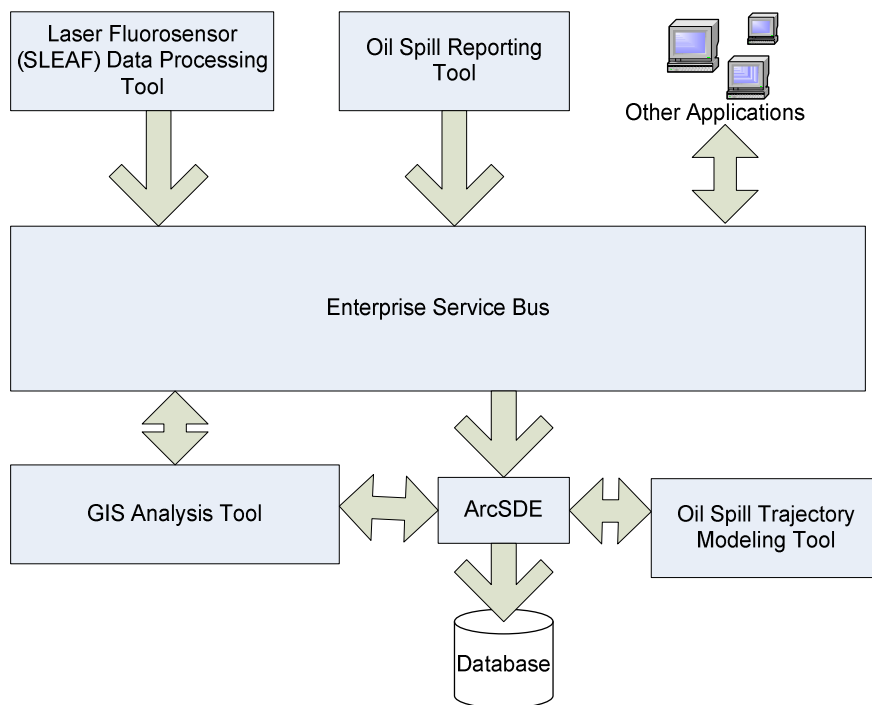


Figure 6.2: System Architecture of Integrated System for Oil Spill Response

6.2 Software Tool Development

A desktop application is developed as an integrated system for oil spill response. There are various components of the system and suitable technologies have to be chosen for developing the prototype system. Environmental Systems Research Inc. (ESRI) is world leader in GIS technologies and provides various GIS products for different kind of users and development tasks. ArcGIS Engine is a development tool provided by ESRI for making customized GIS desktop applications. ArcGIS engine provide access to ArcObjects which are core components of ArcGIS Desktop products. ArcGIS Engine application programming interfaces (APIs) are available in various programming languages such as C++, Java and C#.NET. Moreover, ArcGIS Engine provides various visual components for making development tasks for GIS applications pretty easy and straight forward. Many basic GIS functions such as map manipulation tools e.g. pan, zoom, map selection tools, map searching tools, map measuring tools and simple query tools can be easily implemented. Visual Studio 2005 is Integrated Development Environment (IDE) by Microsoft and suitable for developing Graphical User Interface (GUI) applications. C#.Net is chosen as programming language for the development as it is simple, robust and object oriented language. TIBCO Enterprise Message Service (EMS) is used as ESB for the prototype system. TIBCO EMS can run on multiple platforms including LINUX, Windows servers and desktops, Mac OS X. The EMS provide support for multiple languages such as Java, Microsoft .NET, C and C++ (TIBCO, 2009). Microsoft SQL Server 2005 Express is used as relational database management system (RDBMS) for the system. ArcSDE is used to spatially enable the RDBMS. ArcSDE is used to store and manipulate spatial data in Microsoft SQL Server.

ArcSDE acts as a bridge between user and RDBMS and user has to deal with ArcSDE without caring about particulars of RDBMS.

Figure 6.5 shows the part of the software displaying general information about the system and the tools integrated in the system that are available to the user for oil spill detection and decision support. The main input for SLEAF data processing is a text file which contains information about observed fluorescence spectra for each target point. The reference data is required which consists of fluorescence spectra of oils and background materials collected in laboratory conditions. Laser fluorosensor data processing software component can accept input SELAF file and the reference file from the user. Thresholds can be specified by the user for the oil spill detection and classification process or the default values may be used (Figure 6.6, 6.7). The laser fluorosensor data processing tool processes data based on the proposed oil spill detection and classification scheme. Every sample point is geo-referenced and then classified to determine the oil traces. At the end of this process, a geodatabase containing locations of each sample and associated feature type is obtained. This information should be published to TIBCO EMS so that any applications interested in receiving this information can get it via TIBCO EMS. TIBCO EMS accepts messages in form of XML only. The geodatabase is converted into XML feature class and then published to TIBCO EMS. The laser fluorosensor data processing process can be explained graphically by a flow chart (Figure 6.3).

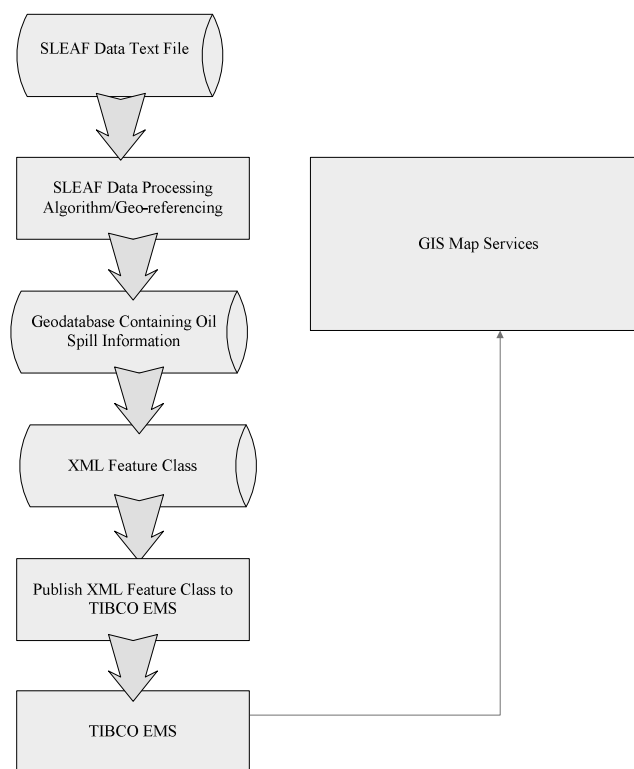


Figure 6.3: SLEAF Data Processing and Analysis Flow Chart

A detailed report is also generated which provides more information about the oil spill detection and classification process. An oil spill incident can also be reported by simply specifying location, date and amount and type of the oil spill (Figure 6.8).

Oil spill trajectory can be modeled by using the ‘Trajectory Modeling’ tool which is based on the previously described CA model. Vector grids for oil mass distribution are created using ‘Hawth’s Analysis Tool’ which is a freely available GIS tool for spatial analysis (Figure 6.4). The detailed information about ‘Hawth’s Analysis Tool’ can be found at Spatial Ecology Website (Spatial ecology, 2009). The grids for wind and current information can also be added to the system to provide information about wind and current velocity for each grid.

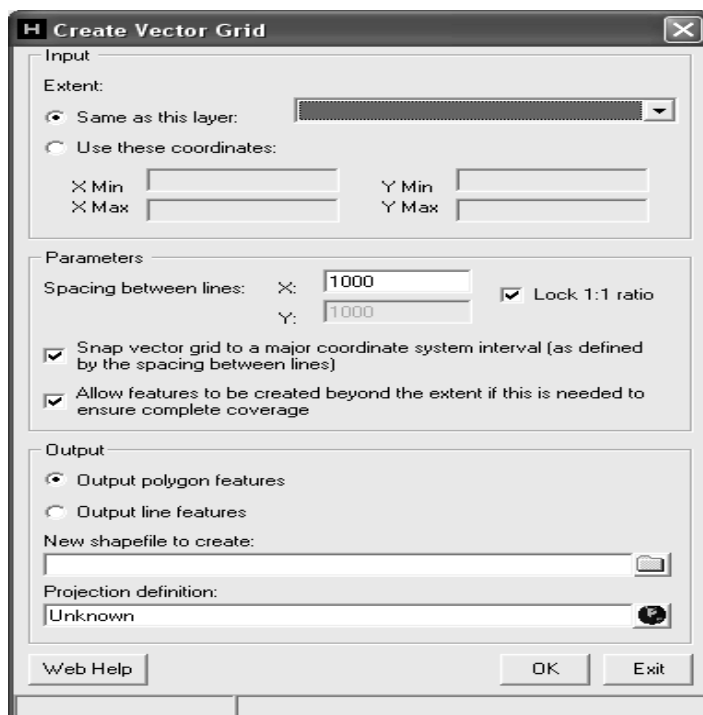


Figure 6.4: Hawth's Analysis Tool for Creating Vector Grids

In the trajectory modeling tool, user is provided with default values of a number of parameters, but it can be changed according to the user's experience and knowledge about the environmental settings (Figure 6.9, 6.10). Users click on grid where oil spill is reported and input the required information and the 'Save' button stores this information into the database (Figure 6.11). The spread of the spill is provided to the user once he/she clicks on the 'Model Trajectory' button (Figure 6.12). GIS analysis tool is provided for advanced GIS analysis (Figure 6.13). Many GIS functions such as map manipulation tools, map searching tools, map measuring tools and simple query tools are made available to the user by using ArcGIS Engine Map Control. Advanced users such as Disaster Managers will have access to this tool. Oil spill disaster products are available

via this tool and other layers can be added by users if desired (Figure 6.14, 6.15, 6.16).

More components can be added to the system to enhance functionality of the system.

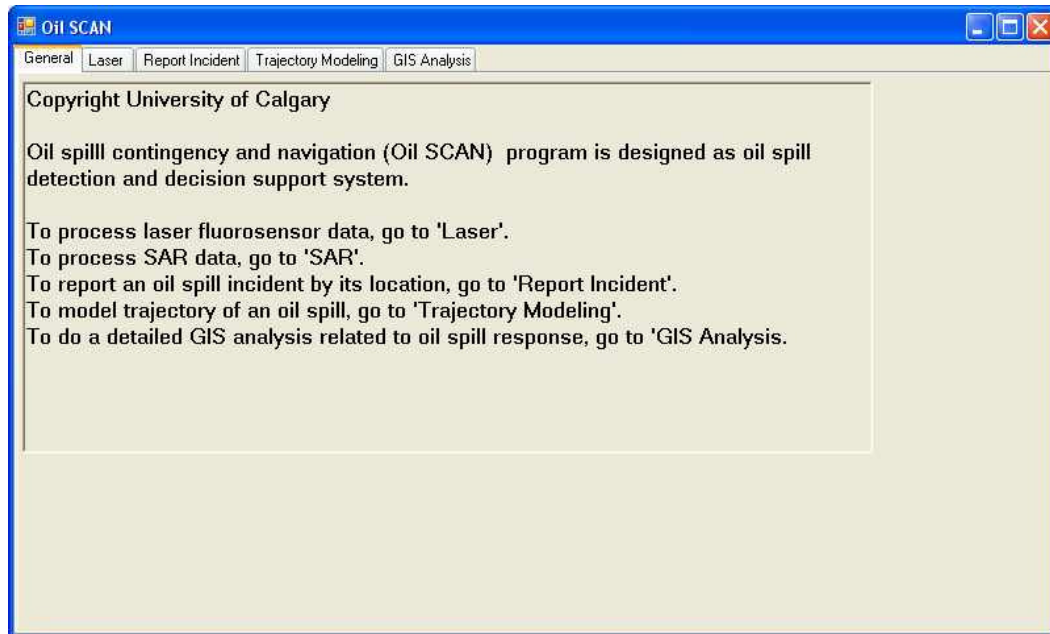


Figure 6.5: Software Tool Providing General Information about the Prototype System

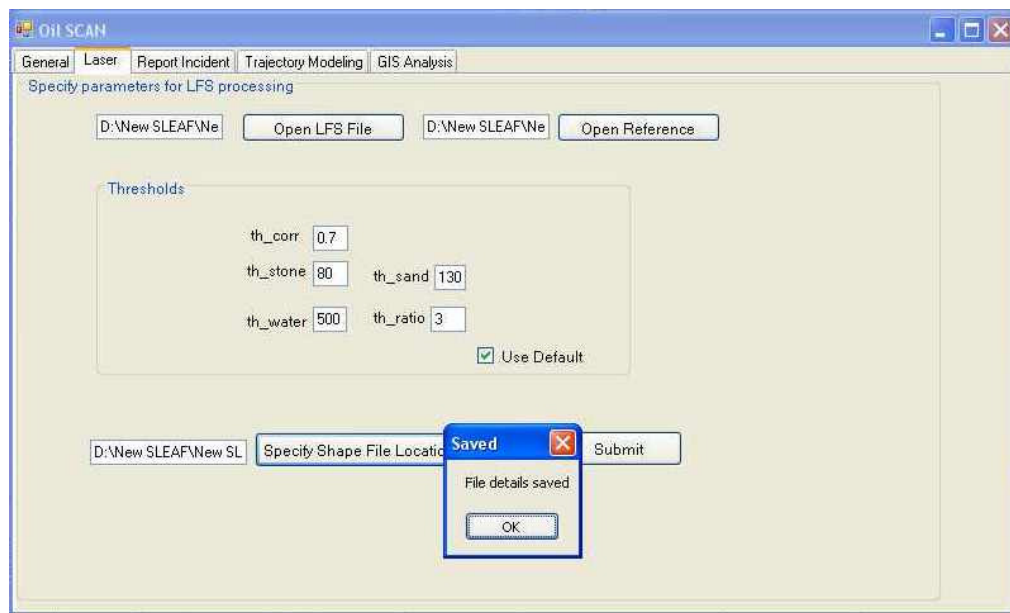


Figure 6.6: Laser Fluorosensor Data Processing Part of the System

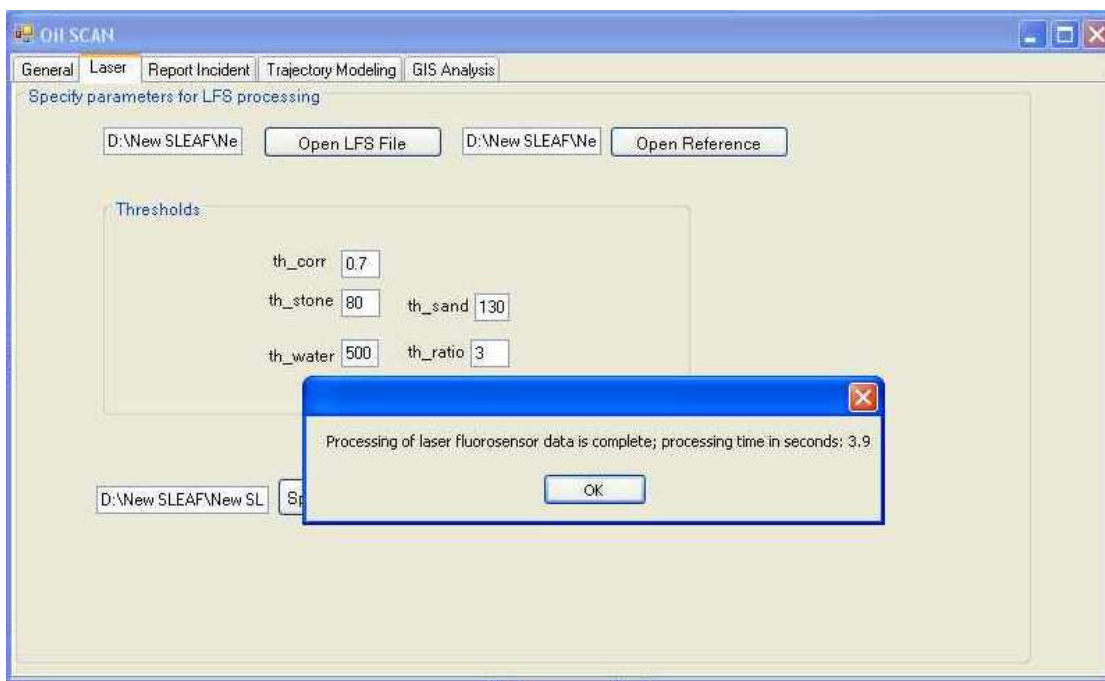


Figure 6.7: Dialog Box Showing that Processing of Laser Fluorosensor Data is Complete

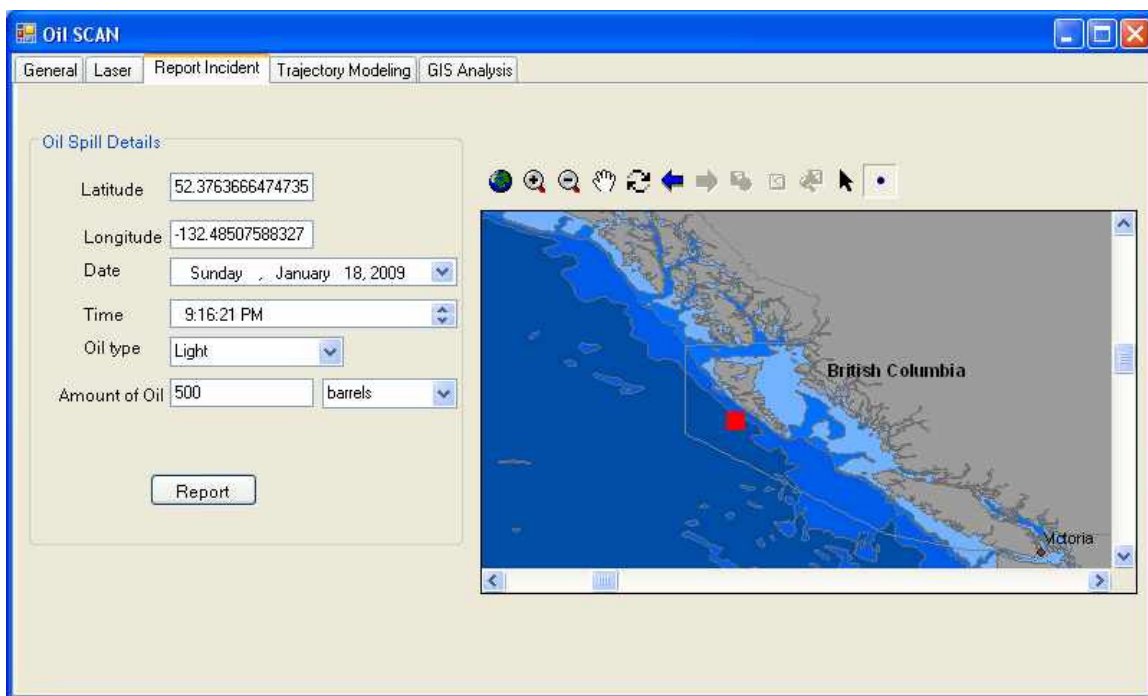


Figure 6.8: Tool for Oil Spill Incident Reporting

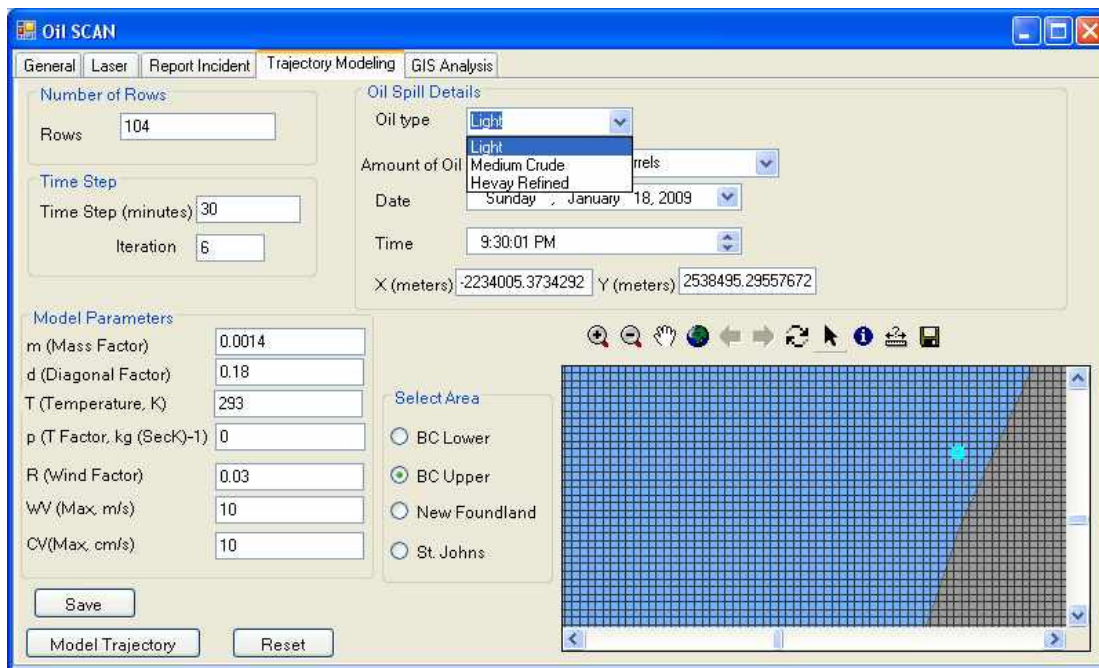


Figure 6.9: Oil Spill Trajectory Modeling Tool Showing Options for Selecting Different Oil Types

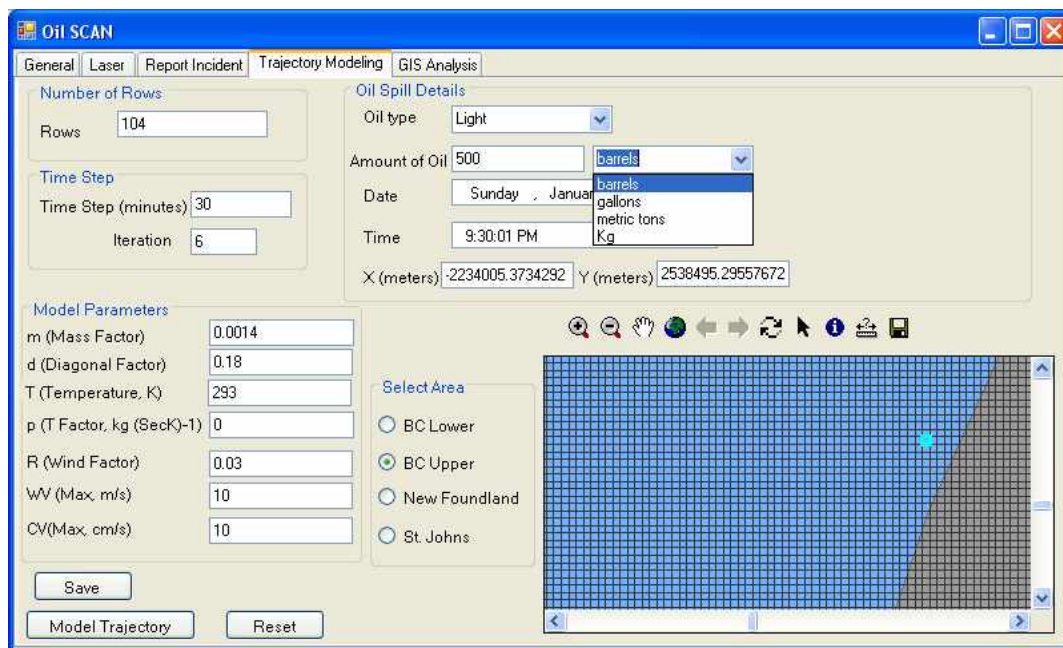


Figure 6.10: Oil Spill Trajectory Modeling Tool Showing Options for Selecting Different Measurement Type for Oil

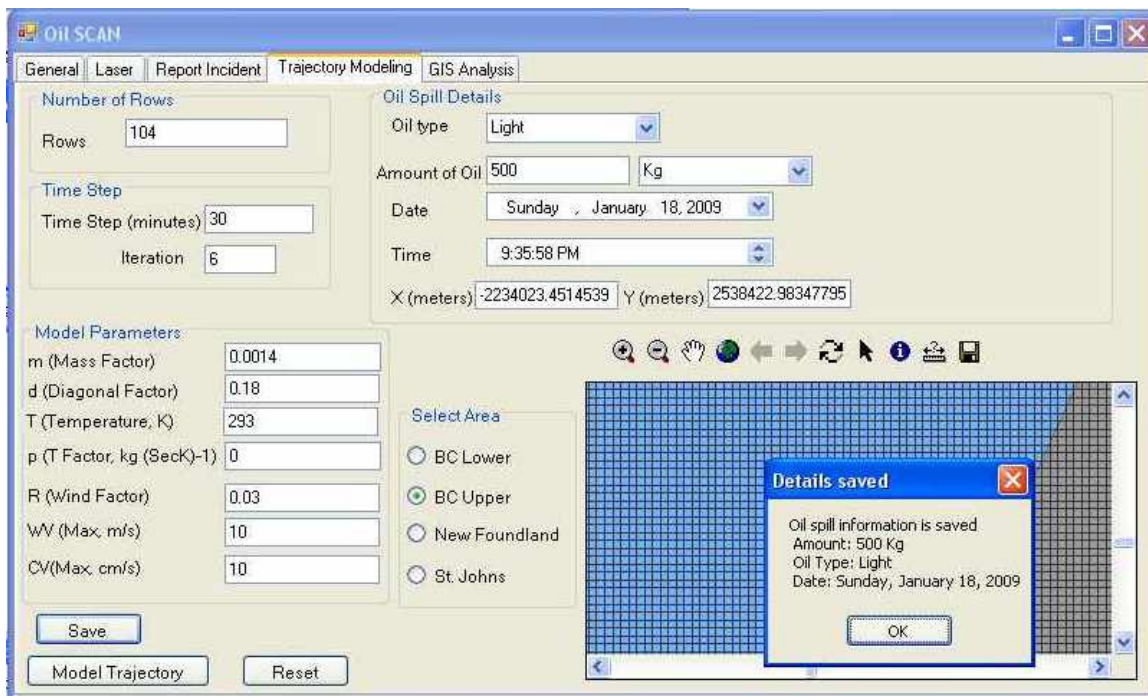


Figure 6.11: Saved Oil Spill Information in Oil Spill Trajectory Modeling Tool

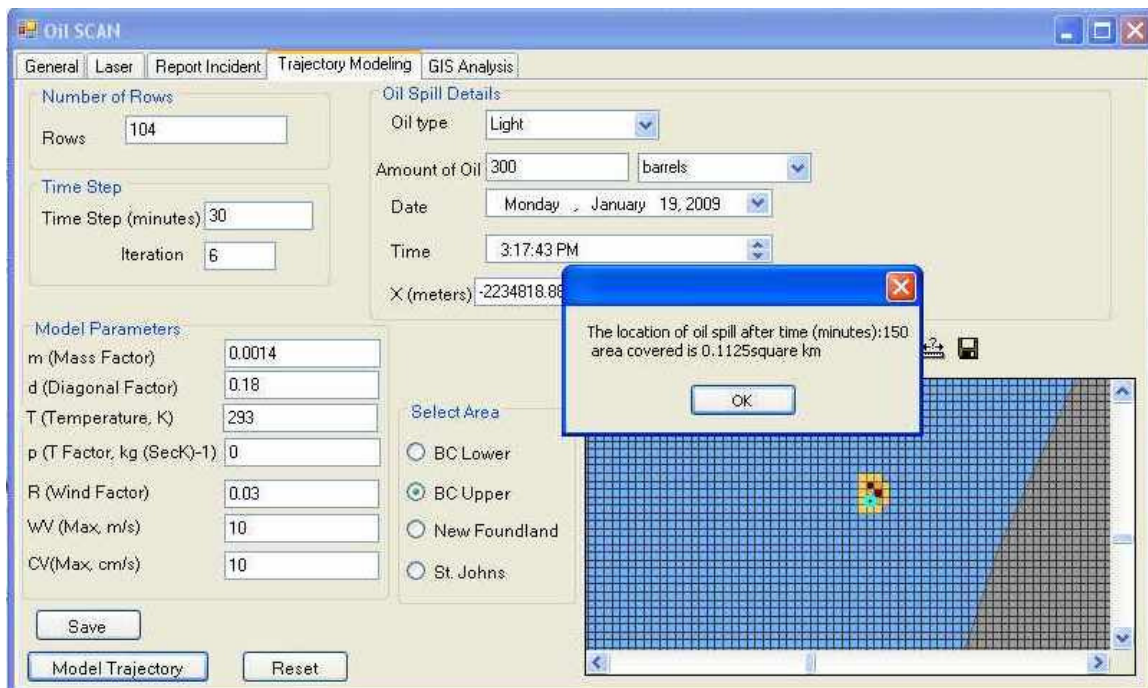


Figure 6.12: Trajectory of Oil Spill after Time Interval of 150 Minutes

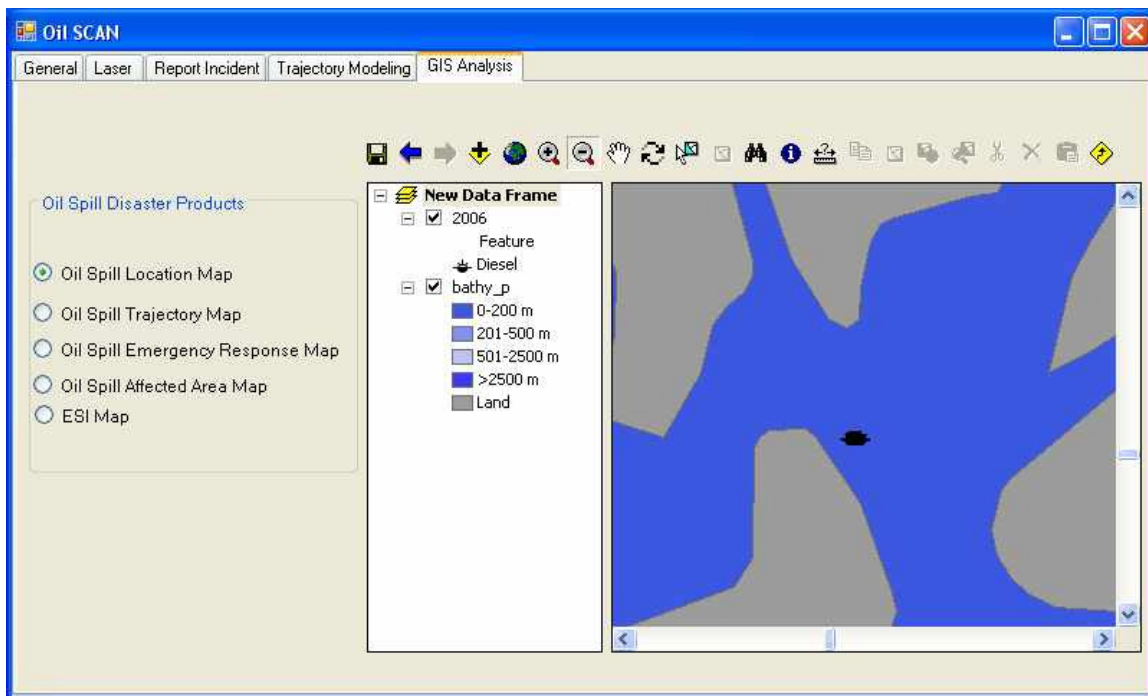


Figure 6.13: GUI for GIS Analysis Component of the System

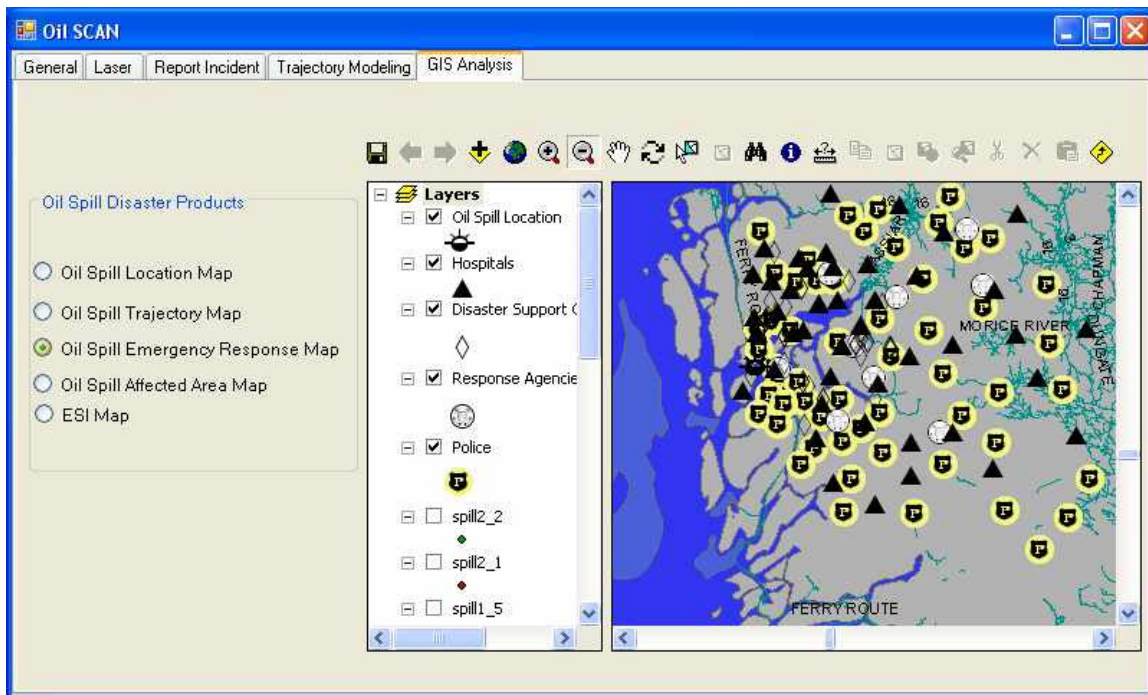


Figure 6.14: Oil Spill Emergency Response Map Displayed in GIS Analysis Tool

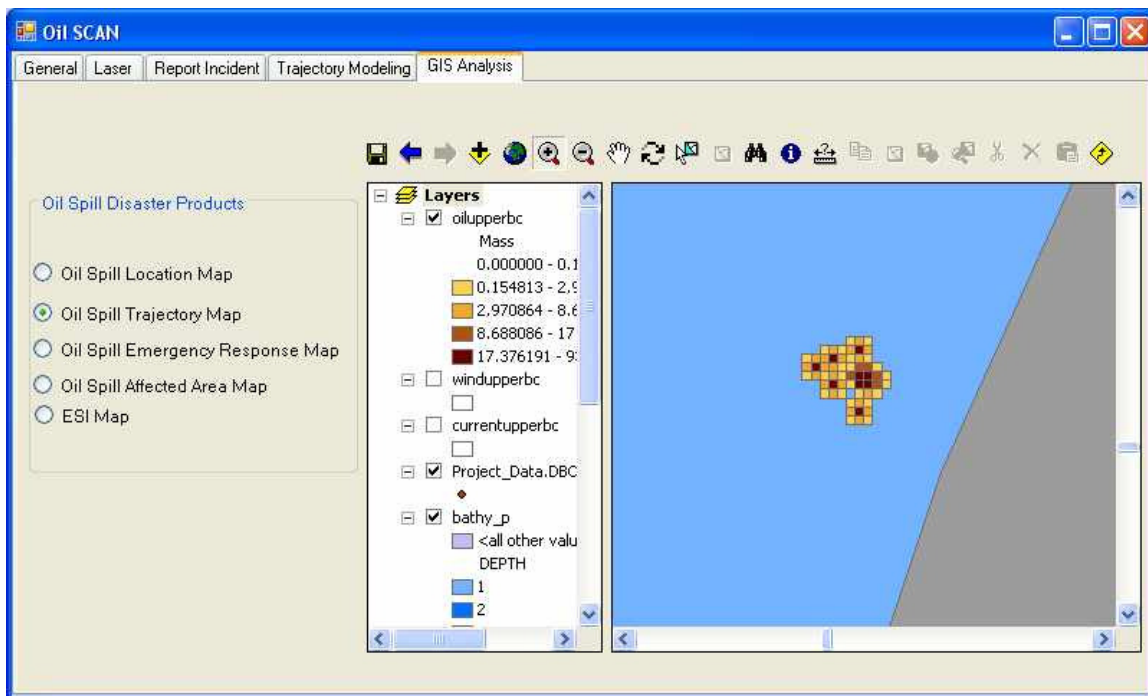


Figure 6.15: Oil Spill Trajectory Map Displayed in GIS Analysis Tool

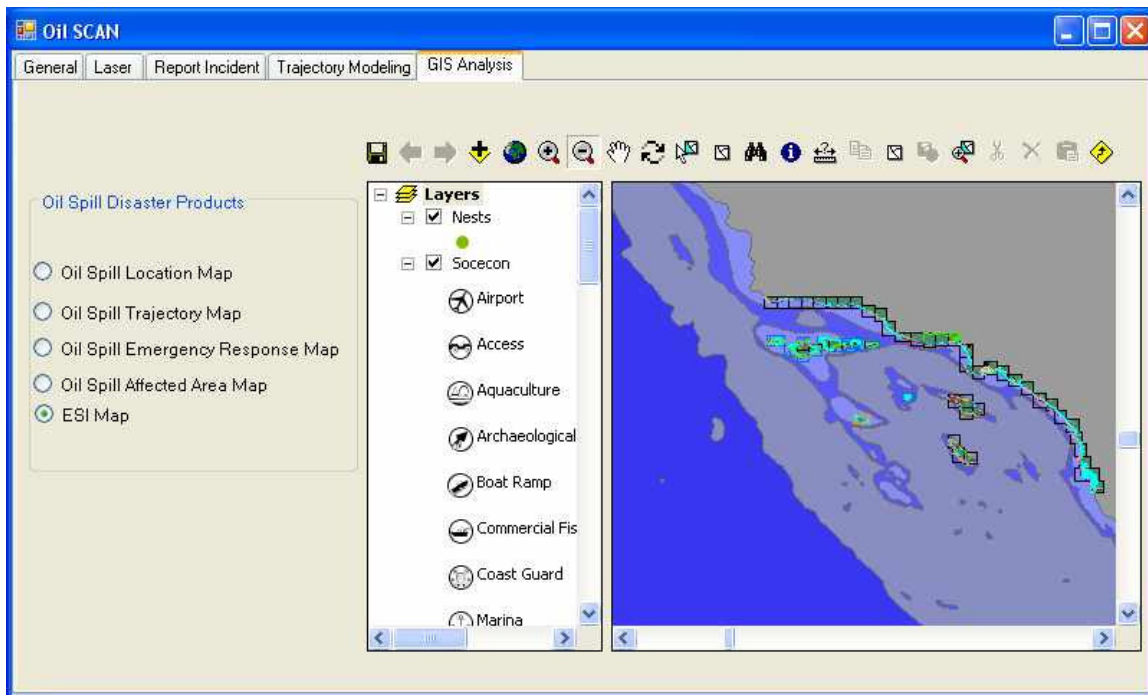


Figure 6.16: ESI Map Displayed in GIS Analysis Tool

Chapter Seven: Conclusions and Recommendations

Oil spills causes significant damage to economy and environment and proper oil spill contingency planning can reduce response time and assist oil spill responders. The research aimed to develop an oil spill detection system based on laser fluorosensor data. Additional GIS tools were developed to assist oil spill responders in case of an oil spill.

7.1 Conclusions

Oil spill surveillance is an important part of oil spill contingency planning. Current remote sensing sensors have been evaluated in terms of their usefulness for detecting and monitoring oil spills. Laser fluorosensors were found to be the best available sensor for oil spill surveillance as they can detect oil on various backgrounds including ice and the shoreline. However, no single sensor had capability to provide all the information needed for oil spill surveillance. Real time remote sensing data is essential for oil spill response so that resources can be immediately directed to sensitive areas for cleaning and containment operations.

The characteristics of laser fluorosensors were studied in detail in this research. SLEAF operated by Environment Canada was found to successfully detect oil in test flights by Environment Canada. An oil detection and classification scheme can make use of various features such as spectral shape, the fluorescence decay time, the position of the fluorescent peak, the fluorescence yield, the depression of water Raman scattering signal, and the variation of these parameters with the excitation wavelength. The broad fluorescence spectrum and water Raman scattering properties was found to be reliable in order to improve oil spill detection and classification. Various algorithms were evaluated in terms of their ability to detect and classify oil from simulated data as well as actual

SLEAF data collected by Environment Canada. PCs of the original reference spectra and Pearson Correlation Coefficient were found to have suitable characteristics for the classification of the simulated data whereas the ratio of channels was found to be unsuitable. The Pearson Correlation Coefficient was used for the classification of SLEAF data as this coefficient only depends on the shape of fluorescence spectra and not on the total fluorescence emission. The high correlation between several oils and background materials were noted and an oil spill detection and classification scheme was proposed to solve this problem. Our proposed detection and classification scheme successfully detected diesel oil slicks in the area around Vancouver Island, which is in accordance with Environment Canada findings.

The need for developing a comprehensive integrated system for oil spill detection and decision support was realized. Oil spill responders can make use of such integrated system for quickly and effectively responding to an oil spill. Oil spill contingency planning is a complex task and involves multiple agencies. Many issues related to any emergency planning are spatial. GIS can help in integrating various operations and can facilitate effective communication between various parties involved. A software system has been developed to provide a tool to oil spill responders in case of an oil spill. Oil spill can be reported by various ways e.g. oil spill can be reported by specifying location and details about the oil spill. Oil spill can also be reported by uploading a SLEAF data file which can be processed by SLEAF data processing scheme for detecting any possible oil slicks. Oil spill trajectory modeling tool was developed as part of this integrated system. Cellular Automata (CA) was used to model trajectory of oil spill based on initial location of oil spill, wind speed and direction, current speed and direction and various other user-

defined parameters. Various oil spill disaster products such as oil spill location map, oil spill risk map and oil spill emergency response map can be made available to the disaster managers.

The system architecture to meet the research objectives was discussed. ESB can provide environment for communication between various system components such as remote sensing image processing system, Web-GIS and database. More components can be added to the system during the development as all components are loosely coupled or independent of each other and only communicate via ESB. A prototype desktop application was developed using Visual Studio 2005 (C#.NET) to demonstrate the feasibility of such as system. ArcGIS Engine was used to develop spatial components of the system. Microsoft SQL Server 2005 Express was used as RDBMS for the system. ArcSDE was used to handle spatial data query and manipulation and it acts as bridge between users and the RDBMS. The developed prototype system displays the feasibility of creating a fully operational comprehensive integrated system for oil spill disaster management. Though, system is specifically designed for handling oil spill disasters, but can be easily extended to handle other disasters such as Urban Fire, Floods etc.

7.2 Recommendations

The objective of this research is to provide a reliable oil spill detection system based on laser fluorosensor data. Some additional tools were developed to assist oil spill responders in case of an oil spill. This research contributed in realizing this goal to some extent, but still a lot of work is needed to achieve the full-fledged system. Reliable oil spill detection and classification is an important part of this work as this can tremendously help in reducing ambiguity in terms of identifying and responding to an oil

spill. Laser fluorosensor can be a useful input for a real-time system as it can be processed for detecting and classifying oil in real-time. An oil spill detection and classification scheme is developed for reliable oil spill detection and classification, but further research is needed to improve and check the reliability of our outlined oil spill detection and classification scheme.

The oil spill trajectory model used in this research is based on many simplifications and has ignored some processes involved in deciding fate and behaviour of oil spill. Oil spill trajectory modeling is complicated and extensive research is needed to understand various aspects of the modeling.

The goal of the research is to develop a web-based GIS system so that it can be accessible from anywhere in the world. A desktop system was developed in this research, but more work is needed to convert this system to a web-based system. The system architecture is designed for an oil spill detection and decision support system and clearly defines system components at high-level. A detailed low-level design based on the user requirements should be prepared based on the real requirements of oil spill disaster managers in case of an oil spill.

References

- Alaruri, S.D., M. Rasas, O. Alamedine, S. Jubian, F. Al-Bahrani and M. Quinn, "Remote Characterization of Crude and Refined Oils using a Laser Fluorosensor System", *Optical Engineering*, 34:01, pp. 214-221, 1995.
- Almhdi, K.H., P. Valigi, V. Gulbinas, R. Westphal and R. Reuter, "Classification with Artificial Neural Networks and Support Vector Machines: Application to Oil Fluorescence Spectra", *EARSeL eProceedings*, 6, 2007.
- ArcGIS Desktop Help, Topic: Projected Coordinate System.
http://webhelp.esri.com/arcgisdesktop/9.3/index.cfm?TopicName=About_projected_coordinate_systems. Last accessed on Aug 14, 2009.
- Armstrong, M.P. and P.J. Densham, "Database organization strategies for spatial decision support system", *International Journal of Geographical Information Systems*, 4:1, pp. 3-20, 1990.
- Babichenko, S., A. Dudelzak and L. Poryvkina, "Laser Remote Sensing of Coastal and Terrestrial Pollution by FLS-LiDAR", *EARSeL eProceedings*, 3, 2004.
- Brebbia, C.A., *Oil Spill Modeling and Processes*, WIT Press, UK, 2001.
- Brekke, C. and A. Solberg, "Oil spill detection by satellite remote sensing", *Remote Sensing of Environment*, 95, pp.1 –13, 2005.
- Brown, C. and M. Fingas, "Review of Oil Spill Remote Sensing", *Spill Science & Technology Bulletin*, 4.4, pp.199-208, 1997.

- Brown, C. and M. Fingas, “New space-borne sensors for oil spill response”, *International SPILL Conference, American Petroleum Institute*, Washington, DC, pp. 911-916, 2001a.
- Brown, C. and M. Fingas, “Upcoming Satellites: Potential Applicability to Oil Spill Remote Sensing”. *Proceedings of the 24th Arctic and Marine Oil Spill Program (AMOP) Technology Seminar*, Environment Canada, Ottawa, ON, Canada, pp. 495-505, 2001b.
- Brown, C. and M. Fingas, “Review of the Development of Laser Fluorosensors for Oil Spill Application”, *Marine Pollution Bulletin*, 47, pp. 477–484, 2003a.
- Brown, C. and M. Fingas, “Development of airborne oil thickness measurements”, *Marine Pollution Bulletin*, 47, pp. 485–492, 2003b.
- Brown, C. and M. Fingas, “A review of current global oil spill surveillance, monitoring and remote sensing capabilities”, *Proceedings of the 28th Arctic and Marine Oil Spill Program (AMOP) Technical Seminar*, Environment Canada, Ottawa, ON, Canada, pp. 789-798, 2005.
- Brown, C., M. Fingas and R. Hawkins, “Synthetic Aperture Radar Sensors: Viable for Marine Oil Spill Response?”, *Proceedings of the 26th Arctic and Marine Oil Spill Program (AMOP) Technology Seminar*, Environment Canada, Ottawa, ON, Canada, pp. 299-310, 2003.

- Brown, C., M. Fingas and R. Marois, "Oil Spill Remote Sensing: Laser Fluorosensor Demonstration Flights off the East Coast of Canada", *Proceedings of the 27th Arctic and Marine Oilspill Program (AMOP) Technical Seminar*, Environment Canada, Ottawa, ON, Canada, pp. 317-334, 2004a.
- Brown, C., M. Fingas, R. Marois, B. Fieldhouse and R. Gamble, "Remote Sensing of Water-In-Oil Emulsions: Initial Laser Fluorosensor Studies", *Proceedings of the 27th Arctic and Marine Oilspill Program (AMOP) Technical Seminar*, Environment Canada, Ottawa, ON, Canada, pp. 295-306, 2004b.
- Brown, C., M. Fingas, J. Monchalin, C. Neron and C. Padioleau, "Airborne measurement of oil slick thickness", *Proceedings of the 29th Arctic and Marine Oilspill Program (AMOP) Technical Seminar*, Environment Canada, Ottawa, ON, pp. 911-919, 2006a.
- Brown, C., M. Fingas and R. Marois, "Oil Spill Remote Sensing Flights around Vancouver Island", *Proceedings of the 29th Arctic and Marine Oilspill Program (AMOP) Technical Seminar*, Environment Canada, Ottawa, ON, Canada, pp. 921-930, 2006b.
- Camagni, P., A. Colombo, C. Koechler, N. Omenetto, P. Qi and G. Rossi, "Fluorescence Response of Mineral Oils: Spectral Yield vs Absorption and Decay Time", *Applied Optics*, 30:1, pp. 26-35, 1991.
- Cova, T.J., "GIS in emergency management, Geographical Information Systems: Principles, Techniques, Applications and Management" (P.A. Longley, M.F.

- Goodchild, D.J. Maguire, D.W. Rhind, editors), *John Wiley & Sons*, New York, pp. 845–858, 1999.
- Dick, R. and M.F. Fingas, “First Results of Airborne Trials of a 64-Channel Laser Fluorosensor for Oil Detection”, *Proceedings of the 15th Arctic and Marine Oilspill Program (AMOP) Technical Seminar*, Environment Canada, Ottawa, ON, Canada, pp. 365-379, 1992.
- Dick, R., M. Fruhwirth, M. Fingas and C. Brown, “Laser Fluorosensor Work in Canada”, *Proceedings of the First Thematic Conference: Remote Sensing for Marine and Coastal Environments*, New Orleans, USA, pp. 223-236, 1992.
- Fant, J. and K. Hansen, “U.S. Coast Guard Laser Fluorosensor Testing”, *Proceedings of the 29th Arctic and Marine Oilspill Program (AMOP) Technical Seminar*, Environment Canada, Ottawa, ON, Canada, pp. 951-964, 2006.
- Fingas, M., *The Basics of Oil Spill Cleanup*, CRC Press, Boca Raton, FL, 2001.
- Fingas, M. and C. Brown, “An Update on Oil Spill Remote Sensors”, *Proceedings of the 28th Arctic and Marine Oilspill Program (AMOP) Technical Seminar*, Environment Canada, Ottawa, ON, pp. 825-860, 2005.
- Fingas, M.F., C.E.Brown and J.V.Mullin, “A comparison of the utility of airborne oil spill remote sensors and satellite sensors”, *Proceedings of the 5th conference on remote sensing for Marine and Coastal Environments*, Environmental research institute of Michigan, ann arbor, Michigan , USA, 1, pp.I-171-I-178, 1998f

- Goodman, R., "Overview and Future Trends in Oil Spill Remote Sensing", *Spill Science & Technology Bulletin*, 1.1, pp.11-21, 1994.
- Graham, G., "Expert Systems for Marine Oil Spill Response Operations", *Georgia Basin/Puget Sound Research Conference Proceedings*, 2004.
- Green, D., "Troubled Waters: Despite tougher maritime legislation, oil spills at sea still foul our coastlines", *Mapping Awareness*, 10:6, pp. 19-22, 1996.
- Grüner, K., R. Reuter and H. Smid, "A New Sensor System for Airborne Measurements of Maritime Pollution and of Hydrographic Parameters", *Geojournal*, 24:1, pp. 103-117, 1991.
- Habib A., "ENGO 531 - Advanced Photogrammetric and Ranging Techniques", *Chapter 7*. http://dprg.geomatics.ucalgary.ca/files/Courses/431/AKAM_431_CH7_6_2008.pdf. Last accessed on June 13, 2009.
- Habib, A., K. Bang, A. Jarvis, and M. N. Jha, "LiDAR System Calibration", *Submitted to the Korean Electronics and Telecommunications Research Institute (ETRI)*, 2007.
- Hoge, F.E. and R.N. Swift, "Oil Film Thickness Measurement using Airborne Laser Induced Water Raman Backscatter", *Applied Optics*, 19, pp. 3269–3281, 1980.
- Howlett, E. and M.R. Bradstreet, "GIS component software for oil spill response", *Earth Observation Magazine*, 5:12, pp. 26-29, 1996.

- Hugh, H. and R.Mendds, "Oil spill contingency planning", *Proceedings of the Second SPE Exposition and Conference*, Port of Spain, 1977.
- Jackson, J.E., *A User's Guide to PCsComponents*, W InterScience, J Wiley & Sons, 1991.
- James, R.T.B. and R. Dick, "Design of Algorithms for the Real-time Airborne Detection of Littoral Oil-Spills by Laser-Induced Fluorescence", *Proceedings of the 19th Arctic and Marine Oilspill Program (AMOP) Technical Seminar*, Environment Canada, Ottawa, ON, Canada, pp.1599-1608, 1996.
- Jha, M.N. and Y. Gao, "Oil Spill Contingency Planning using Laser Fluorosensors and Web-Based GIS", *Proceedings of MTS/IEEE Oceans Conference*, Quebec City, 2008.
- Jha, M.N., J. Levy and Y. Gao, "Advances in Remote Sensing for Oil Spill Disaster Management: State-of-the-Art Sensors Technology for Oil Spill Surveillance", *Sensors*, 8, pp. 236-255, 2008a.
- Jha, M.N., Y. Gao and J. Levy, "An Analysis of Oil Spill Detection Algorithms using Laser Fluorosensor Data", *Proceedings of the 31st Arctic and Marine Oilspill Program (AMOP) Technical Seminar*, Environment Canada, Ottawa, ON, Canada, pp. 741-758, 2008b.
- Karafyllidis, I., "A model for the prediction of oil slick movement and spreading using cellular automata", *Environment International*, Elsevier, 23:6, pp. 839-850, 1997.

- Lennon, M., S. Babichenko, N. Thomas, V. Mariette, G. Mercier and A. Lisin, “Detection and Mapping of Oil Slicks in the Sea by Combined Use of Hyperspectral Imagery and Laser Induced Fluorescence”, *EARS eProceedings*, 5, pp 1-9, 2006.
- Li, J., “Spill Management for the Toronto AOC: The City of Toronto Study”, *Report and factsheet prepared for the Great Lakes Sustainability Fund, Burlington, Ontario, Canada, 2002.*
- Liu, S., Y. Gao and S. Li, “Emergency Management System using Event-driven GIS”, *Proceedings of the 31st Arctic and Marine Oilspill Program (AMOP) Technical Seminar*, Environment Canada, Ottawa, ON, Canada, pp. 405-414, 2008.
- Natural Resources Canada Website,
http://ccrs.nrcan.gc.ca/resource/tutor/fundam/chapter5/28_e.php. Last accessed on June 13, 2009.
- National Oceanic and Atmospheric Administration (NOAA), USA website.
<http://response.restoration.noaa.gov/>. See Topic: Emergency Response, Responding to Oil Spills. Last accessed on June 13, 2009.
- O’Neil, R.A., L. Buja-Bijunas and D.M. Rayner, “Field Performance of a Laser Fluorosensor for the Detection of Oil Spills”, *Applied Optics*, 19:6, 1980.
- Ornitz, B. and M. Champ, *Oil spill first principles: Prevention and best response*, NY: Elsevier, 2002.

- Patsayeva S., V. Yuzhakov, V. Varlamov, R. Barbini, R. Fantoni, C. Frassanito and A. Palucci, "Laser Spectroscopy of Mineral Oils on Water Surface", *EARSeL eProceedings, 1*, pp. 106-115, 2000.
- Plaza, J., R. Pérez, A. Plaza, P. Martínez and D. Valencia, "Mapping oil spills on sea water using spectral mixture analysis of hyperspectral image data", *Proceedings of SPIE, 5995, 599509-1*, 2001.
- Prentki, R., "Oil Spill Modeling towards the Close of the 20th Century: Overview of the State of the Art", *Spill Science & Technology Bulletin, 5:1* , pp. 3 – 16, 1999.
- Quinn, M.F., A.S. Al-Otaibi, P.S. Sethi, F. Al-Bahrani and O. Alamedine, "Measurement of Analysis Procedures for Remote Identification of Oil Spills using a Laser Fluorosensor", *International Journal of Remote Sensing, 15:13*, pp. 2637 – 2658, 1994.
- Ranger, R.L. and D.B. Casas, Casas, "Computer enhancement of spill response decision support", *Proceedings of the 18th Arctic and Marine Oilspill Program (AMOP) Technical Seminar*, Environment Canada, Ottawa, ON, Canada, pp. 297-312, 1995.
- Rogerson, P., *Statistical Methods for Geography*. Sage Publications, London, 2001.
- Rusinovic, Z. and N. Bogunovic, "Cellular automata based model for the prediction of oil slicks behaviour", *28th International Conference Information Technology Interfaces*, pp. 569 – 574, 2006.

- Salem, F. and M. Kafatos, "Hyperspectral image analysis for oil spill mitigation", 22nd *Asian Conference on Remote Sensing*, Singapore, 1, pp. 748–753, 2001.
- Salisbury, J., D. D'aria and F. Sabins, "Thermal Infrared Remote Sensing of Crude Oil Slicks", *Remote Sensing of Environment*, 45, pp. 225-231, 1993.
- Samberg, A., "Advanced oil pollution detection using an airborne hyperspectral LiDAR technology", *Proceedings of SPIE, the International Society for Optical Engineering*, 5791, pp. 308-317, 2005.
- Spatial Ecology Website, <http://www.spataleecology.com/htools/>. Last accessed on June 13, 2009.
- TIBCO EMS Website, <http://www.tibco.com/software/messaging/enterprise-message-service/default.jsp>. Last accessed on June 13, 2009.
- Trieschmann, O., Th. Hunsänger, and U. Barjenbruch, "A multiple remote sensor system for the aerial surveillance of the north sea and baltic sea", *Presented at the Fifth International Airborne Remote Sensing Conference*, San Francisco, California, pp. 17-20 2001. Available on <http://www.bafg.de/servlet/is/5863/proceedings.pdf>.
- Wadsworth, A., W. J. Looyen, R. Reuter, and M. Petit, "Aircraft experiments with visible and infrared sensors", *International Journal of Remote Sensing*, 13:6, pp. 1175 – 1199, 1992.
- Wehr, A. and U. Lohr. "Airborne laser scanning—an introduction and overview", *ISPRS Journal of Photogrammetry & Remote Sensing*, 54, pp. 68–82, 1999.